Chapter 1

Update on Ozone-Depleting Substances (ODSs) and Other Gases of Interest to the Montreal Protocol

Lead Authors
A. Engel
M. Rigby

Coauthors
J.B. Burkholder
R.P. Fernandez
L. Froidevaux
B.D. Hall
R. Hossaini
T. Saito
M.K. Vollmer
B. Yao

Contributors
E. Altas
P. Bernath
D.R. Blake
G. Dutton
P. Krummel
J.C. Laube
E. Mahieu
S.A. Montzka
J. Mühle
G. Nedoluha
S.J. O'Doherty
D.E. Oram
K. Pfeilsticker
R.G. Prinn
B. Quack
I.J. Simpson
R.F. Weiss

Review Editors
Q. Liang
S. Reimann

Cover photo: View of the high-altitude Jungfraujoch research station, perched at ca. 3,500 m in the Swiss Alps. Both in-situ atmospheric background measurements of halocarbons and related species, as well as remote sensing measurements of halogen species taken at the Jungfraujoch, have contributed to this report. Photo: Courtesy of jungfraujoch.ch.

Chapter 1

Update on Ozone-Depleting Substances (ODSs) and Other Gases of Interest to the Montreal Protocol

CONTENTS

Chapter 1

Update on Ozone-Depleting Substances (ODSs) and Other Gases of Interest to the Montreal Protocol

SCIENTIFIC SUMMARY

This chapter concerns atmospheric changes in ozone-depleting substances (ODSs), such as chlorofluorocarbons (CFCs), halons, chlorinated solvents (e.g., CCl_4 and CH_3CCl_3) and hydrochlorofluorocarbons (HCFCs), which are controlled under the Montreal Protocol. Furthermore, the chapter updates information about ODSs not controlled under the Protocol, such as methyl chloride (CH_3Cl) and very short-lived substances (VSLSs). In addition to depleting stratospheric ozone, many ODSs are potent greenhouse gases.

Mole fractions of ODSs and other species are primarily measured close to the surface by global or regional monitoring networks. The surface data can be used to approximate a mole fraction representative of the global or hemispheric tropospheric abundance. Changes in the tropospheric abundance of an ODS result from a difference between the rate of emissions into the atmosphere and the rate of removal from it. For gases that are primarily anthropogenic in origin, the difference between northern and southern hemispheric mole fractions is related to the global emission rate because these sources are concentrated in the northern hemisphere.

- **The abundances of the majority of ODSs that were originally controlled under the Montreal Protocol are now declining, as their emissions are smaller than the rate at which they are destroyed. In contrast, the abundances of most of the replacement compounds, HCFCs and hydrofluorocarbons (HFCs, which are discussed in Chapter 2), are increasing.**

TROPOSPHERIC CHLORINE

Total tropospheric chlorine is a metric used to quantify the combined globally averaged abundance of chlorine in the troposphere due to the major chlorine-containing ODSs. The contribution of each ODS to total tropospheric chlorine is the product of its global tropospheric mean mole fraction and the number of chlorine atoms it contains.

- **Total tropospheric chlorine (Cl) from ODSs continued to decrease between 2012 and 2016.** Total tropospheric chlorine in 2016[1] was 3,287 ppt (where ppt refers to parts per trillion as a dry air mole fraction), 11% lower than its peak value in 1993, and about 0.5% lower than reported for 2012 in the previous Assessment. Of the 2016 total, CFCs accounted for about 60%, CH_3Cl accounted for about 17%, CCl_4 accounted for about 10%, and HCFCs accounted for about 9.5%. The contribution from CH_3CCl_3 has now decreased to 0.2%. Very short-lived source gases (VSL SGs), as measured in the lower troposphere, contributed approximately 3%.
    - During the period 2012–2016, the observed rate of decline in tropospheric Cl due to *controlled substances* was 12.7 ± 0.9[2] ppt Cl yr^{-1}, similar to the 2008–2012 period (12.6 ± 0.3 ppt Cl yr^{-1}). This rate of decrease was close to the projections from the A1 scenario[3] in the previous Assessment. However, the net rate of change was the result of a slower than projected decrease in CFCs and a slower HCFC increase than in the A1 scenario, which assumed that HCFC production from Article 5 countries would follow the maximum amount allowed under the Montreal Protocol.

[1] Here and throughout this chapter, values that are given for a specific year represent annual averages, unless mentioned otherwise.

[2] The ranges given here represent the interannual variability in observed growth rate or rate of decrease.

[3] A1 Scenario is given in Table 5A-2 of Harris and Wuebbles et al. (2014).

  - When substances *not controlled* under the Montreal Protocol are also included, the overall decrease in tropospheric chlorine was 4.4 ± 4.1 ppt Cl yr^{-1} during 2012–2016. This is smaller than the rate of decline during the 2008–2012 period (11.8 ± 6.9 ppt Cl yr^{-1}) and smaller than the rate of decline in controlled substances because VSLSs, predominantly anthropogenic dichloromethane (CH_2Cl_2), and methyl chloride (CH_3Cl), which is mostly from natural sources, increased during this period.

- **Starting around 2013, the rate at which the CFC-11 mole fraction was declining in the atmosphere slowed unexpectedly, and the interhemispheric difference in its mole fraction increased. These changes are very likely due to an increase in emissions, at least part of which originate from eastern Asia.** Assuming no change in atmospheric circulation, an increase in global emissions of approximately 10 Gg yr^{-1} (~15%) is required for 2014–2016, compared to 2002–2012, to account for the observed trend and interhemispheric difference. The rate of change and magnitude of this increase is unlikely to be explained by increasing emissions from banks. Therefore, these findings may indicate new production not reported to the United Nations Environment Programme (UN Environment). If the new emissions are associated with uses that substantially increase the size of the CFC-11 bank, further emissions resulting from this new production would be expected in future.

- **Compared to 2008–2012, for the period 2012–2016, mole fractions of CFC-114[4] declined more slowly, CFC-13 continued to rise, and CFC-115 exhibited positive growth after previously showing near-zero change. These findings likely indicate an increase or stabilization of the emissions of these relatively low abundance compounds, which is not expected given their phaseout for emissive uses under the Montreal Protocol.** For CFC-114 and -115, regional analyses show that some of these emissions originate from China. There is evidence that a small fraction of the global emissions of CFC-114 and -115 are due to their presence as impurities in some HFCs. However, the primary processes responsible are unknown.

- **The rate at which carbon tetrachloride (CCl_4) has declined in the atmosphere remains slower than expected from its reported use as a feedstock. This indicates ongoing emissions of around 35 Gg yr^{-1}. Since the previous Assessment, the best estimate of the global atmospheric lifetime of CCl_4 has increased from 26 to 32 years, due to an upward revision of its lifetime with respect to loss to the ocean and soils. New sources have been proposed including significant by-product emissions from the production of chloromethanes and perchloroethylene and from chlor-alkali plants.** With these changes in understanding, the gap between top-down and bottom-up emissions estimates has reduced to around 10 Gg yr^{-1}, compared to 50 Gg yr^{-1} previously.

- **Combined emissions of the major HCFCs have declined since the previous Assessment.** Emissions of HCFC-22 have remained relatively stable since 2012, while emissions of HCFC-141b and -142b declined between 2012 and 2016, by around 10% and 18%, respectively. These findings are consistent with a sharp drop in reported HCFC consumption after 2012, particularly from Article 5 countries.

- **Emissions of the compounds HCFC-133a and HCFC-31, for which no current intentional use is known, have been detected from atmospheric measurements.** Research to date suggests that these gases are unintentional by-products of HFC-32, HFC-134a, and HFC-125 production.

TROPOSPHERIC BROMINE

Total tropospheric bromine is defined in analogy to total tropospheric chlorine. Even though the abundance of bromine is much smaller than that of chlorine, it has a significant impact on stratospheric ozone because it is around 60–65 times more efficient than chlorine as an ozone-destroying catalyst

[4] Here, CFC-114 refers to the combination of the CFC-114 and CFC-114a isomers.

- **Total tropospheric bromine from controlled ODSs (halons and methyl bromide) continued to decrease and by 2016 was 14.6 ppt, 2.3 ppt below the peak levels observed in 1998.** In the 4-year period prior to the last Assessment, this decrease was primarily driven by a decline in methyl bromide (CH_3Br) abundance, with a smaller contribution from a decrease in halons. These relative contributions to the overall trend have now reversed, with halons being the main driver of the decrease of 0.15 ± 0.04 ppt Br yr^{-1} between 2012 and 2016.

- **The mole fractions of halon-1211, halon-2402, and halon-1202 continued to decline between 2012 and 2016. Mole fractions of halon-1301 increased during this period, although its growth rate dropped to a level indistinguishable from zero in 2016.** Emissions of halon-2402, halon-1301, and halon-1211, as derived from atmospheric observations, declined or remained stable between 2012 and 2016.

- **Methyl bromide (CH_3Br) mole fractions continued to decline between 2012 and 2015 but showed a small increase (2–3%) between 2015 and 2016. This overall reduction is qualitatively consistent with the controls under the Montreal Protocol.** The 2016 level was 6.8 ppt, a reduction of 2.4 ppt from peak levels measured between 1996 and 1998. The increase between 2015 and 2016 was the first observation of a positive global change for around a decade or more. The cause of this increase is yet to be explained. However, as it was not accompanied by an increased interhemispheric difference, it is unlikely that this is related to anthropogenic emissions in the Northern Hemisphere. By 2016, controlled CH_3Br consumption dropped to less than 2% of the peak value, and total reported fumigation emissions have declined by more than 85% since their peak in 1997. Reported consumption in quarantine and pre-shipment (QPS) uses of CH_3Br, which are not controlled under the Montreal Protocol, have not changed substantially over the last two decades.

HALOGENATED VERY SHORT-LIVED SUBSTANCES (VSLSs)

VSLSs are defined as trace gases whose local lifetimes are shorter than 0.5 years and have nonuniform tropospheric abundances. These local lifetimes typically vary substantially over time and space. Of the very short-lived source gases (VSL SGs) identified in the atmosphere, brominated and iodinated species are predominantly of oceanic origin, while chlorinated species have significant additional anthropogenic sources. VSLSs will release the halogen they contain almost immediately once they enter the stratosphere and will thus play an important role in the lower stratosphere in particular. Due to their short lifetimes and their atmospheric variability the quantification of their contribution is much more difficult and has much larger uncertainties than for long-lived compounds.

- **Total tropospheric chlorine from VSL SGs in the background lower atmosphere is dominated by anthropogenic sources. It continued to increase between 2012 and 2016, but its contribution to total chlorine remains small.** Global mean chlorine from VSLSs in the troposphere has increased from about 90 ppt in 2012 to about 110 ppt in 2016. The relative VSLS contribution to stratospheric chlorine input derived from observations in the tropical tropopause layer has increased slightly from 3% in 2012 to 3.5% in 2016.

- **Dichloromethane (CH_2Cl_2), a VSL SG that has predominantly anthropogenic sources, accounted for the majority of the change in total chlorine from VSLSs between 2012 and 2016 and is the main source of VSLS chlorine.** The global mean abundance reached approximately 35–40 ppt in 2016, which is about a doubling compared to the early part of the century. The increase slowed substantially between 2014 and 2016. Emissions from southern and eastern Asia have been detected for CH_2Cl_2.

- **There is further evidence that VSLSs contribute ~5 (3–7) ppt to stratospheric bromine, which was about 25% of total stratospheric bromine in 2016. The main sources for brominated VSLSs are natural, and no long-term change is observed.** While the best estimate of 5 ppt has remained unchanged from the last

Assessment, the assessed uncertainty range has been reduced. Due to the decline in the abundance of regulated bromine compounds, the relative contribution of VSLSs to total stratospheric bromine continues to increase.

STRATOSPHERIC CHLORINE AND BROMINE

In the stratosphere, chlorine and bromine can be released from organic source gases to form inorganic species, which participate in ozone depletion. In addition to estimates of the stratospheric input derived from the tropospheric observations, measurements of inorganic halogen loading in the stratosphere are used to determine trends of stratospheric chlorine and bromine.

- **Hydrogen chloride (HCl) is the major reservoir of inorganic chlorine (Cl_y) in the mid to upper stratosphere. Satellite-derived measurements of HCl (60°N–60°S) in the middle stratosphere show a long-term decrease of HCl at a rate of around 0.5% yr^{-1}, in good agreement with expectations from the decline in tropospheric chlorine.** In the lower stratosphere, a decrease was observed over the period from 1997 to 2016, while significant differences in the trends are seen over the period 2005 to 2016 between various datasets and altitude/geographical regions. A similar behavior is observed for total column measurements, likely reflecting variability in stratospheric dynamics and chemistry. Total chlorine input to the stratosphere of 3,290 ppt is derived for 2016 from measurements of long-lived ODSs at the surface and VSLSs in the upper troposphere. About 80% of this input is from substances controlled under the Montreal Protocol.

- **Total stratospheric bromine, derived from observations of bromine monoxide (BrO), continued to decrease at a rate of about 0.75% yr^{-1} from 2004 to 2014.** This decline is consistent with the decrease in total tropospheric organic bromine, based on measurements of CH_3Br and the halons. A total bromine input to the stratosphere of 19.6 ppt is derived for 2016, combined from 14.6 ppt of long-lived gases and 5 ppt from VSLSs not controlled under the Montreal Protocol. Anthropogenic emissions of all brominated long-lived gases are controlled, but as CH_3Br also has natural sources, more than 50% of the bromine reaching the stratosphere is now estimated to be from sources not controlled under the Montreal Protocol. There is no indication of a long-term change in natural sources to stratospheric bromine.

EQUIVALENT EFFECTIVE STRATOSPHERIC CHLORINE (EESC)

EESC is the chlorine-equivalent sum of chlorine and bromine derived from ODS tropospheric abundances, weighted to reflect their expected depletion of stratospheric ozone. The growth and decline in EESC depends on a given tropospheric abundance propagating to the stratosphere with varying time lags (on the order of years) associated with transport. Therefore, the EESC abundance, its peak timing, and its rate of decline are different in different regions of the stratosphere. Recent suggestions of a refinement in the calculation method for EESC result in somewhat lower estimates on how far the stratospheric reactive halogen loading has recovered.

- **By 2016, EESC had declined from peak values by about 9% for polar winter conditions and by about 13–17% for mid-latitude conditions.** This drop is 31–43% of the decrease required for EESC in mid-latitudes to return to the 1980 benchmark level, and about 18–19% of the decrease required for EESC in polar regions to return to the 1980 benchmark level[5]. The rate at which EESC is decreasing has slowed, in accordance with a slowdown of the decrease in tropospheric chlorine. The ranges given reflect the different methods for calculating EESC. Differences in halogen recovery levels from previous Assessments are also due to differences in assumed fractional release factors.

[5] As in previous Assessments, 1980 levels of EESC are used as a benchmark for recovery, although this value is somewhat arbitrary and some ozone loss had occurred prior to 1980. Also, recovery of EESC to 1980 values does not necessarily imply a recovery of ozone to 1980 levels, as other parameters, e.g. stratospheric circulation, may change.

TROPOSPHERIC AND STRATOSPHERIC FLUORINE

While fluorine has no direct impact on stratospheric ozone, many fluorinated gases are strong greenhouse gases, and their emission is often related to the replacement of chlorinated substances regulated under the Montreal Protocol. For this reason, trends in fluorine are also assessed in this report.

- **The main sources of fluorine in the troposphere and in the stratosphere are CFCs, HCFCs, and HFCs. In contrast to total chlorine, total fluorine in the troposphere continued to increase between 2012 and 2016, at a rate of 1.7% yr^{-1}.** This increase shows the decoupling of the temporal trends in fluorine and chlorine due to the increasing emissions of HFCs (see **Chapter 2**). The total atmospheric-column abundance of inorganic fluorine, which is mainly stratospheric, has continued to increase at a rate of about 1% yr^{-1} over the period 2007–2016.

EFFECT OF OZONE-DEPLETING SUBSTANCES (ODSs) ON CLIMATE

- **The total direct radiative forcing[6] of CFCs continues to be much higher than that of HCFCs.** However, radiative forcing from CFCs has dropped by about 7% since its peak in 2000 to about 250 mW m^{-2} in 2016 (approximately 13% that of CO_2), while radiative forcing from HCFCs increased to 58 mW m^{-2} in 2016 (approximately 3% that of CO_2). The total direct radiative forcing due to CFCs, HCFCs, halons, CCl_4 and CH_3CCl_3 was 327 mW m^{-2} in 2016 (approximately 16% that of CO_2).

- **CO_2-equivalent emissions[7] of CFCs and HCFCs were approximately equal in 2016.** The CO_2-equivalent emission from the sum of all CFCs or the sum of all HCFCs was approximately 0.8 Gt in 2016. The CO_2-equivalent emission from the sum of CFCs, HCFCs, Halons, CCl_4 and CH_3CCl_3 was approximately 1.7 Gt in 2016.

OTHER GASES THAT AFFECT OZONE AND CLIMATE

- **Mole fractions of many other gases that affect both ozone and climate have changed since the previous Assessment.** The atmospheric abundance of methane has continued to increase following a period of stagnation in the early 2000s. The drivers of the changing trend are disputed. Nitrous oxide continues to grow relatively steadily in the atmosphere. The global mole fractions of the fluorinated species sulfur hexafluoride (SF_6), nitrogen trifluoride (NF_3), sulfuryl fluoride (SO_2F_2), and the perfluorocarbons (PFCs such as CF_4 and C_2F_6) have continued to grow. In contrast, the abundance of the sulfur-containing compounds sulfur dioxide (SO_2) and carbonyl sulfide (COS) has not changed substantially.

[6] A measure of the change in net irradiance (incoming minus outgoing) at the tropopause.

[7] CO_2 equivalents are determined here by weighting emissions estimates by the global warming potential (GWP) of each gas, integrated over a 100-year time horizon.

Chapter 1

Update on Ozone-Depleting Substances (ODSs) and Other Gases of Interest to the Montreal Protocol

1.1 SUMMARY OF FINDINGS FROM THE PREVIOUS OZONE ASSESSMENT

Chapter 1 of the 2014 Assessment report (Carpenter and Reimann et al., 2014) provided updates on ozone-depleting substances (ODSs) and other gases of interest to the Montreal Protocol. These included hydrofluorocarbons (HFCs), which have been used to replace ODSs; they are not ozone-depleting substances, but they do add to climate warming.

Chapter 1 from the 2014 Assessment showed that, in the 5-year period 2008–2012, total tropospheric chlorine from substances regulated under the Montreal Protocol had declined at an average rate of 13.4 ± 0.9 ppt yr^{-1} (ppt defined as dry air mole fraction in parts per trillion), while bromine from regulated substances was declining at a rate of 0.14 ± 0.02 ppt yr^{-1}. All major CFCs (chlorofluorocarbons) showed decreasing mole fractions and continued to be the main carriers of chlorine, with a contribution of 61% to total tropospheric chlorine. The only class of compounds that were regulated yet still showed increasing mole fractions were hydrochlorofluorocarbons (HCFCs). A continuing discrepancy in the emissions of CCl_4 inferred from observations versus those derived from reports to the United Nations Environment Programme (UN Environment) was documented.

An increase in lower tropospheric abundances of chlorinated very short-lived substances (VSLSs) was observed. Dichloromethane (CH_2Cl_2) increased particularly strongly; the global mean mole fraction had increased by about 60% between 2001 and 2012. However, the total contribution of VSLSs to stratospheric chlorine remained small at approximately 3% in 2012, including the contribution of inorganic product gases entering the stratosphere.

Total tropospheric bromine showed an overall decline, consistent with the projections from the scenarios in the 2010 Assessment. The decline was driven by the continued decrease of CH_3Br and, for the first-time, an observed decrease in total tropospheric bromine from halons, with all halons except for halon-1301 decreasing in the atmosphere. The relative contribution of brominated VSLSs to total bromine was much larger than the contribution of chlorinated VSLSs to total chlorine, with about 5 ppt of the total 20 ppt of stratospheric bromine attributed to short-lived substances. Input of bromine from VSLSs to the stratosphere in both organic and inorganic forms was included.

Equivalent effective stratospheric chlorine (EECS), which is the chlorine-equivalent sum of chlorine and bromine derived from ODS tropospheric abundances weighted to reflect their expected depletion of stratospheric ozone, was assessed to have declined from its maximum value in polar regions by about 10% and in mid-latitudes by about 15%; this is equivalent to about 20% and 40% of the decline required to return to 1980 benchmark levels, respectively.

The influence of ODS and HFC emissions on climate was assessed in terms of their equivalent in gigatonnes of carbon dioxide (CO_2-equivalent emissions) using 100-year Global Warming Potential (GWP). The CO_2-equivalent emissions of CFCs, HCFCs, and HFCs were roughly equal to each other in 2012 with respect to their climate influence. However, the emissions of HFCs were increasing, while the emissions of CFCs were declining and those of HCFCs remained relatively constant.

1.2 UPDATED ABUNDANCES, TRENDS, LIFETIMES, AND EMISSIONS OF LONGER-LIVED HALOGENATED SOURCE GASES

Observations of ODSs have been carried out over multiple decades by several groups with different sampling strategies, who have, in most cases, developed independent, but regularly compared, calibration scales (**Figure 1-1**, **Table 1-1**). Global and hemispheric mean mole fractions are derived using data from networks with air sampling stations that are distributed

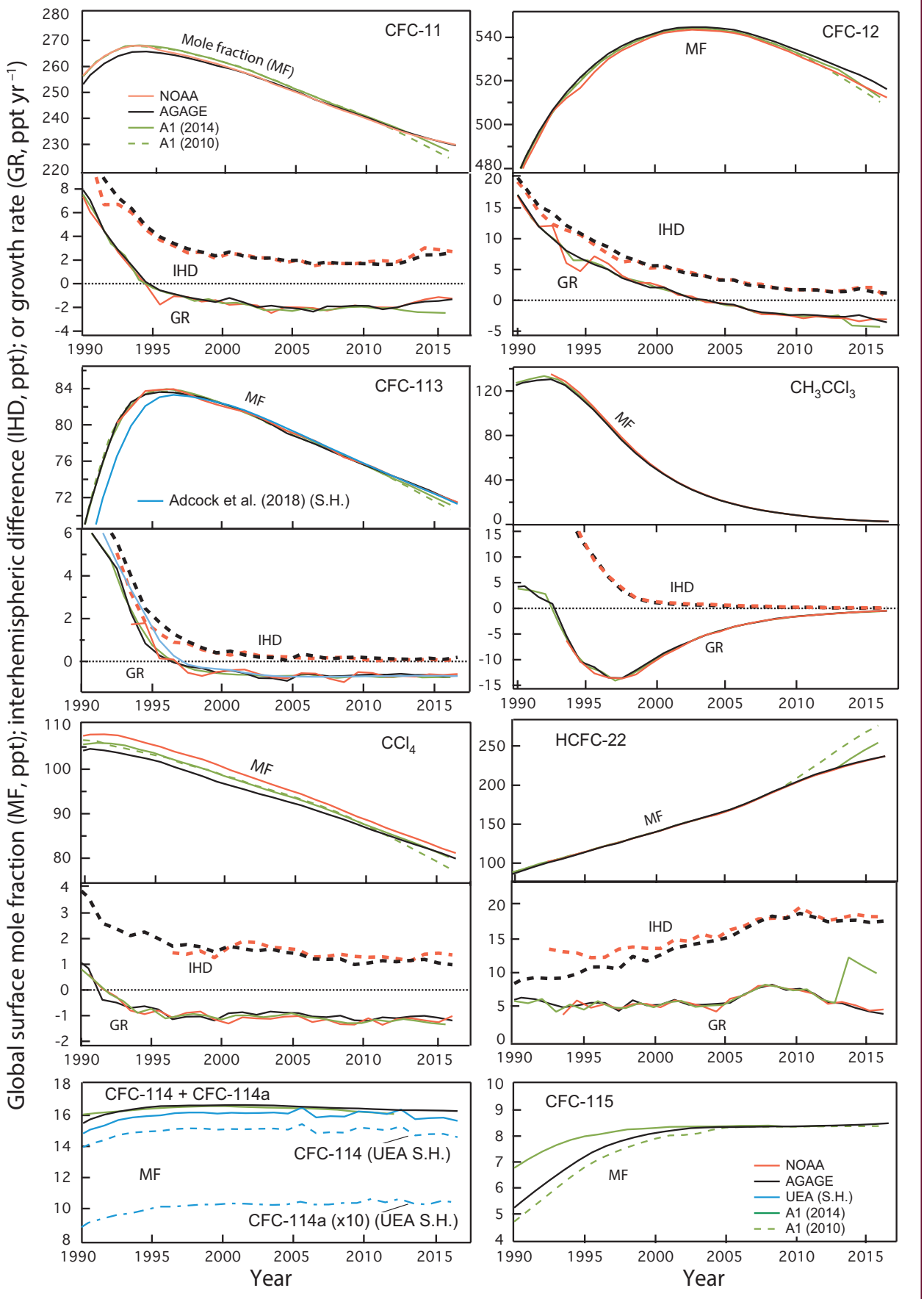
Global surface mole fraction (MF, ppt); interhemispheric difference (IHD, ppt); or growth rate (GR, ppt yr⁻¹)
CFC-11
Mole fraction (MF)
NOAA
AGAGE
A1 (2014)
A1 (2010)
IHD
GR
CFC-12
MF
IHD
GR
CFC-113
MF
Adcock et al. (2018) (S.H.)
IHD
GR
CH3CCl3
MF
IHD
GR
CCl4
MF
IHD
GR
HCFC-22
MF
IHD
GR
CFC-114 + CFC-114a
CFC-114 (UEA S.H.)
MF
CFC-114a (x10) (UEA S.H.)
CFC-115
MF
NOAA
AGAGE
UEA (S.H.)
A1 (2014)
A1 (2010)
Year
Year

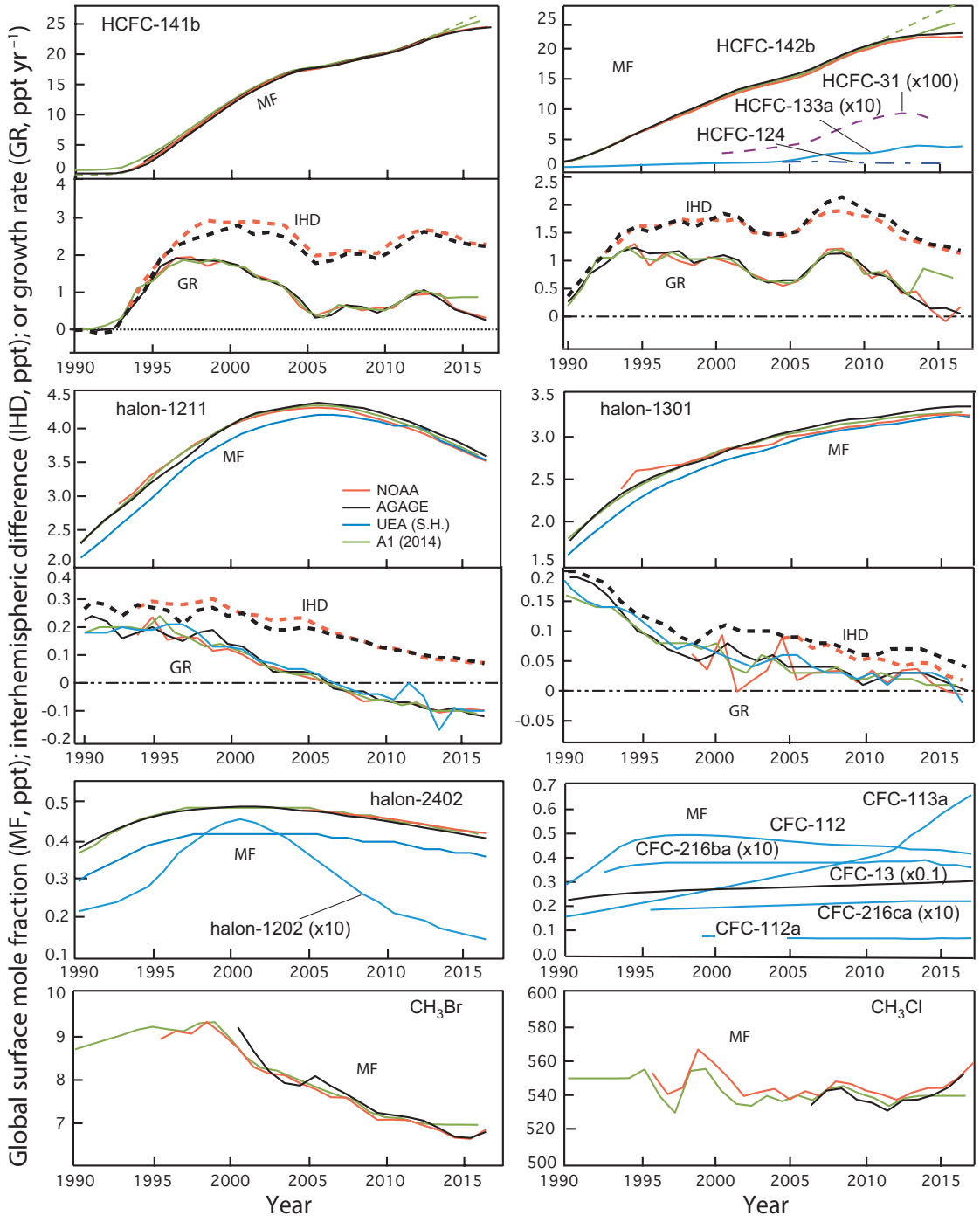

Figure 1-1. Annual mean global surface mole fractions (MF; expressed as dry air mole fractions in parts per trillion or ppt) of ozone-depleting substances from independent sampling networks and from scenario A1 of the previous Ozone Assessments over the past 26 years (1990–2016) (Daniel and Velders, 2011; Harris and Wuebbles et al., 2014). The baseline scenarios from previous Assessments (A1-2010, A1-2014) are projections from 2009 and 2013, respectively. Only A1-2014 data are shown for some species. Shown are measured global surface annual means from the NOAA network (red) and AGAGE network (black). Southern Hemispheric data obtained by the University of East Anglia (UEA) (blue) are shown for some species. NOAA and AGAGE CFC-113 data likely represent some combination of CFC-113 and CFC-113a (although the influence of CFC-113a on NOAA and AGAGE measurements of CFC-113 is likely small), whereas UEA measures CFC-113 and CFC-113a separately (Adcock et al., 2018). UEA CFC-113 data (annual Southern Hemispheric means from Adcock et al., 2018) were adjusted downward by 2% to be consistent with the NOAA scale determined by gas chromatography-mass spectrometry (GC-MS) as opposed to gas chromatography-electron capture detection (GC-ECD). HCFC-124 data were taken from Simmonds et al. (2017). HCFC-31 data were taken from Schoenenberger et al. (2015). For some gases, we also show growth rates (GR) and interhemispheric differences (IHD; NH mean minus SH mean) in a second panel, using the same color scheme as in the corresponding upper panel.

Table 1-1. Measured mole fractions and changes of ozone-depleting gases from ground-based sampling networks (expressed in dry air mole fractions as parts per trillion (ppt), or relative units).

Chemical Formula	Common or Industrial Name	Annual Mean Mole Fraction (ppt) 2012	2015	2016	Change (2015–2016) (ppt yr^{-1})	(% yr^{-1})	Network, Method
CFCs							
CCl_3F	CFC-11	**235.5**	**230.9**	**229.6**	**-1.3**	**-0.6**	AGAGE, in situ[1]
		235.2	**231.1**	**229.8**	**-1.3**	**-0.6**	NOAA[2], flask & in situ
		235.3	**229.2**	**227.4**	**-1.8**	**-0.8**	UCI, flask
CCl_2F_2	CFC-12	**527.8**	**519.7**	**516.1**	**-3.6**	**-0.7**	AGAGE, in situ
		524.7	**515.3**	**512.2**	**-3.1**	**-0.6**	NOAA, flask & in situ
		522.5	**519.5**	**515.6**	**-3.9**	**-0.8**	UCI, flask
$CClF_3$	CFC-13	**2.94**	**3.01**	**3.04**	**0.03**	**1.0**	AGAGE, in situ
CCl_2FCCl_2F	CFC-112	*0.44*	*0.42*	*0.42*	*0.00*	*0.0*	UEA, flask (Cape Grim)
CCl_3CClF_2	CFC-112a	*0.066*	*0.066*	*0.067*	*0.001*	*1.5*	UEA, flask (Cape Grim)
CCl_2FCClF_2	CFC-113	**74.0**	**72.1**	**71.4**	**-0.7**	**-0.9**	AGAGE, in situ[3]
		74.0	**72.1**	**71.5**	**-0.6**	**-0.8**	NOAA, flask[3]
		74.2	**71.8**	**71.1**	**-0.7**	**-1.0**	UCI, flask[3]
CCl_3CF_3	CFC-113a	*0.43*	*0.62*	*0.66*	*0.04*	*6.5*	UEA, flask (Cape Grim)
$CClF_2CClF_2$	CFC-114	**16.3**	**16.3**	**16.3**	**0.0**	**-0.1**	AGAGE, in situ[4]
		15.2	*14.8*	*14.6*	*-0.2*	*-1.4*	UEA, flask (Cape Grim)[5]
CCl_2FCF_3	CFC-114a	*1.05*	*1.05*	*1.04*	*-0.01*	*-1.0*	UEA, flask (Cape Grim)[5]
$CClF_2CF_3$	CFC-115	**8.40**	**8.46**	**8.49**	**0.03**	**0.4**	AGAGE, in situ
		8.48	*8.63*	*8.67*	*0.04*	*0.5*	NIES, in situ (Japan)
HCFCs[6]							
$CHClF_2$	HCFC-22	**219.3**	**233.6**	**237.4**	**3.8**	**1.6**	AGAGE, in situ
		218.0	**233.0**	**237.5**	**4.5**	**1.9**	NOAA, flask
		214.5	**238.0**	**242.3**	**4.3**	**1.8**	UCI, flask
CH_2ClCF_3	HCFC-133a	*0.31*	*0.37*	*0.39*	*0.02*	*5.4*	UEA, flask (Cape Grim)
CH_3CCl_2F	HCFC-141b	**22.45**	**24.22**	**24.47**	**0.25**	**1.0**	AGAGE, in situ
		22.27	**24.22**	**24.53**	**0.31**	**1.3**	NOAA, flask
		21.80	**24.49**	**24.59**	**0.10**	**0.4**	UCI, flask
CH_3CClF_2	HCFC-142b	**21.92**	**22.51**	**22.56**	**0.05**	**0.2**	AGAGE, in situ
		21.36	**21.84**	**22.01**	**0.17**	**0.8**	NOAA, flask
		21.80	**23.26**	**23.16**	**-0.10**	**-0.4**	UCI, flask
Halons							
CBr_2F_2	halon-1202	*0.018*	*0.015*	*0.014*	*-0.001*	*-6.7*	UEA, flask (Cape Grim)[5]
$CBrClF_2$	halon-1211	**4.01**	**3.71**	**3.59**	**-0.12**	**-3.2**	AGAGE, in situ
		3.92	**3.61**	**3.52**	**-0.09**	**-2.5**	NOAA, flask

Chemical Formula	Common or Industrial Name	Annual Mean Mole Fraction (ppt) 2012	2015	2016	Change (2015–2016) (ppt yr^{-1})	(% yr^{-1})	Network, Method
$CBrClF_2$ (continued)	halon-1211 (continued)	**3.96**	**3.66**	**3.54**	**-0.12**	**-3.3**	NOAA, in situ
		3.97	*3.61*	*3.51*	*-0.10*	*-2.8*	UEA, flask (Cape Grim)
		4.14	**3.80**	**3.70**	**-0.10**	**-2.6**	UCI, flask
$CBrF_3$	halon-1301	**3.30**	**3.36**	**3.36**	**0.00**	**0.0**	AGAGE, in situ
		3.19	**3.25**	**3.25**	**0.00**	**-0.1**	NOAA, in situ
		3.10	*3.17*	*3.17*	*0.00*	*0.0*	UEA, flask (Cape Grim)
$CBrF_2CBrF_2$	halon-2402	**0.44**	**0.42**	**0.41**	**-0.01**	**-2.4**	AGAGE, in situ[7]
		0.44	**0.42**	**0.42**	**-0.01**	**-1.2**	NOAA, flask
		0.39	*0.37*	*0.36*	*-0.01*	*-2.7*	UEA, flask (Cape Grim)[5]
Chlorocarbons							
CH_3Cl	methyl chloride	**539.9**	**544.7**	**552.7**	**8.0**	**1.5**	AGAGE, in situ
		541.4	**550.0**	**559.1**	**9.1**	**1.7**	NOAA, flask
CCl_4	carbon tetrachloride	**84.2**	**81.1**	**79.9**	**-1.2**	**-1.5**	AGAGE, in situ
		85.7	**82.2**	**81.2**	**-1.0**	**-1.2**	NOAA, flask & in situ
		86.7	**82.2**	**81.9**	**-0.3**	**-0.3**	UCI, flask
CH_3CCl_3	methyl chloroform	**5.21**	**3.09**	**2.61**	**-0.48**	**-16**	AGAGE, in situ
		5.25	**3.07**	**2.60**	**-0.47**	**-15**	NOAA, flask
		5.7	**3.48**	**3.05**	**-0.43**	**-12**	UCI, flask
Bromocarbons							
CH_3Br	methyl bromide	**7.06**	**6.66**	**6.80**	**0.14**	**2.1**	AGAGE, in situ
		6.95	**6.64**	**6.86**	**0.22**	**3.3**	NOAA, flask

Mole fractions in this table represent independent estimates measured by different groups for the years indicated. Results in bold text are estimates of global surface mean mole fractions. Regional data from relatively unpolluted sites are shown (in italics) where global estimates are not available, where global estimates are available from only one network, or where regional data provide additional long-term records. Absolute changes (ppt yr^{-1}) are calculated as the difference between 2015 and 2016 annual means; relative changes (% yr^{-1}) are the same difference relative to the 2015 value. Small differences between values reported in previous Assessments are due to changes in calibration scale and methods for estimating global mean mole fractions from a limited number of sampling sites.

These observations are published in or are updated from the following sources: (Adcock et al., 2018; Butler et al., 1998; Laube et al., 2016; Laube et al., 2014; Montzka et al., 2003; Montzka et al., 2018; Montzka et al., 2015; Newland et al., 2013; Prinn et al., 2018; Rigby et al., 2014; Simmonds et al., 2017; Simpson et al., 2007; Vollmer et al., 2016, 2018; Yokouchi et al., 2006); AGAGE, Advanced Global Atmospheric Gases Experiment (http://agage.mit.edu/; Prinn et al., 2018); NOAA, National Oceanic and Atmospheric Administration, USA (http://www.esrl.noaa.gov/gmd/dv/site/); UEA, University of East Anglia, United Kingdom (http://www.uea.ac.uk/environmental-sciences/research/marine-and-atmospheric-sciences-group); UCI, University of California, Irvine, USA (http://ps.uci.edu/~rowlandblake/research_atmos.html); NIES, National Institute for Environmental Studies, Japan (http://db.cger.nies.go.jp/gem/moni-e/warm/Ground/st01.html); Cape Grim: Cape Grim Baseline Air Pollution Station, Australia.

Notes:

[1] Global mean estimates from AGAGE are calculated using atmospheric data and a 12-box model (Cunnold et al., 1983; Rigby et al., 2014; Rigby et al., 2013). [2]The NOAA CFC-11 data have been updated following a calibration scale change in 2016 (Montzka et al., 2018). [3]Measurements of CFC-113 likely represent a combination of CFC-113 and CFC-113a due to co-elution, with the effect of CFC-113a on CFC-113 dependent on the analytical method. [4]AGAGE measurements of CFC-114 are a combination of the CFC-114 and CFC-114a isomers, with a relative contribution of ~7% CFC-114a (Laube et al., 2016). At UEA, CFC-114 and CFC-114a are quantified separately. [5]Mole fractions for 2016 represent averages from January to July for UEA data for these compounds. [6]Updates to HCFC-124 mole fractions are not provided as the AGAGE calibration scale has not been finalized. [7]Compared to the previous Assessment, AGAGE halon-2402 data are now on an independent calibration scale.

around the world: the Advanced Global Atmospheric Gases Experiment (AGAGE) network, the National Oceanic and Atmospheric Administration (NOAA) network, and the University of California, Irvine (UCI) network. Further data representative of regional or hemispheric scales are available for some species from the National Institute for Environmental Studies (NIES) and the University of East Anglia (UEA). Because these networks maintain independent calibration scales, and because they have different sampling locations and frequencies, small differences are observed (typically on the order of a few percent or less; see **Table 1-1**) in the burden and trend estimated from each dataset. Therefore, for much of this section, global trends and inferred emissions are given separately for each network. Data from regionally representative (e.g., Southern Hemisphere) sites are used when global network data are not available. In some circumstances, these data can be extrapolated to derive global-scale mole fractions or emissions using an atmospheric transport model (e.g., **Box 1-1**). This is the case where AGAGE mole fraction records have been extended back before Northern Hemispheric air samples were available, through the assimilation of Cape Grim Air Archive (CGAA; Langenfelds et al., 1996) data into an AGAGE 12-box model inversion (e.g. Rigby et al., 2014). Column observations are also available for some species based on ground-based or satellite-based remote sensing methods (**Figure 1-2**, **Table 1-2**).

For the long-lived ODSs that are primarily of anthropogenic origin, we derive radiative forcing from global mean near-surface mole fractions using the methods outlined in Ramaswamy et al. (2001) (**Figure 1-3**). Emissions, along with global and hemispheric mean mole fractions, are estimated using a box model of atmospheric transport and chemistry, constrained using baseline atmospheric data, following Rigby et al. (2014) (**Figure 1-4, Box 1-1**). The model includes estimates of the major loss processes, the magnitudes of which are mostly based on the SPARC Lifetimes assessment (SPARC, 2013) (**Table A-1**, **Figure 1-4**). Emissions estimates were combined with estimates of 100-year time horizon Global Warming Potentials (GWPs) and Ozone Depletion Potentials (ODPs), as summarized in **Table A-1**, to calculate CO_2-equivalent and CFC-11-equivalent emissions of ODSs and related substances (**Figure 1-5**).

1.2.1 Chlorofluorocarbons (CFCs)

Observations of Atmospheric Abundance

Mole fractions of the three most abundant CFCs—CFC-12 (CCl_2F_2), CFC-11 (CCl_3F), and CFC-113 (CCl_2FCClF_2)—continued to decline since 2012, reaching approximately 514 ppt, 230 ppt, and 71 ppt, respectively in 2016 (**Figure 1-1**). The atmospheric abundance of CFC-12 has fallen increasingly rapidly throughout this period, with the rate of decline increasing from 2.9 ppt yr^{-1} in 2011–2012 to around 3.6 ppt yr^{-1} in 2015–2016 (**Figure 1-1**, **Table 1-1**). The

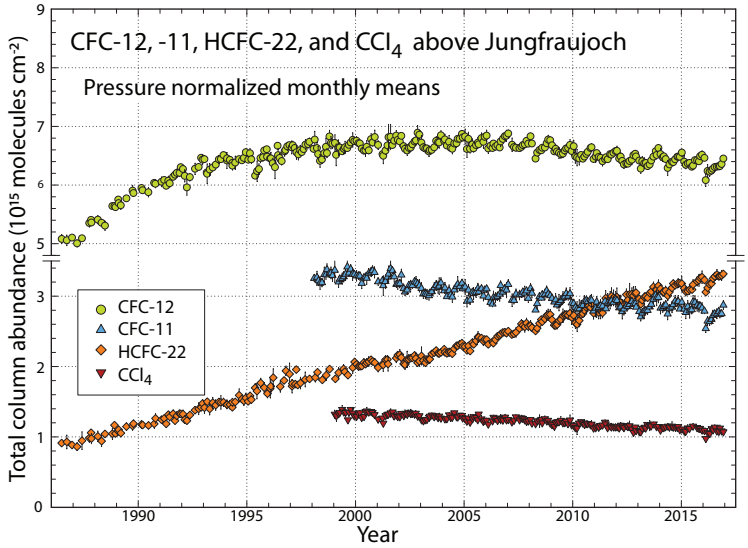

Figure 1-2. Monthly mean total vertical column abundances (in molecules per square centimeter) for CFC-12, CFC-11, CCl_4, and HCFC-22 above Jungfraujoch station, Switzerland, from 1986 to 2016 (updated from Zander et al., 2008 and Rinsland et al., 2012). The bootstrap resampling tool described by Gardiner et al. (2008) and Rinsland et al. (2012) was used for the trend evaluations (see **Table 1-2**). Note the discontinuity in the vertical scale.

rate of decline in CFC-113 has remained relatively constant at around 0.7 ppt yr^{-1}. In contrast, there was a slowdown in the rate at which the global abundance of CFC-11 was falling, starting around 2013 (Montzka et al., 2018): Rates of decline remained relatively close to 2.0 ppt yr^{-1} (0.8% yr^{-1}) between around 2002 and 2012 (±0.2 ppt yr^{-1} interannual variability, 1-sigma), but that rate has since dropped to approximately 1.3 ppt yr^{-1} (0.6% yr^{-1}) between 2014 and 2016. Coincident with this feature, the interhemispheric difference (IHD; the difference between Northern Hemisphere and Southern Hemisphere mean mole fractions) of CFC-11 increased from 1.8 ppt in 2012 to 2.7 ppt in 2016, suggesting that the increase is driven by Northern Hemispheric sources.

Measurements of the 2010–2016 trends in Northern Hemispheric CFC-11 and CFC-12 abundances made using ground-based Fourier transform infrared (FTIR) spectroscopy at Jungfraujoch, Switzerland, agree within uncertainties with those derived using surface-based in situ observations (**Table 1-2**, **Figure 1-2**). However, in contrast to the surface data, column CFC-11 trends were not found to be statistically different between the periods 2008–2012 (–1.24 ± 0.23% yr^{-1}) and 2013–2016 (–1.28 ± 0.42% yr^{-1}). This discrepancy is likely due to the larger interannual variability found in the column data, which complicates the comparison between column and surface trends over short timescales.

A full atmospheric history of CFC-13 ($CClF_3$) has recently been published based on samples from firn, archived air, and AGAGE in situ measurements (Vollmer et al., 2018). This compound increased relatively rapidly in the atmosphere until the mid-1990s, after which growth slowed but remained positive until the most recent measurements in 2016, when the global mole fraction reached 3.04 ppt (mean growth rate since 1996 of 0.02 ppt yr^{-1}). This new

Table 1-2. Comparison of annual trends of ODSs, CF_4, and SF_6 from in situ and remote sensing measurements. Relative trends in ODSs and halogenated greenhouse gases for the 2010–2016 time period derived from surface measurements and remote sensing observations. This time period was selected because interannual variability in remote sensing data makes robust quantification of trends challenging over shorter periods. Surface in situ trends were derived from monthly mean mole fractions, weighted by the surface area in the region 30°N to 90°N. Shown are the averages of trends derived independently from NOAA and AGAGE data (% yr^{-1} relative to 2013 annual mean). Uncertainties were estimated from uncertainties in the linear trends and differences between trends derived from independent networks. For CF_4, only AGAGE in situ data were used, and the uncertainty was derived from the uncertainty in the slope. For remote sensing observations, relative annual rates of change were computed over the 2010–2016 time period from FTIR observations at Jungfraujoch station, Switzerland, with the bootstrap resampling tool described in Gardiner et al. (2008), using the year 2013 as reference. All uncertainties are estimated at 2-sigma.

Annual Trend 2010–2016 (% yr^{-1} relative to 2013)			
Substance	**In situ**	**Remote sensing**	**References**
CFC-11	-0.64 ± 0.05	-0.70 ± 0.17	Updated from Zander et al. (2008) and references in Table 1-1.
CFC-12	-0.55 ± 0.05	-0.47 ± 0.08	Updated from Zander et al. (2008) and references in Table 1-1.
CCl_4	-1.32 ± 0.09	-1.03 ± 0.23	Updated from Rinsland et al. (2012) and references in Table 1-1.
HCFC-22	2.21 ± 0.10	2.54 ± 0.14	Updated from Zander et al. (2008) and references in Table 1-1.
HCFC-142b	0.97 ± 0.17	-0.6 ± 1.1	Updated from Mahieu et al. (2017) and references in Table 1-1.
SF_6	3.90 ± 0.06	4.34 ± 0.19	Updated from Zander et al. (2008) and Hall et al. (2011).
CF_4	0.94 ± 0.01	1.11 ± 0.09	Updated from Mahieu et al. (2014b) and references in Table 1-1.

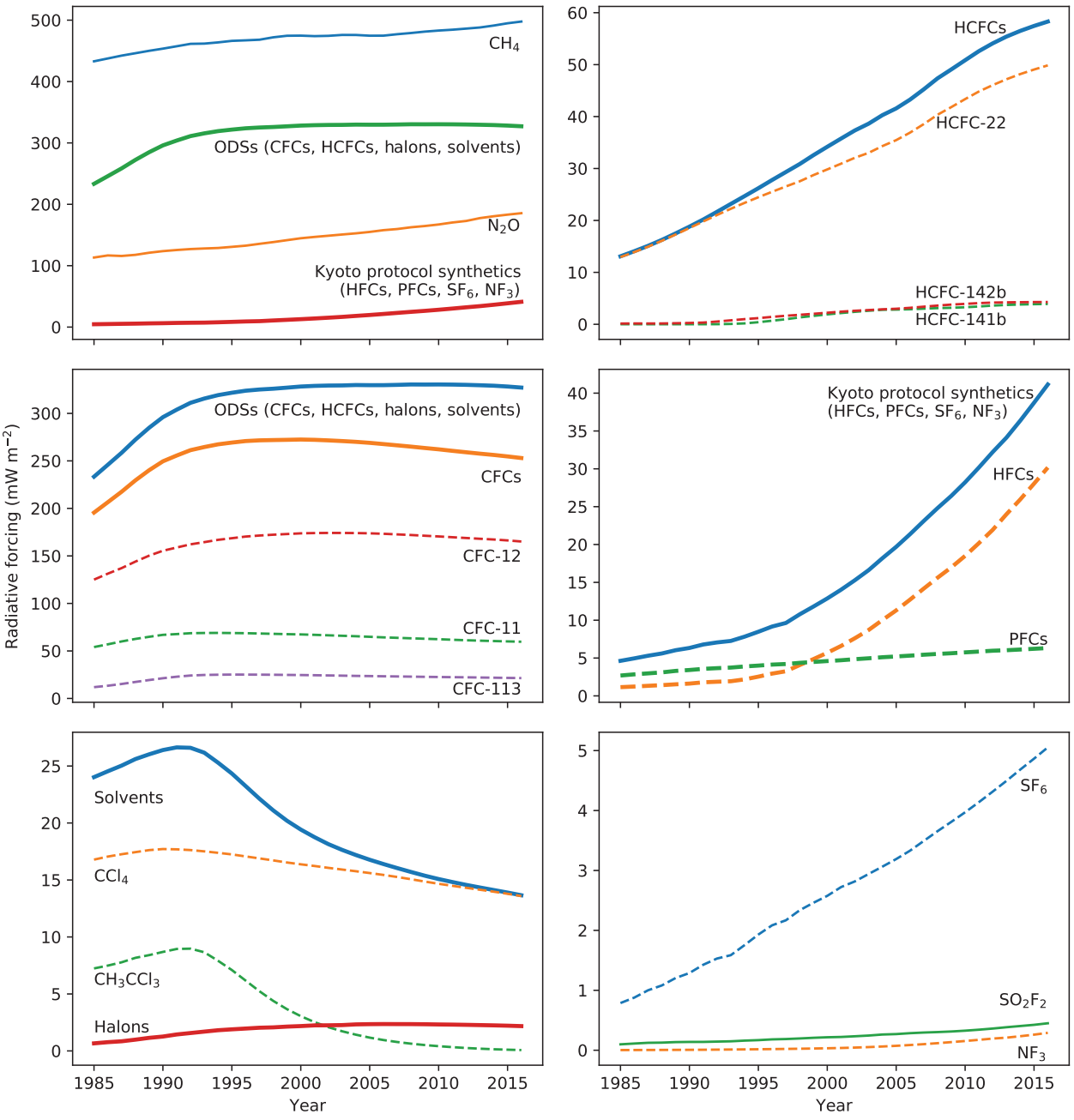

Figure 1-3. Direct radiative forcing due to ODSs, HFCs, CH_4, N_2O, and other greenhouse gases. Selected groupings of gases are shown in bold and selected compounds or collections of compounds that fall within these groupings are shown as dashed lines. The ODS group here refers to combined CFCs, HCFCs, halons, and solvents (CCl_4 and CH_3CCl_3). Kyoto protocol synthetics are defined as HFCs (see **Chapter 2**), perfluorocarbons (PFCs, which include CF_4 and C_2F_6), SF_6, and NF_3 (**Section 1.5**). Lower tropospheric annual mean mole fractions were taken from AGAGE data (**Table 1-1**, **Figure 1-1**). Radiative forcing was calculated using the expressions in Ramaswamy et al. (2001), with radiative efficiencies as summarized in **Table A-1** and preindustrial global surface mean mole fractions of 722 ppb, 270 ppb, and 36 ppt for CH_4, N_2O, and CF_4, respectively. For comparison, the radiative forcing due to CO_2 was approximately 2 W m^{-2} in 2016.

measurement time series is around 25% lower than previous records, due primarily to differences in calibration scales (Culbertson et al., 2004; Oram, 1999).

The previous Assessment reported a slowly declining combined mole fraction of the CFC-114 ($CClF_2CClF_2$) and CFC-114a (CCl_2FCF_3) isomers. This downward trend has continued but at a slower rate than was reported between 2011 and 2012 (**Figure 1-1**, **Table 1-1**; Vollmer et al., 2018). In 2016, the global mean mole fraction of combined CFC-114 and CFC-114a was approximately 16 ppt, and the mole fraction of CFC-114a measured in the CGAA was around 1 ppt. The 2014 Assessment estimated a 10% contribution of CFC-114a to total CFC-114 in the atmosphere. A new study using CGAA samples shows the CFC-114a contribution to total CFC-114 increasing from 4.1% in the late 1970s to 6.5% in the mid-2010s (Laube et al., 2016). The sum of the abundances of the two CFC-114 isomers in the CGAA agree between this and another recently published record of combined-isomer measurements (Laube et al., 2016; Vollmer et al., 2018).

The 2010 and 2014 Assessments found that mole fractions of CFC-115 ($CClF_2CF_3$) had stabilized at approximately 8.4 ppt since around 2000. However, mole fractions have grown since 2012, reaching 8.5 ppt in 2016 (Vollmer et al., 2018). While the magnitude of this change is comparable with the uncertainties on the observations (around 0.1 ppt in 2016), the fact that it is observed at all remote AGAGE stations strongly suggests a renewed global increase (Vollmer et al., 2018).

Since the last Assessment, CFC-112 (CCl_2FCCl_2F), which had a Southern Hemispheric mole fraction of 0.42 ppt in 2016, has continued to decline in the atmosphere, and CFC-112a ($CClF_2CCl_3$) has remained relatively stable at close to 0.07 ppt in the Southern Hemisphere (update to Laube et al., 2014; see **Table 1-1**). In contrast, CFC-113a has continued to increase in the Southern Hemisphere at an accelerated rate since 2012, reaching 0.68 ppt in 2016 (Adcock et al., 2018).

CFC-216ba ($CClF_2CClFCF_3$) and CFC-216ca ($CClF_2CF_2CClF_2$) were measured for the first time in the CGAA (Kloss et al., 2014). The Southern Hemispheric mole fraction of CFC-216ba was found to be relatively constant over the last 20 years at 0.04 ppt. CFC-216ca exhibited a small positive trend, with a mole fraction in the CGAA of 0.02 ppt in 2012.

With respect to their influence on climate, in 2016, CFCs contributed 77% of the total direct radiative forcing due to ODSs regulated under the Montreal Protocol, with a combined radiative forcing of 250 mW m^{-2} (**Figure 1-3**). The radiative forcing due to CFCs has declined by 7% since its peak in 2000, driven primarily by the reduction in abundance of CFC-11 and CFC-12; by 2016 the radiative forcing due to each gas had declined by 9 mW m^{-2} from their respective peaks in 1994 and 2002.

Emissions and Lifetimes

Since the previous Assessment, there has been little new work on CFC lifetimes. Therefore, our lifetimes estimates for these compounds are still based on SPARC (2013), as summarized in **Table A-1**.

Given the global phaseout of the production of CFCs for dispersive uses under the Montreal Protocol, emissions to the atmosphere are now expected to be due only to leakage from banks. These emissions are generally expected to decline with time as the size of the banks decrease, as is reflected in the monotonically decreasing emissions in previous baseline (A1) scenarios of CFC emissions (Harris and Wuebbles et al., 2014). One potential exception was identified in the IPCC/TEAP Special Report: Safeguarding the Ozone Layer and the Global Climate System (Ashford et al., 2005), where a global increase in emissions could coincide with the decommissioning of buildings with foams containing CFCs (primarily CFC-11).

Broadly in line with the expectation of declining emissions from banks, inferred emissions of CFC-12 have continued to fall since the previous Assessment, with 2016 emissions being approximately 35 Gg yr^{-1}, around 20% lower than in 2012, and 93% lower than their peak value in 1988 (**Figure 1-4**). Emissions of CFC-113 have remained at very low levels (<10 Gg yr^{-1}, compared to a maximum of around 243 Gg yr^{-1} in 1988).

The findings, since the previous Assessment, of a slowdown in the rate of decline of CFC-11 and an increase in the IHD suggest an increase in emissions, although changes in atmospheric transport could also play a role (Montzka et al., 2018; Prinn et al., 2018). **Figure 1-4** shows CFC-11 emissions inferred from AGAGE and NOAA data, assuming interannually repeating transport and a global lifetime of 52 years (also shown

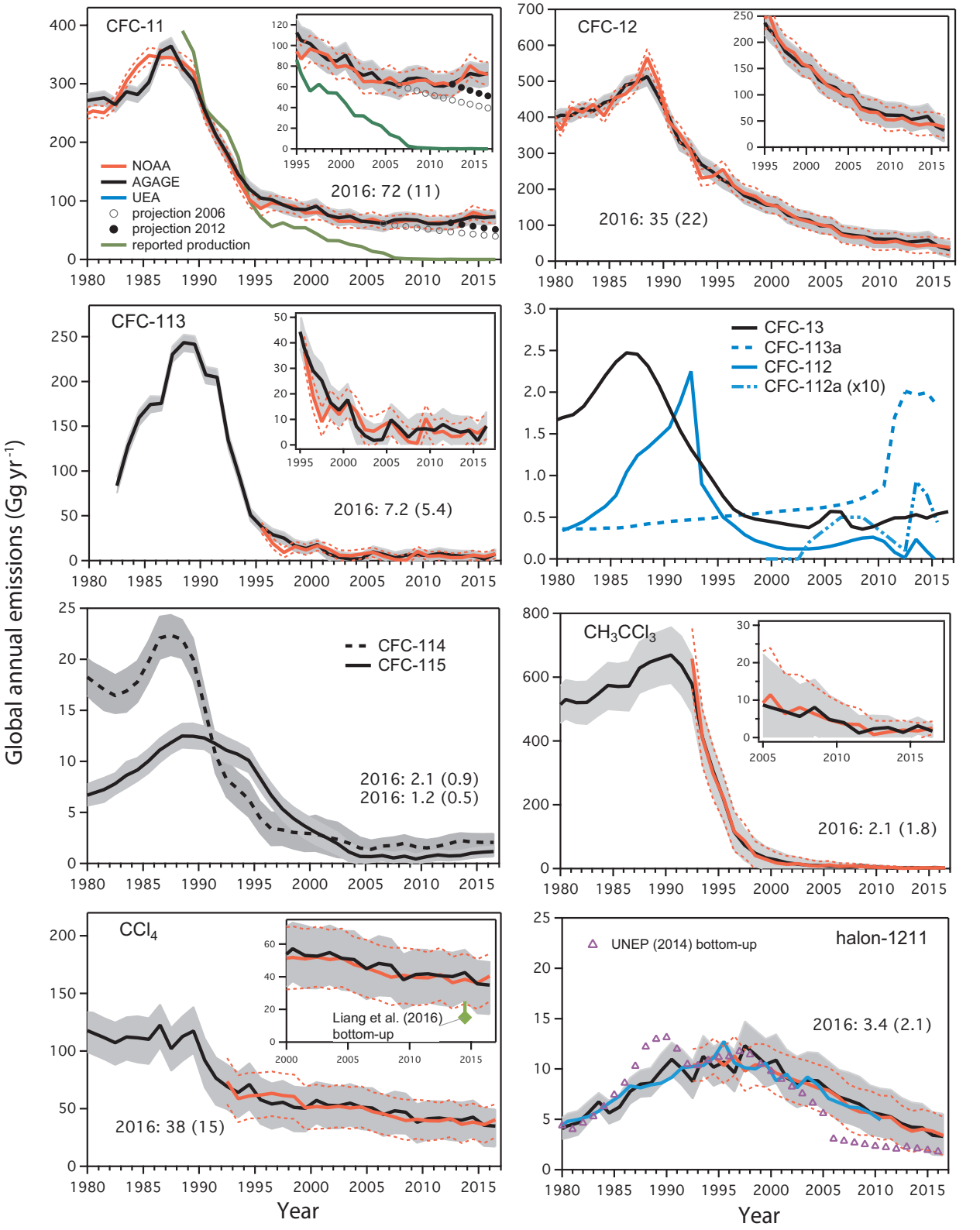
CFC-11
NOAA
AGAGE
UEA
projection 2006
projection 2012
reported production
2016: 72 (11)
CFC-12
2016: 35 (22)
CFC-113
2016: 7.2 (5.4)
CFC-13
CFC-113a
CFC-112
CFC-112a (x10)
CFC-114
CFC-115
2016: 2.1 (0.9)
2016: 1.2 (0.5)
CH3CCl3
2016: 2.1 (1.8)
CCl4
Liang et al. (2016) bottom-up
2016: 38 (15)
UNEP (2014) bottom-up
halon-1211
2016: 3.4 (2.1)
Global annual emissions (Gg yr-1)
Year

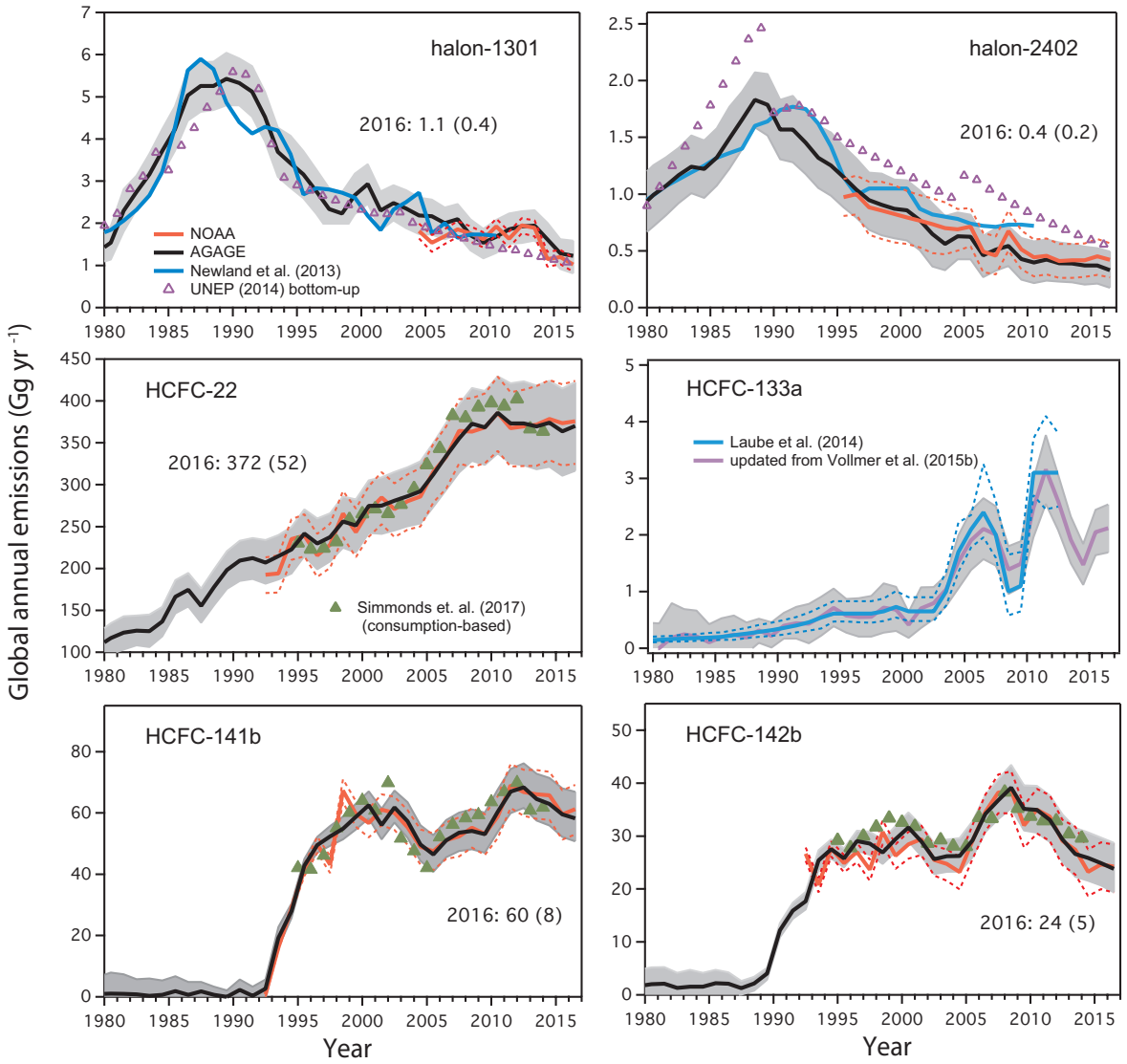

Figure 1-4. Top-down and bottom-up global emission rate estimates (Gg yr^{-1}) for ozone-depleting substances. Top-down emissions rates from AGAGE (black) and NOAA (red) atmospheric data were calculated using a global 12-box model (**Box 1-1;** Cunnold et al., 1983; Rigby et al., 2013). For the CFCs, stratospheric lifetimes were assumed to be equal to the total lifetimes from **Table A-1** (no other losses were assumed). For the halons, lifetimes are summarized in Vollmer et al. (2016). A lifetime of 32 years was used, derived from stratospheric, ocean, and soil lifetimes of CCl_4 (Butler et al., 2016; Rhew and Happell, 2016; SPARC, 2013). For the other species, stratospheric lifetimes from **Table A-1** were imposed, with OH rate constants from Burkholder et al. (2015). Global steady-state lifetimes for each species were: CFC-11 (52 years), CFC-12 (101 years), CFC-13 (640 years), CFC-113 (93 years), combined CFC-114/CFC-114a (189 years), CFC-115 (540 years), halon-1211 (16 years), halon-1301 (72 years), halon-2402 (28 years), HCFC-22 (11.6 years), HCFC-141b (9.2 years), HCFC-142b (17.6 years), and HCFC-133a (4.6 years). For some of these species, small differences can be seen between these global steady-state lifetimes calculated using the 12-box model and those in Appendix **Table A-1**, due to differences in assumed OH and model transport. Emissions were estimated using a Bayesian inverse method, in which the emissions growth rates from bottom-up inventories were used as *a priori* constraints (Rigby et al., 2011; Rigby et al., 2014) with minor update in Vollmer et al. (2018). Descriptions of bottom-up datasets are given in Rigby et al. (2014); Rigby et al. (2013); Simmonds et al. (2017); Vollmer et al. (2016); and

Vollmer et al. (2018). As described in Vollmer et al. (2018), the uncertainty in the *a priori* emissions growth rate was assumed to be 20% of maximum prior emissions. Posterior uncertainties (gray shading for AGAGE and red dashed lines for NOAA) include contributions from the observations, the model, the prior constraint, and the lifetime uncertainties from SPARC (2013), using the method in Rigby et al. (2014). For CFC-11, uncertainties are larger here than presented in the Executive Summary, as the systematic components of the uncertainty (i.e. due to lifetime and calibration scale) are omitted from Figure ES.2. For CFC-112, CFC-112a, CFC-113a, and the halons, emissions were calculated using UEA data from the Southern Hemisphere (blue; Laube et al. 2014). Emissions were calculated from 2013 to 2015 for CFC-112, CFC-112a, and CFC-113a using a 1-box model and scaled to match those reported in Laube et al. (2014) for previous years. HCFC-133a emissions were taken from Vollmer et al. (2015b) and Laube et al. (2014). Uncertainties for CFC-112, CFC-112a, and CFC-113a are not shown for clarity (see Laube et al., 2014). Numerical values of emissions estimates for 2016, shown in some panels, were calculated as the mean of estimates based on AGAGE and NOAA network data, with 1-sigma uncertainties (in parentheses) taken from the AGAGE estimates. For CCl_4, the bottom-up industrial estimate from Liang et al. (2016) is shown as a green diamond in the CCl_4 inset, with the potential magnitude of legacy emissions shown as a green bar extending upwards. Bottom-up estimates for halons (violet triangles) were updated from (UNEP, 2014a). For the major HCFCs, consumption-based estimates from Simmonds et al. (2017) are shown (solid green triangles). These estimates are calculated from reported consumption and estimates of immediate and ongoing release rates that were chosen to be consistent with the top-down emissions estimates.

in Executive Summary Figure ES.2). Following an initial decline after the late 1980s, emissions did not drop substantially after about 2002–2005, with the 2002–2012 average being 66 Gg yr^{-1} or 64 Gg yr^{-1} (using AGAGE or NOAA observations, respectively), which is about 82% lower than the peak in 1987. The inversions then show an increase in emissions beginning around 2013 and reaching an average of 72 or 75 Gg yr^{-1} between 2014 and 2016 (for AGAGE or NOAA data, respectively). This represents a 7 Gg yr^{-1} (or 10%) to 11 Gg yr^{-1} (or 17%) increase in emissions over the 2002 to 2012 average. These emissions are higher overall than the NOAA-data-based estimate of Montzka et al. (2018), who assumed a longer lifetime than the SPARC (2013) estimate used here. However, due to the use of a different inverse modeling approach, they found a slightly larger magnitude of the post-2013 increase, of 13 ± 5 Gg yr^{-1} (25 ± 13%) for 2014–2016 compared to 2002–2012. Considered together, these estimates using AGAGE and NOAA data show an increase in emissions of around 10 Gg yr^{-1} between these two periods. Following the methodology used in previous Assessments and Montzka et al. (2018), two projections were created to examine the expected decline in emissions after 2006 (near the beginning of the period during which emissions did not decline) and 2012 (after which emissions increased) (**Figure 1-4** and Executive Summary Figure ES-2). These projections are based on reported CFC-11 production history, an estimate of the magnitude of the bank for the year 2002 (IPCC/TEAP, 2005), and the assumption of a constant release fraction from the bank following 2006 or 2012. The release fractions used in the projections were estimated as the mean release fractions during the 7-year periods prior to 2006 or 2012 and were based on the yearly inferred bank size and top-down emissions over these periods. The projections indicate that emissions may have been higher than expected since the mid-2000s, although this has only recently become clear given the relatively large uncertainties considered in the past on top-down emissions and on projections. The projections also highlight that the recent emissions increase may be significantly larger than 10 Gg yr^{-1}, when considered relative to the expected emissions decline during this period. Montzka et al. (2018) argue that the recent increase is too large and too rapid to be explained by the release of CFC-11 from its bank, including from the decommissioning of old buildings, given our understanding of the bank size and past release rates. Therefore, they propose that new production is taking place that has not been reported to the UN Environment Ozone Secretariat. This would be inconsistent with the CFC-11 phaseout agreed under

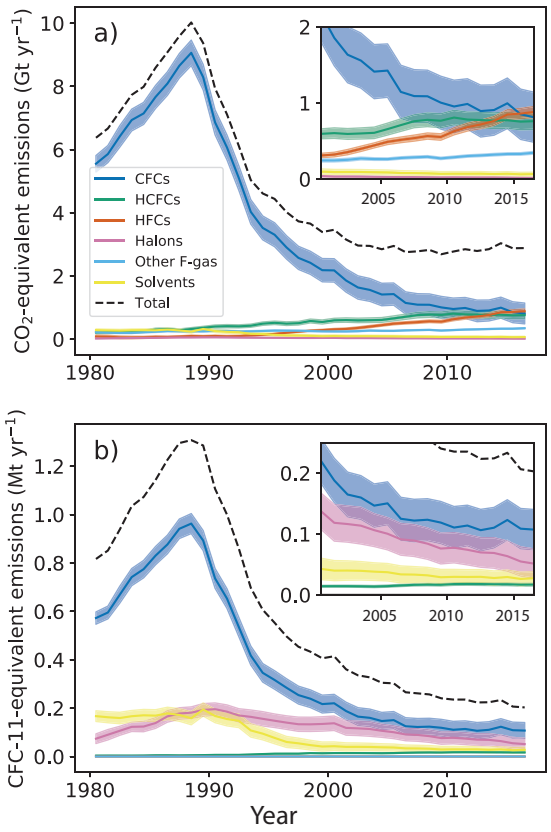

Figure 1-5. (a) 100-year GWP-weighted emissions and (b) ODP-weighted emissions. Emissions are the average of those derived from AGAGE and NOAA data, converted to CO_2-equivalents and CFC-11-equivalents using 100-year time horizon GWPs and ODPs from **Table A-1.** Species are grouped into CFCs, HCFCs, HFCs (see **Chapter 2**), halons, solvents (CCl_4 and CH_3CCl_3), and other F-gases (SF_6, CF_4, C_2F_6, C_3F_8, NF_3, SO_2F_2, see **Section 1.5**). Totals are shown as dashed black lines and shading indicates the 1-sigma uncertainty.

the Montreal Protocol. If the new emissions are associated with uses that substantially increase the size of the CFC-11 bank, further emissions resulting from this new production would be expected in future. The recent increase in emissions and any associated future emissions will delay the expected rate of recovery of stratospheric ozone relative to previous projections.

Inferred emissions of the lower-abundance compound CFC-13 show a strong decline in the first decade following a maximum in emissions in the late 1980s of 2.5 Gg yr^{-1} (Vollmer et al., 2018). However, for the last decade, emissions have plateaued at around 0.5 Gg yr^{-1} (approximately 85% lower than their peak value). CFC-13 was used primarily in refrigeration; the size of the CFC-13 bank and rate of release from it were expected to continue to decline with time.

Emissions of the combined CFC-114/CFC-114a isomers have plateaued for at least the last decade, at 1.9 Gg yr^{-1}, which is about 10% of the maximum value, reached in the late 1980s (Vollmer et al., 2018). Based on a study that can separate the two isomers (Laube et al., 2016), stagnant emissions were found for CFC-114 (1.8 Gg yr^{-1}; data through 2014), while those of the minor CFC-114a isomer have slightly declined. This indicates that the sources of the two isomers are, at least in part, decoupled. Laube et al. (2016) speculated that emissions of CFC-114a could be linked to the production of HFC-125 and HFC-143a.

Global emissions of CFC-113a increased strongly between 2009 and 2012 and since then have remained at approximately 1.7 Gg yr^{-1} (Adcock et al., 2018). This is opposite to the trend exhibited by the major isomer CFC-113 and, similar to the relative changes in CFC-114 and CFC-114a, indicates that the two isomers may have some different sources.

Emissions of CFC-115 appear to have increased since the previous Assessment, with Vollmer et al. (2018) reporting mean emissions for 2015–2016 of 1.14 ± 0.5 Gg yr^{-1}, which is approximately double that of the period 2007–2010, when emissions were at a minimum (**Figure 1-4**). Recent emissions are around 5–10% of the maximum, found in the late 1980s. While some CFC-115 was found as an impurity in samples of the refrigerant HFC-125 (CHF_2CF_3), this was not thought to be significant enough of a source to explain global emissions. Therefore, the cause of this emissions increase is unknown.

Several regional studies have examined CFC emissions using atmospheric observations. Between 2008 and 2014, emissions within the USA of the three major CFCs (CFC-11, CFC-12, and CFC-113) were estimated to have declined (L. Hu et al., 2017). These results suggest that the USA is unlikely to be the

Box 1-1. Inferring Emissions Using Atmospheric Data

In this Assessment, as in previous reports, emissions of ODSs (and of HFCs in Chapter 2) are inferred using atmospheric observations and a model of atmospheric transport and chemistry. Here, we describe the principle considerations behind these "top-down," or "inverse," calculations. An overview of the various methods for estimating ODS emissions can be found in Montzka and Reimann et al. (2010).

If we assume that the atmosphere consists of a single box into which trace gases are emitted, and within which some loss takes place, mass balance considerations allow the rate of change in the burden (B, the total mass of the gas in the atmosphere) to be written as:

$$\frac{dB}{dt} = Q - \frac{B}{\tau}$$

Here, Q is the globally integrated emission rate (in mass per unit time) and τ is the overall lifetime of the gas in the atmosphere. The latter is determined by a variety of sinks such as photolysis (e.g., in the stratosphere), reaction with oxidants (e.g., the hydroxyl radical), and loss at the surface (e.g., to soils or the ocean). The previous Assessment discussed how the lifetimes from these different processes can be combined to calculate overall lifetimes.

For long-lived gases ($\tau \geq 0.5$yr) that are relatively well mixed throughout the atmosphere, surface mole fraction data from global networks such AGAGE and NOAA provide estimates of the trace gas global burden and its rate of change.

For the majority of gases in this chapter, the magnitudes of the global lifetimes are relatively well known, compared to uncertainties in bottom-up emissions estimates. These lifetimes estimates, primarily taken from the SPARC Lifetimes assessment (SPARC, 2013), are based on a combination of satellite observations, in situ measurements of tracer-tracer correlations, photochemical model simulations, and estimates of oceanic and terrestrial fluxes, which are independent of the observations used to infer emissions in this chapter. However, it should be noted that SPARC (2013) also included lifetimes estimates inferred using AGAGE and NOAA observations for some species, which leads to some circularity if used to infer emissions.

We can rearrange Equation 1 to infer global emissions rates (Q) from the information on the global burden (B) and its trend (dB/dt) and estimates of the global lifetime (τ). Such emissions estimates are sensitive to uncertainties in the observed burden (e.g., random and representation errors in the observations and systematic calibration scale errors) and uncertainties in the lifetime, both of which should be propagated through to the uncertainties in the inferred emissions (e.g. Rigby et al., 2014).

While this discussion illustrates the broad principles behind the inference of emissions at the global scale, some additional factors are introduced in the calculations presented in this chapter. Firstly, a model of atmospheric transport and chemistry is used to simulate the nonuniform distribution of gases in the atmosphere, improving our estimates of the global burden compared to the single-box approach above. The model primarily used in this chapter is the AGAGE 12-box model, which separates the atmosphere into boxes with latitudinal boundaries at 90°N, 30°N, 0°N, 30°S, and 90°S, and vertical boundaries at 1000 hPa, 500 hPa, 200 hPa and 0 hPa (Cunnold et al., 1994; Cunnold et al., 1983; Rigby et al., 2013). Transport of each gas occurs via parameterized mixing and advection between boxes. Removal from the atmosphere takes place via reaction with the hydroxyl radical, via first-order processes parameterizing non-OH photochemical losses and via loss to the ocean or land. This model was designed to simulate baseline mole fractions (i.e.,

Box 1-1, continued.

observations that have not been strongly influenced by nearby sources and can be considered representative of zonal averages) for long-lived gases that have small spatial gradients in the atmosphere. However, for shorter-lived substances, which exhibit strong spatial and temporal variability, atmospheric distributions may be more poorly represented. Secondly, a Bayesian statistical approach is employed that allows prior beliefs about emissions to be incorporated into the inversion and provides a framework for propagating prior and observational uncertainty through to the derived emissions estimates (e.g., see the supplementary materials in Rigby et al., 2014).

Regional emissions estimates are possible where spatially and/or temporally dense measurements are made within or downwind of certain areas (e.g., Graziosi et al., 2015; L. Hu et al., 2017). The regional approach requires a model that can simulate the three-dimensional atmospheric transport of a gas from the source to the measurement points. Such simulations can then be compared to the data and fluxes at regional and national scales inferred through examination of the difference between the two. In contrast to global estimates, for long-lived compounds, regional flux inversions are insensitive to uncertainties in the atmospheric lifetime. However, significant uncertainties can arise through the need to accurately simulate trace gas transport at high resolution.

source of the increase in global CFC-11 emissions that started in 2013. In aggregate, the emissions of these gases agreed well with bottom-up estimates by the US Environmental Protection Agency (EPA). However, species-specific differences were found, particularly for CFC-113. Where the emissions inventory had predicted negligible emissions since 1996, emissions inferred from atmospheric concentrations were statistically higher than zero (by around 0.5–3 Gg yr^{-1}) until 2013. While regional inverse modeling of CFC-11 emissions from eastern Asia has not yet been carried out, Montzka et al. (2018) note increased variability in CFC-11 measured at Mauna Loa, Hawai'i, beginning after 2012, along with emerging correlations with other anthropogenic species during the autumn months, when this site is strongly influenced by flows from eastern Asia. These signals are consistent with an increase in CFC-11 emissions from eastern Asia. Regional inverse modeling using data from the Gosan Station, South Korea, showed evidence of emissions of combined CFC-114/CFC-114a and CFC-115 from China (Vollmer et al., 2018). The inferred emissions for each of these gases were of a magnitude that was a significant fraction of the respective global total. Persistent sources of CFC-113a and CFC-114a from eastern Asia were also identified (Adcock et al., 2018; Laube et al., 2016).

In summary, while emissions of almost all CFCs have declined substantially since their peaks in the 1980s or 1990s, and emissions of CFC-12 and -113 continue to decline, there are strong indications that emissions of several CFCs are no longer following the downward trajectory expected under a scenario of globally depleting banks. Most important, CFC-11 emissions have increased by around 10 Gg yr^{-1} for 2014–2016, relative to 2002–2012. A study into these CFC-11 trends proposes that new production not reported to the UN Environment Ozone Secretariat may be taking place and that at least some of the new emissions originate from eastern Asia (Montzka et al., 2018). Regional studies find evidence for continuing or increasing emissions of some of the more minor CFCs from eastern Asia (Vollmer et al., 2018).

In terms of both CO_2- and CFC-11-equivalents, inferred combined emissions of all CFCs have declined markedly since the late 1980s (**Figure 1-5**). In 2016, CO_2-equivalent emissions of the CFCs were 0.8 ± 0.3 Gt yr^{-1}, approximately 90% lower than the highest inferred value of 9.1 ± 0.4 Gt yr^{-1} in 1988. If the recent change in the CFC-11 growth rate is due to emissions alone, the increase since 2013 has added around 0.05 Gt yr^{-1} CO_2-equivalent to this total. Total ODP-weighted emissions for all CFCs dropped by around 90% since the peak (in 1987) and reached 110 ± 30 Gg yr^{-1} CFC-11-equivalent in 2016.

1.2.2 Halons

Observations of Atmospheric Abundance

Halon-1211 ($CBrClF_2$), halon-2402 ($CBrF_2CBrF_2$), and halon-1202 (CBr_2F_2) abundances continued to decline from their peak values, observed in the early and mid-2000s. Global surface mean mole fractions of approximately 3.5 ppt and 0.42 ppt were observed for halon-1211 and -2402, respectively, in 2016, and Southern Hemispheric mole fractions of approximately 0.014 ppt were recorded for halon-1202 (**Table 1-1**, **Figure 1-1**) (Newland et al., 2013; Vollmer et al., 2016). Halon-1301 (CF_3Br) growth rates, which were reported as being positive in the previous Assessment, declined to <0.01 ppt yr^{-1} in 2016, when a global mean mole fraction of 3.36 ppt or 3.25 ppt was reached for AGAGE and NOAA, respectively.

New measurements of halon-2311 ($CF_3CHClBr$, halothane, an anesthetic that is no longer widely used) show low abundances in the atmosphere with a mole fraction that declined from 0.025 ppt in 2000 to <0.01 ppt in 2016 in the Northern Hemisphere (update of Vollmer et al., 2015c).

The direct contribution of halons to global radiative forcing was small, 2.2 mW m^{-2} in 2016, equivalent to 0.9% of the radiative forcing of CFCs (**Figure 1-3**). When their influence on ozone depletion is also considered, radiative forcing due to halons is negative (Daniel et al., 1995).

Emissions and Lifetimes

Lifetimes of the three most abundant halons are taken from SPARC (2013), and are summarized in **Table A-1.** For these three halons, emissions derived from observations generally agree within their uncertainties for the estimates made from NOAA, AGAGE, and UEA measurements (**Figure 1-4;** Vollmer et al., 2016; Newland et al., 2013). For each gas, these emissions have continued to decline since the previous Assessment. Bottom-up emissions were revised in 2014 by the Halon Technical Options Committee (HTOC), and updates are provided here (UNEP, 2014a).

Top-down estimates of emissions of halon-1211 show a decline to 3.4 ± 2.1 Gg yr^{-1} in 2016 (average of emissions inferred from AGAGE and NOAA data), 70% lower than the peak value in 1998. Compared to previous bottom-up estimates (UNEP, 2011), the most recent HTOC emissions for this species have been revised downward for the last decade, creating a larger gap (~50%) with the observation-based values. In contrast, for halon-1301, bottom-up and observation-based emissions now show closer agreement than in the previous Assessment, with top-down values for 2016 of 1.1 ± 0.4 Gg yr^{-1} and HTOC estimates of 1.1 Gg yr^{-1}. The 2016 top-down values are 80% lower than their peak of 5.4 ± 0.6 in 1989. Halon-2402 bottom-up emissions are now available for a longer time period than in the previous Assessment and are significantly larger than previously estimated (UNEP, 2014a). They show a similar trend to emissions inferred from observations, which grew until 1988 and then declined. However, the HTOC estimates were larger throughout, at 0.56 Gg yr^{-1} in 2016, compared to top-down estimates of 0.37 ± 0.2 Gg yr^{-1}; these are 80% lower than their peak value.

Global emissions of the lower-abundance halon-2311 inferred from atmospheric observations declined from 0.49 Gg yr^{-1} in 2000 to 0.25 Gg yr^{-1} in 2014, likely reflecting a continuing reduction of its use as an anesthetic (Vollmer et al., 2015c).

Total CO_2-equivalent halon emissions were small in 2016, 2% that of CFCs, as shown in **Figure 1-5**. However, due to their high ODPs (**Table A-1**), their contribution to ozone depletion remains significant, with ODP-weighted emissions of 50 ± 20 Gg yr^{-1} CFC-11-equivalent in 2016, just under half that of global CFC emissions.

1.2.3 Carbon Tetrachloride (CCl_4)

Observations of Atmospheric Abundance

Carbon tetrachloride (CCl_4) has continued to decline at a rate similar to that reported in the previous Assessment. AGAGE observations showed a decline of 1.5% between 2015 and 2016, with a mole fraction of 79.9 ppt in 2016, and NOAA reported a decline of 1.2% during the same period and a 2016 mole fraction of 81.2 ppt (**Table 1-1**, **Figure 1-1**). These differences are broadly consistent with known calibration scale differences, although the level of agreement has changed over time, suggesting some drift in one or both scales or time-dependent analytical issues. Data from UCI show a smaller decline, of 0.3%, between

these years and a 2016 mole fraction of 81.9 ppt. The IHD, estimated from AGAGE and NOAA networks, has exhibited a gradual decline since 2000, with a rate of 0.04 and 0.03 ppt yr^{-1}, respectively, for each network.

Ground-based remote sensing observations of CCl_4 from Jungfraujoch show a slightly lower rate of decline between 2010 and 2016 than the AGAGE and NOAA networks, although the uncertainties overlap at the 2-sigma level (**Table 1-2**). New observations with global coverage in the upper troposphere and lower stratosphere have become available from the MIPAS instrument, onboard the Envisat satellite (Eckert et al., 2017; Valeri et al., 2017). The upper-tropospheric trends derived from these observations between 2002 and 2012 confirm that atmospheric mole fractions declined during this period with a magnitude that was broadly consistent with the ground-based measurements (Valeri et al., 2017). However, stratospheric trends derived from these observations were found to be nonuniform, with some (generally non-statistically significant) positive trends even being found in the middle stratosphere in the Southern Hemisphere (Eckert et al., 2017). This high variability, compared to surface data, reflects the additional impact of variability in transport on the temporal evolution of trace gases in the stratosphere.

Radiative forcing due to CCl_4 declined to 14 mW m^{-2} in 2016, equivalent to 6% of the radiative forcing due to CFCs (**Figure 1-3**).

Emissions and Lifetime

Previous Assessments highlighted a significant discrepancy between CCl_4 trends observed in atmospheric data and those calculated from known sources and our understanding of atmospheric sinks (Carpenter and Reimann et al., 2014; Montzka and Reimann et al., 2010). In the previous Assessment, the best estimate of the CCl_4 lifetime was 26 years, which led to a top-down global emissions estimate of 57 (40–74) Gg yr^{-1}. In contrast, bottom-up estimates of emissions due to feedstock use, based on the difference between reported production and destruction (Montzka and Reimann et al., 2010), were less than 4 Gg yr^{-1} in 2012 (Carpenter and Reimann et al., 2014). In light of these discrepancies, the CCl_4 budget was re-examined in the 2016 SPARC Report on the Mystery of Carbon Tetrachloride (Liang et al., 2016). Here we summarize the primary findings of this report, along with additional studies that have been carried out in the interim period.

The global lifetime of CCl_4 has been revised upward from 26 years, initially to 33 (28–41) years in Liang et al. (2016), primarily due to an increase in the estimated lifetime due to ocean loss and uptake from soils. This has subsequently been reduced slightly to 32 (26–43) years, following a revision to the lifetime with respect to ocean loss, the best estimate for which is now 183 (147–241) years (Butler et al., 2016). The current best estimate for the lifetime due to soil uptake is 375 (228–536) years, which has increased from the previously estimated 195 years (Rhew and Happell, 2016). Estimates of the lifetime due to stratospheric loss remained unchanged at 44 (36–58) years (SPARC, 2013). Of these sinks, the remaining uncertainties in the ocean uptake were found to have the potential to most significantly alter model estimates of the atmospheric trend (Chipperfield et al., 2016).

Global emissions, derived from atmospheric trends and a model parameterized with a 33-year lifetime, were reduced to 40 ± 15 Gg yr^{-1} (2007–2014 average) in Liang et al. (2016), compared to 57 ± 17 Gg yr^{-1} in the previous Assessment (2011–2012 average). Estimates based on the observed atmospheric IHD were found to be similar to the trend-based estimate, at 30 ± 5 Gg yr^{-1} (2010–2014 average; update of Liang et al., 2014b). Updated estimates (**Figure 1-4**), using the new lifetime of 32 years and AGAGE and NOAA observations, show a relatively rapid drop in emissions in the late-1980s and early-1990s, then a relatively slow decline since the late-1990s. Since 2000, emissions have been declining at a rate of ~1.2 Gg yr^{-1} per year (**Figure 1-4**). Emissions inferred here for 2016 from the AGAGE and NOAA data, respectively, were 35 ± 16 Gg yr^{-1} and 40 ± 15 Gg yr^{-1} (around 30% of the peak value, which occurred in the mid-to-late 1980s).

Since the previous Assessment, global bottom-up estimates have been made of emissions from a range of industrial sources. Liang et al. (2016) and Sherry et al. (2017) proposed that 13 Gg yr^{-1} may be due to unreported, non-feedstock emissions from chloromethane and perchloroethylene production plants. In addition, unreported, inadvertent emissions during chlorine production (e.g., from chlor-alkali plants) and usage (e.g., in industrial and domestic bleaching) and legacy

emissions from landfills and contaminated soil were estimated to contribute up to 10 Gg yr^{-1} (which is towards the lower end of estimates previously made by Fraser et al. (2014)). Similar to previous Assessments, 2 Gg yr^{-1} fugitive emissions from feedstock usage were estimated (e.g., in the production of HFCs and other compounds). Together, these sources could total around 25 Gg yr^{-1}.

Regional studies of CCl_4 emissions have been carried out for the USA, Europe, and East Asia. NOAA observations across the USA were used to infer fluxes of 4.0 (2.0–6.5) Gg yr^{-1} from 2008 to 2012 (L. Hu et al., 2016a), a value two orders of magnitude larger than reported by the US Environmental Protection Agency (EPA) and around 10% of the global top-down value estimated here during the same period. The spatial distribution of emissions derived for the USA was found to be more consistent with the location of industrial sources in the EPA reports (e.g., chlor-alkali plants) than other potential sources that would be more widely distributed (e.g., uncapped landfill). This suggests that emissions may be underreported for these industries. Similarly, using European AGAGE data, Graziosi et al. (2016) found that the spatial distribution of emissions in Europe was similar to that of industrial sources in the European Pollutant Release and Transfer Register and the location of chlor-alkali plants. Also in common with the USA, these top-down emissions estimates are significantly larger than the bottom-up reports. The top-down mean European emission rate was estimated to be 2.2 ± 0.8 Gg yr^{-1} from 2006 to 2014 (around 5% of the global mean estimated here during the same period), declining at an average rate of 6.9% yr^{-1}. Bottom-up estimates for China showed an increase in emissions during the 1990s, which reached a peak in 2002 of 14.0 (9.1–19.5) Gg yr^{-1} (Bie et al., 2017). This was followed by a decline to 5.2 (2.4–8.8) Gg yr^{-1} in 2014, with the sharpest drop occurring between 2009 and 2011. It was proposed that this decrease was primarily due to a reduction in CCl_4 use as a process agent. Top-down estimates for China from late 2006 to early 2008 by Vollmer et al. (2009) are consistent with these bottom-up values, within uncertainties (15 (10–22) Gg yr^{-1}). However, the subsequent decline estimated by Bie et al. (2017) has not yet been confirmed by atmospheric observations at the national scale. The sum of the available regional top-down studies suggests emissions of around 20 Gg yr^{-1}, although it should be emphasized that these studies cover different time periods and that this cannot be considered a global total, as several potentially important regions are not observed by the current monitoring network (e.g., India, Russia, Africa, and South America).

In summary, the upward revision of the atmospheric lifetime and the proposal of significant emissions from sources such as chloromethane, perchloroethylene, and chlor-alkali plants have substantially reduced the gap in the CCl_4 budget since the previous Assessment. Regional inverse modeling studies in the USA and Europe support the idea that reported emissions are significantly underestimated and that industrial sources could be much larger than previously thought. However, there remains a difference of around 10 Gg yr^{-1} between the global top-down estimate, based on our updated knowledge of the sinks, and recent global bottom-up estimates.

CO_2-equivalent CCl_4 emissions were relatively small in 2016, 8% that of the CFCs (**Figure 1-5**). However, ODP-weighted emissions were significant, at 27 ± 10 Gg yr^{-1} in 2016, 23% as large as the CFCs.

1.2.4 Methyl Chloroform (CH_3CCl_3)

Observations of Atmospheric Abundance

The global mean mole fraction of methyl chloroform (1,1,1-trichloroethane, CH_3CCl_3) continued to decline between 2012 and 2016, decreasing to 2.6 ± 0.7 ppt in 2016, 2% of its maximum value of 133 ± 4 ppt, which was reached in 1992 (**Figure 1-1**, **Table 1-1**). The IHD reached a maximum in 1990 (28 ppt) and has since declined to 0.078 ppt in 2016. The radiative forcing due to methyl chloroform is now negligible (**Figure 1-3**).

Emissions and Lifetime

Assuming a constant CH_3CCl_3 global lifetime of 5.0 years (SPARC, 2013), we infer emissions that have continued to decline since 2012 (**Figure 1-1**, **Table 1-1**), with mean values of 1.7 and 2.5 Gg yr^{-1} in 2016 (AGAGE and NOAA, respectively); the emissions are not statistically different from zero at the 1-sigma level. Using global box models, non-zero emissions have been inferred for up to at least 2014 (Rigby et

al., 2017; Turner et al., 2017), with estimated global emissions in the range of 0.5 to 2 Gg yr^{-1} in 2014. Observations of above-baseline mole fractions at one AGAGE station (Scripps Institution of Oceanography, La Jolla, California, USA) confirm the continued release of CH_3CCl_3 near this location until at least 2014 (Rigby et al., 2017). Above-baseline events were also found up until 2012 at Monte Cimone, Italy, and Jungfraujoch, Switzerland, with inferred emissions in Europe declining from around 1.1 Gg yr^{-1} in 2002 to 0.2 Gg yr^{-1} in 2012 (Maione et al., 2014).

Rigby et al. (2017) and Turner et al. (2017) used methyl chloroform observations from AGAGE and NOAA to infer changes in tropospheric hydroxyl radical (OH) concentrations, the primary sink for CH_3CCl_3, between the 1980s and the mid-2000s. They both found maximum likelihood tropospheric concentrations of OH that increased during the late 1990s and early 2000s and fell afterwards. However, both studies noted that the uncertainty in these inferred changes was large, such that a solution with no OH variability (and therefore no change in CH_3CCl_3 lifetime) was also possible. Rigby et al. (2017) inferred a global mean OH concentration that was 5–10% higher than was estimated in Rigby et al. (2013) and SPARC (2013), suggesting that the CH_3CCl_3 lifetime (and that of many other compounds whose primary sink is OH) may be shorter than the SPARC estimate, although their uncertainties suggest that this difference is not statistically significant.

The influence of CH_3CCl_3 emissions on climate and ozone depletion is now very small (**Figure 1-5**). In 2016, 100-year-GWP-weighted emissions were 0.3 ± 0.3 Mt yr^{-1} (0.04% as large as the CFCs), and ODP-weighted emissions were 0.3 ± 0.3 Gg yr^{-1} (0.3% as large as the CFCs).

1.2.5 Hydrochlorofluorocarbons (HCFCs)

Observations of Atmospheric Abundance

The global surface mean mole fraction of the most abundant HCFC, HCFC-22 ($CHClF_2$), has continued to increase since the previous Assessment and was around 237 ppt in 2016 (**Figure 1-1**, **Table 1-1**). However, its growth rate has declined relative to previous years (**Figure 1-1**) and is now comparable to the growth rate observed in the early 2000s. Growth rates of the less abundant HCFCs—HCFC-141b (CH_3CCl_2F) and HCFC-142b (CH_3CClF_2)—have declined substantially since 2012 (**Figure 1-1**). Global mean mole fractions of these two gases were about 24.5 ppt and 22 ppt in 2016, respectively. Abundances of all three HCFCs have grown more slowly than projected in the previous Assessment, with 2016 mole fractions being about 7.5%, 4.5%, and 8% lower than the A1-2014 scenario for HCFC-22, HCFC-141b, and HCFC-142b, respectively. This scenario assumed that after 2012, all Article 5 countries would continue producing HCFCs at the maximum level allowed under the Montreal Protocol.

Recent trends of HCFC-22 and HCFC-142b are compared between surface in situ (including grab samples) and ground-based total column remote sensing methods (**Table 1-2**). Trends calculated during the period 2010–2016 are similar for the two methods for HCFC-22 but do not agree for HCFC-142b. For HCFC-142b, the remote sensing observations show a trend that is not statistically different from zero, while in situ observations show a small positive (1% yr^{-1}) trend.

Upper tropospheric trends based on global satellite observations of HCFC-22 from MIPAS agree with surface trends measured by AGAGE and NOAA networks for the period from 2005 to 2012 (Chirkov et al., 2016). Stratospheric trends determined from satellite data largely reflect tropospheric trends but with additional variability, possibly caused by variability in stratospheric circulation.

HCFC-133a (CH_2ClCF_3), which is an intermediate in HFC-125, HFC-134a, and HFC-143a production, has increased only slightly since 2012, and its abundance remains less than 1 ppt. HCFC-31 (CH_2ClF), a relatively short-lived compound with an atmospheric lifetime of 1.2 years, is an intermediate in the synthesis of HFC-32 (CH_2F_2) and was first reported by Schoenenberger et al. (2015). It was found to be present in the Northern Hemisphere at 0.17 ppt in 2011, and updates to these measurements have shown a decline to 0.11 ppt in 2016. The compound HCFC-225ca ($CF_3CF_2CHCl_2$), which was used as a drop-in replacement for CFC-113, has been measured in the CGAA since the previous Assessment (Kloss et al., 2014). It appeared in the observational record in the early 1990s, and its abundance peaked at 0.05 ppt in

2001, after which it declined to 0.02 ppt in 2012.

The radiative forcing due to HCFCs reached 58 mW m^{-2} in 2016 (**Figure 1-3**), which is comparable to that of CFC-11 (60 mW m^{-2}) and 23% as large as total CFC radiative forcing. The major contributor to total HCFC radiative forcing was HCFC-22, which was responsible for 50 mW m^{-2} in 2016.

Emissions and Lifetimes

Lifetimes of the major of HCFCs have not been significantly updated since (SPARC, 2013), the values from which are used here (**Table A-1**).

Emissions of HCFC-22 inferred from atmospheric observations have remained relatively constant at ~370 Gg yr^{-1} since 2012 (**Figure 1-4**), while emissions of HCFC-141b and HCFC-142b have declined by approximately 10 Gg yr^{-1} (~10%) and 6 Gg yr^{-1} (~18%), respectively, between 2012 and 2016, reaching values of around 60 Gg yr^{-1} and 24 Gg yr^{-1} in 2016. For all three of these gases, the top-down emissions trends generally agree with consumption-based estimates (Simmonds et al., 2017) (**Figure 1-4**).

Emissions of HCFCs as a whole, expressed as CO_2-equivalent, have declined since the previous Assessment (**Figure 1-5**). This is contrary to the projected increase in emissions in the A1 scenarios, which were based on the assumption that Article 5 countries would produce the maximum amount of HCFCs allowed under the Montreal Protocol (Harris and Wuebbles et al., 2014; Simmonds et al., 2017). This emissions decrease is consistent with a sharp drop in reported HCFC consumption after 2012, particularly in Article 5 countries. By 2016, reported HCFC consumption in Article 5 countries declined by 30% compared to the 2008–2012 average (UNEP, 2017). These recent changes suggest that the 2007 adjustment to the Montreal Protocol has been highly effective in limiting emissions of these gases (Montzka et al., 2015; Simmonds et al., 2017).

Emissions trends have been inferred for some of the more minor HCFCs. Emissions of HCFC-124 ($CHClFCF_3$) have declined from ~7 Gg yr^{-1} in 2003 to ~3.5 Gg yr^{-1} in 2015 (Simmonds et al., 2017). Emissions of HCFC-133a (**Figure 1-4**), which had been reported as increasing prior to the previous Assessment (Laube et al., 2014), were found to suddenly decline after reaching a peak of 3 Gg yr^{-1} in 2011 and were at 1.5 Gg in 2014 (Vollmer et al., 2015b). As this compound is thought to be an intermediate during the manufacture of HFC-134a, HFC-143a, and HFC-125, this reduction may be related to better containment during production of these HFCs (Vollmer et al., 2015b). However, the trend appears to have reversed again after 2014. (**Figure 1-4**). Emissions of the compound HCFC-31 were recently inferred for the first time from atmospheric observations (Schoenenberger et al., 2015). Emissions were found to increase from 2000 to 2011, reaching 0.9 (0.7–1.0) Mg yr^{-1}, before declining until the last available measurements in 2014. The reasons for the decline are unknown but may be related to changes in HFC-32 production methods. Emissions of HCFC-225ca were inferred to increase between 1992 and 1999, reaching 1.5 Gg yr^{-1} before declining to 0.5 Gg yr^{-1} in 2011 (Kloss et al., 2014). This trend was thought to be consistent with an increase due to its use as a CFC replacement, then subsequent phasedown due to controls on HCFCs.

Regional emissions estimates using atmospheric observations indicate substantial declines in HCFC-22 and HCFC-142b emissions in the USA and HCFC-22 emissions in Europe, as would be expected from the phasedown schedule for non–Article 5 countries (**Figure 1-6**) (Graziosi et al., 2015; Hu et al., 2017). However, in both regions, significant differences with the bottom-up estimates were found, perhaps indicating incomplete or inaccurate reporting and assumptions relating to release rates and/or atmospheric modeling uncertainties. Because the phaseout of HCFCs in Article 5 countries is delayed compared to non–Article 5 countries (e.g., the USA and European countries), recent emissions estimates using bottom-up methods suggest a continued increase of HCFC-22, HCFC-141b, and HCFC-142b emissions from China since the 1990s (**Figure 1-6**) (Han et al., 2014; Li et al., 2016; Wang et al., 2015b). A number of observation-based estimates are generally consistent with these bottom-up estimates (Fang et al., 2012; Li et al., 2011; Liu et al., 2015; Stohl et al., 2010; Stohl et al., 2009; Vollmer et al., 2009; Wang et al., 2014; Yokouchi et al., 2006).

In terms of CO_2-equivalent emissions, HCFCs were comparable to the CFCs (and HFCs; **Chapter 2**) in 2016, at 0.8 ± 0.1 Gt CO_2 yr^{-1} (**Figure 1-5**). The major

contributor to this total was HCFC-22, with emissions of 0.7 ± 0.1 Gt yr^{-1} CO_2-equivalent in 2016. CO_2-equivalent emissions due to all HCFCs peaked in 2010 and then declined 6% by 2016. When weighted by their ODPs, emissions of HCFCs were relatively small in 2016, at 17 ± 2 Gg yr^{-1}, 16% as large as the CFCs. ODP-weighted emissions reached a maximum in 2011 and have declined by 6% since.

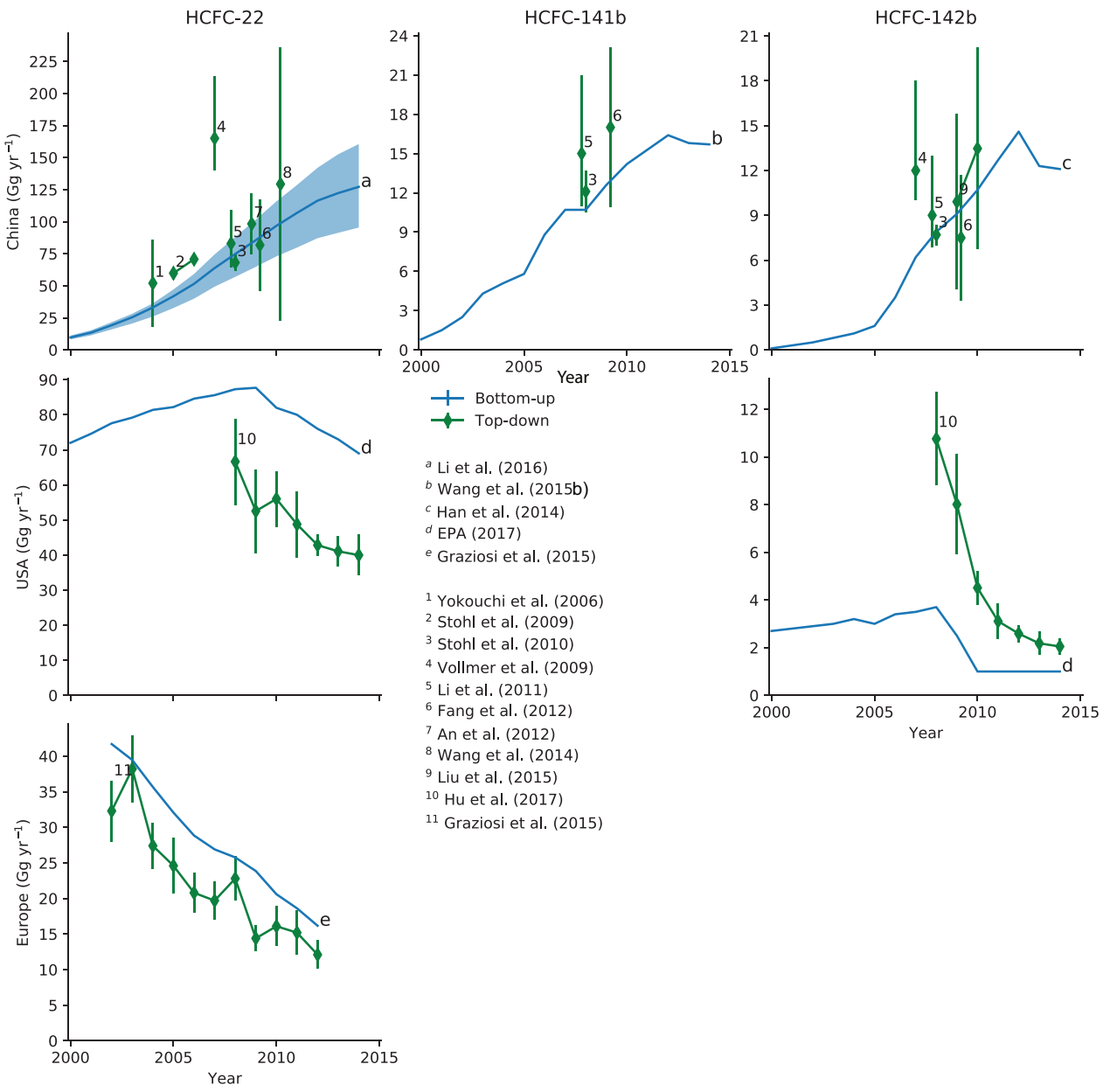

Figure 1-6. Regional emissions estimates of (*left to right*) HCFC-22, HCFC-141b, and HCFC-142b from (*top to bottom*) China, USA, and Europe. Bottom-up estimates are shown as solid blue lines with shading indicating uncertainty (where available). Top-down estimates from a variety of studies and 1-sigma uncertainties are shown in green.

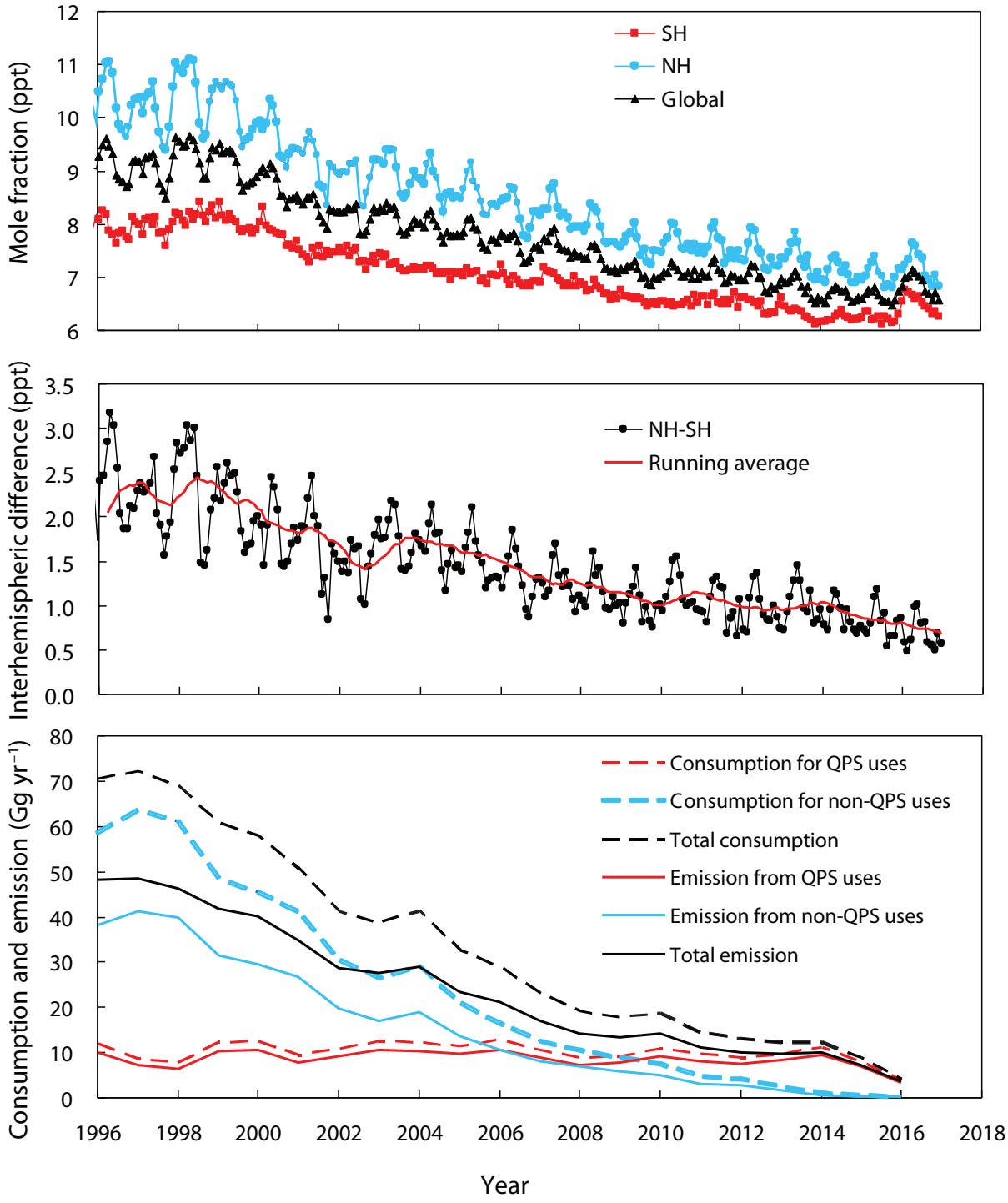

Figure 1-7. *Upper panel:* Trends in methyl bromide monthly mean mole fractions for the NH (blue), SH (red), and globe (black) from NOAA data (Montzka et al., 2003, updated). *Middle panel*: Interhemispheric difference (NH–SH) as monthly means (black) and as a 12-month running average (red). *Lower panel*: Consumption (dashed lines) as reported in the UNEP database (UNEP, 2017), for non-QPS uses (blue) and QPS uses (red), and emissions (solid lines) from non-QPS uses (blue) and QPS uses (red). Total consumption and emissions are shown as black dashed and solid lines, respectively. Soil fumigation emission rates are estimated as 65% of reported consumption (UNEP, 2006) and QPS emission rates are estimated as 84% of reported consumption (UNEP, 2006).

1.2.6 Methyl Chloride (CH_3Cl)

Observations of Atmospheric Abundance

Methyl chloride (CH_3Cl) is largely natural in origin and is not controlled under the Montreal Protocol. The 2016 global mean mole fraction determined from the AGAGE and NOAA global networks was 553 and 559 ppt, respectively (**Table 1-1**). These values are around 2–3% higher than the 2012 values reported in the previous Assessment, although such changes are consistent with historical variability (**Figure 1-1**).

Emissions and Lifetime

The estimate of the total global lifetime of CH_3Cl (0.9 years) remains unchanged from the previous Assessment. Major sinks include oxidation by the hydroxyl radical, uptake by soils, degradation in oceans, and photolysis in the stratosphere. Among the sinks, only the partial lifetime due to loss in the stratosphere has been addressed since the last Assessment. The estimate of a 35 ± 7-year stratospheric lifetime (Umezawa et al., 2015) is consistent with the 30.4-year estimate in the last Assessment.

The major sources of methyl chloride are tropical and subtropical plants, biomass burning, the ocean, salt marshes, and fungi. The major anthropogenic source is thought to be coal combustion (McCulloch et al., 1999). The previous Assessment summarized known CH_3Cl sources, highlighting that the global source strength is about 20% lower than the magnitude of known sinks. A recent study based on atmospheric observations from Gosan, South Korea, found that CH_3Cl emissions from industrialized regions of China may have been underestimated (Li et al., 2017) and suggested that the chemical industry may be a source that has not been accounted for in previous budgets. If confirmed, these findings could substantially reduce the gap in the CH_3Cl budget. Emissions from bread-baking have also been proposed, although the magnitude was thought to be small compared to other sources (Thornton et al., 2016).

Some process-level studies have investigated emissions of CH_3Cl from a range of natural and anthropogenic sources, including coastal salt marshes and an invasive plant (perennial pepperweed) in North America (Khan et al., 2013; Rhew et al., 2014), a fern species (Yokouchi et al., 2015), and coastal heathland fires in Australia (Lawson et al., 2015). However, the implications of these studies for the global budget have not yet been established.

1.2.7 Methyl Bromide (CH_3Br)

Observations of Atmospheric Abundance

The 2016 global mean surface mole fractions of methyl bromide from the AGAGE and NOAA networks, respectively, were 6.80 ppt and 6.86 ppt (**Figure 1-1**, **Figure 1-7,** and **Table 1-1**), ~25% lower than the peak of about 9.2 ppt observed between 1996-1998 and around 1.3 ppt (~25%) higher than the preindustrial Southern Hemisphere mole fraction of 5.5 ± 0.2 ppt from ice core measurements (Carpenter and Reimann et al., 2014). The global mean mole fraction declined until 2015, when it reached 6.6 ppt. However, between 2015 and 2016, NOAA and AGAGE observations showed positive growth rates of 0.22 ppt yr^{-1} (3.3%) and 0.14 ppt yr^{-1} (2.1%), respectively. This is the highest growth rate observed in the last decade or more. The annual mean IHD has continued to decline since the previous Assessment, with the NOAA value reaching 0.68 ppt in 2016, 70% lower than the peak in 1996–1998. The increase in growth between 2015 and 2016 does not appear to coincide with an increase in IHD.

Emissions and Lifetime

The global total lifetime of CH_3Br is estimated to be 0.8 years, unchanged from the previous Assessment.

Atmospheric CH_3Br has both natural and anthropogenic sources. Its use is controlled under the Montreal Protocol for the fumigation of soils, post-harvest storage of commodities, and the fumigation of structures, although some "critical use" exemptions from these controls have been awarded (e.g.UNEP, 2014b). Quarantine and pre-shipment (QPS) use of CH_3Br, mainly for pest control for the transport of agricultural products, is exempt from the phaseout. Natural or partly anthropogenic sources include biomass burning and emissions from oceanic and terrestrial ecosystems (for further details, see Table 1-4 in the previous Assessment; Carpenter and Reimann et al., 2014). Reported non-QPS consumption dropped to 0.94 Gg in 2016, around 1% of its peak value (UNEP, 2017; **Figure 1-7**). The reported consumption for QPS

was 8.4 Gg yr^{-1} in 2016. Compared to the non-QPS consumption, this value has been relatively stable for the previous two decades (UNEP, 2017). Combined reported consumption from these uses has decreased by approximately 87% since its peak, which occurred in the late-1990s. This decrease is qualitatively consistent with the observed decline in atmospheric mole fraction and IHD. The cause of the anomalous growth observed between 2015 and 2016 is not yet known. However, the fact that the growth increase did not coincide with an increase in IHD suggests that the associated changes in sources and/or sink must be distributed across hemispheres.

The previous Assessments noted a discrepancy between total known sources of CH_3Br and its total loss rate, with the sinks being around 39 Gg yr^{-1} larger than emissions. Some recent studies have investigated potentially new or poorly studied sources that could reduce this gap. Thornton et al. (2016) found a relatively minor contribution to the global budget from emissions occurring during bread-baking (<1%). Similarly, seagrass meadows are not thought to contribute significantly to the global budget (Weinberg et al., 2015). Several regional or process-level studies have been carried out focusing on subtropical salt marshes, peatland pastures, heathland fires, or the photochemical halogenation of terrestrial dissolved organic matter in estuarine outflow (Khan et al., 2013; Lawson et al., 2015; Mendez-Diaz et al., 2014; Rhew et al., 2014). However, the implications of these studies for the global budget have not yet been established. Therefore, the cause of the discrepancy identified in the previous Assessment remains unknown.

1.3 VERY SHORT-LIVED HALOGENATED SUBSTANCES (VSLSs)

As in the last Assessment, VSLSs are considered to include source gases (SGs; i.e., very short-lived halogenated substances present in the atmosphere in the form they were emitted from natural and anthropogenic sources), halogenated product gases (PGs) arising from SG degradation, and other sources of tropospheric inorganic halogens. VSLSs have tropospheric lifetimes of around 0.5 years or less. While longer-lived ODSs account for the majority of the present-day stratospheric halogen loading, there is strong evidence that VSLSs make a significant contribution to stratospheric bromine and that they contribute to stratospheric chlorine (Carpenter and Reimann et al., 2014; Montzka and Reimann et al., 2010), and possibly iodine. These gases thus contribute to stratospheric ozone destruction, but their radiative forcing is small due to their short lifetimes. Also, due to their short lifetimes, VSLSs show much higher variability in the troposphere than long-lived ODSs and are partly chemically broken down during the transport to the stratosphere. In order to assess the amount of halogen delivered to the stratosphere, the sources, transport pathways, and the chemical transformation of VSLSs during transit need to be understood. In this section, we use data from global networks to assess the mean tropospheric mixing ratios, whereas observations close to the tropical tropopause are used to infer the input of VSL SGs to the stratosphere.

1.3.1 Tropospheric Abundance, Trends, and Emissions of Very Short-Lived Source Gases (VSL SGs)

For the principal VSL SGs, a detailed compilation of local lifetimes was given in Table 1-5 of Carpenter and Reimann et al. (2014), and is updated in **Table A-1** of this Assessment. Box 1-1 in the 2014 Assessment provides a discussion of different VSL SGs' lifetimes.

1.3.1.1 Chlorine-Containing Very Short-Lived Source Gases

This section focuses on the chlorinated VSLSs most widely reported in the background atmosphere: dichloromethane (CH_2Cl_2), chloroform (trichloromethane, $CHCl_3$), tetrachloroethene (perchloroethylene, CCl_2CCl_2, shortened to C_2Cl_4), trichloroethene (C_2HCl_3) and 1,2-dichloroethane (CH_2ClCH_2Cl). Long-term measurements are available from both the NOAA and AGAGE surface networks for CH_2Cl_2 and C_2Cl_4, while $CHCl_3$ is available from AGAGE only. Hemispheric mean mole fractions and annual emissions derived from these data using a global 12-box model (see **Box 1-1**) are shown in **Figure 1-8** and **Table 1-3**. It should be noted that because these relatively short-lived compounds exhibit spatial gradients that will not be well represented at the coarse resolution of a box model, these estimates are likely to be subject to significant, but poorly quantified, representation uncertainties. Industrial emissions dominate over natural sources for these gases except for

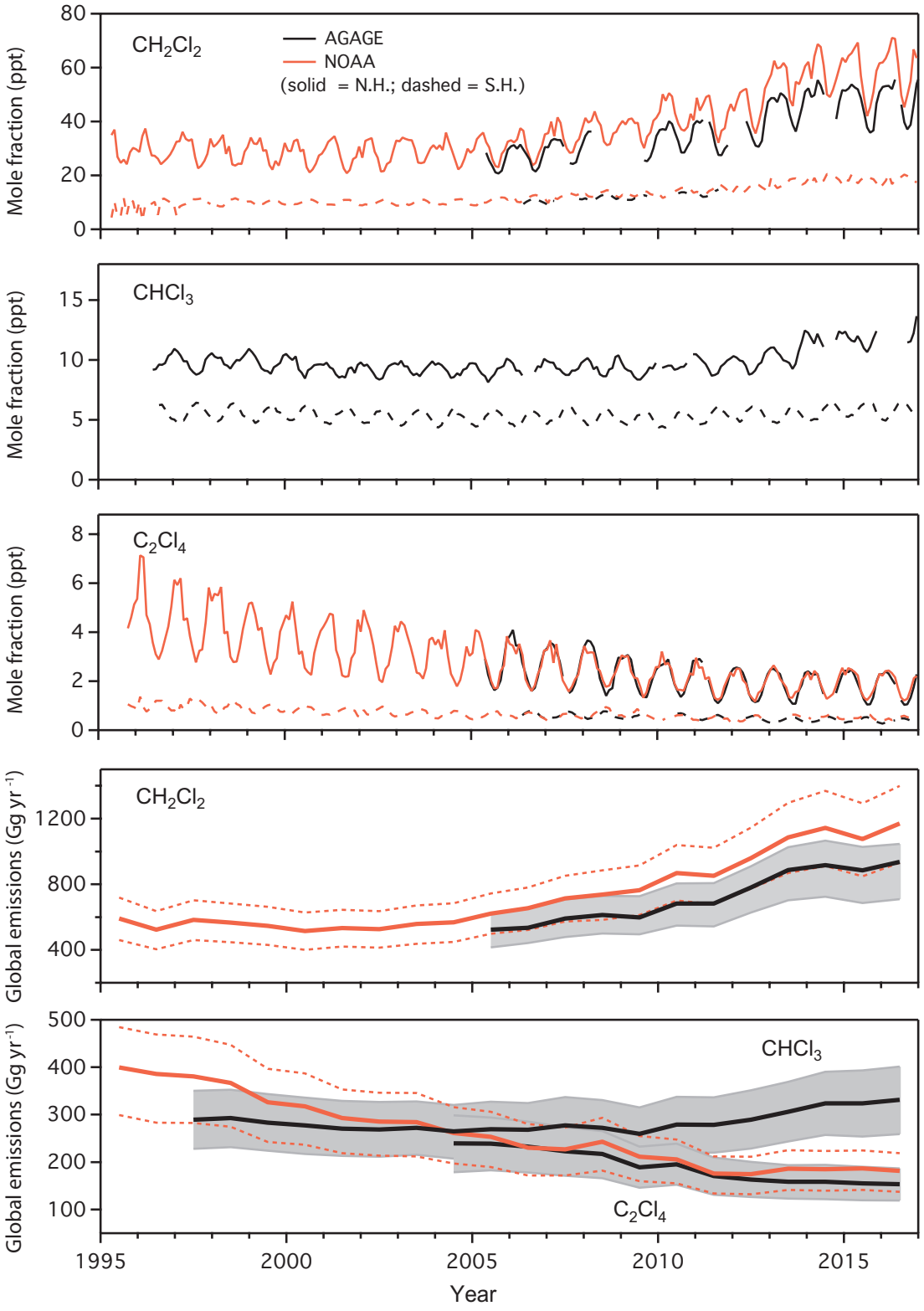

Figure 1-8. *Upper three panels:* Monthly hemispheric mean mole fractions of CH_2Cl_2, $CHCl_3$, and C_2Cl_4 derived from AGAGE (black) and NOAA (red) observations in the NH (solid lines) and SH (dashed lines). *Lower two panels:* Global emissions estimates (Gg yr^{-1}) calculated using a global 12-box model (using methods described in **Box 1-1** and **Figure 1-4**), with 1-sigma uncertainties indicated by shading (AGAGE) or dotted lines (NOAA).

Table 1-3. Annual global mean mole fractions of chlorinated VSL source gases and estimated emissions from the global networks. Emissions based on AGAGE and NOAA surface data were calculated using a global 12-box model (Cunnold et al., 1983; Rigby et al., 2013), identical to the global emissions shown in **Figure 1-4** for longer-lived ODSs. The calculations assume parameterized global total steady-state lifetimes of 0.54, 0.58, and 0.38 years for CH_2Cl_2, $CHCl_3$, and C_2Cl_4, respectively.

Formula	Annual Mean Mole Fraction (ppt)			Growth (2015–2016)		Annual Global Emissions (Gg yr^{-1})			Network
	2012	2015	2016	ppt yr^{-1}	% yr^{-1}	2012	2015	2016	
CH_2Cl_2	26.0	32.0	32.7	0.7	2.2	780 (±135)	885 (±164)	937 (±172)	AGAGE
	30.4	37.8	39.2	1.4	3.7	881 (±169)	957 (±204)	1037 (±213)	NOAA
$CHCl_3$	7.6	8.7	8.9	0.2	2.3	290 (±60)	324 (±69)	331 (±70)	AGAGE
C_2Cl_4	1.17	1.10	1.07	-0.03	-2.7	87 (±18)	84 (±17)	83 (±17)	AGAGE
	1.16	1.22	1.20	-0.02	-1.6	97 (±20)	103 (±22)	103 (±21)	NOAA

$CHCl_3$ (Montzka and Reimann et al., 2010). Detailed information on industrial uses is available on the U.S. Environmental Protection Agency's (https://www.epa.gov) and the EU European Chemicals Agency's (https://echa.europa.eu/) websites.

Dichloromethane (CH_2Cl_2) exhibits a strong IHD, with NH (Northern Hemisphere) mole fractions a factor of ~3 larger than those in the SH (Southern Hemisphere), reflecting NH industrial sources (e.g., **Figure 1-8**; Hossaini et al., 2017). Measurements from the NOAA network suggest CH_2Cl_2 emissions increased by a factor of ~2 between 2000 (~508 ± 109 Gg yr^{-1}) and 2016 (1037 ± 213 Gg yr^{-1}). The annual mean mole fraction in 2016 was 39.2 ppt based on the NOAA network, which is about a doubling compared to the beginning of the century. Global mean mole fractions increased by 12.3 ppt between 2007 and 2016 (a relative increase of 60%), reaching 32.7 ppt in 2016 based on the AGAGE record. Particularly large CH_2Cl_2 growth occurred between 2012 and 2013 (~6 ppt yr^{-1} from NOAA and ~4 ppt yr^{-1} from AGAGE), though more recent growth rates (2015 to 2016) are comparatively small (1.4 ppt yr^{-1} for NOAA and 0.7 ppt yr^{-1} for AGAGE) (**Table 1-3**). At present, it cannot be assessed if this recent decrease in growth rate reflects a stabilization of emissions or is a transient effect reflecting the large atmospheric variability. The discrepancy between the two CH_2Cl_2 datasets of about 13 ppt of tropospheric chlorine in 2016 reflects differences in calibration scales, which are on the order of 10%, and also differences in sampling locations between the networks. The latter is particularly evident in the 0–30° northern latitude band, where NOAA observations (from the Pacific: Mauna Loa and Cape Kumukahi, Hawai'i) are around 30% higher than the AGAGE measurements (from the Atlantic: Ragged Point, Barbados). It is beyond the capability of the 12-box model used here to resolve such differences, which may be due to longitudinal gradients in the atmosphere.

The upward CH_2Cl_2 trend during the last decade is corroborated by upper tropospheric aircraft data from the CARIBIC (Civil Aircraft for the Regular Investigation of the atmosphere Based on an Instrument Container) mission (Leedham Elvidge et al., 2015a; Oram et al., 2017). The contribution of regional CH_2Cl_2 sources to global emission trends are not well quantified, though emissions from the Indian subcontinent may have increased by a factor of 2–4 between 1998–2000 and 2008 (Leedham Elvidge et al., 2015a) and substantial emissions from eastern Asia have been proposed (Oram et al., 2017).

Table 1-4. Summary of observed mole fractions (in ppt) of VSL source gases from the marine boundary layer (MBL) to the tropical tropopause layer (TTL) and above. Note, many of the upper tropospheric measurements were made at least one decade ago in the case of brominated and iodinated SGs. As chlorinated SGs have significant anthropogenic sources and some show trends, data are based on measurements from 2013/2014 only.

	Marine Boundary Layer (MBL)		Lower TTL		LZRH (z_0)[1]		Upper TTL		Tropical Tropopause	
Height Range			**12–14 km**		**14.5–15.5 km**		**15.5–16.5 km**		**16.5–17.5 km**	
Potential Temperature Range			**340–355 K**		**355–365 K**		**365–375 K**		**375–385 k**	
	Median[2]	**Range[3]**	**Mean[2]**	**Range[3]**	**Mean[2]**	**Range[3]**	**Mean[2]**	**Range[3]**	**Mean[2]**	**Range[3]**
CH_2Cl_2	57.5	46.6–68.1	42.0	36.4–47.6	36.4	29.6–44.3	33.9	28.4–41.6	32.5	26.3–38.5
$CHCl_3$	10.3	8.5–12.3	7.9	7.1–8.7	7.1	6.4–8.0	6.8	6.2–7.8	6.5	5.7–7.2
CH_2ClCH_2Cl	12.8	10.4–18.3	9.0	6.8–11.3	7.4	5.2–9.5	6.9	5.4–8.3	6.6	5.7–7.5
C_2HCl_3	0.2	0.1–0.9	0.14	0.02–0.25	0.08	0.00–0.16	0.06	0.0–0.13	0.04	0.00–0.08
C_2Cl_4	1.3	1.0–2.2	0.87	0.68–1.05	0.73	0.49–0.95	0.66	0.49–0.83	0.52	0.38–0.71
CH_2Br_2	0.9	0.6–1.7	0.96	0.72–1.15	0.81	0.59–0.98	0.73	0.43–0.94	0.64	0.32–0.89
$CHBr_3$	1.2	0.4–4.0	0.57	0.30–1.11	0.36	0.05–0.72	0.28	0.02–0.64	0.19	0.01–0.54
CH_2BrCl	0.10	0.07–0.12	0.12	0.07–0.16	0.13	0.08–0.20	0.14	0.10–0.20	0.12	0.07–0.20
$CHBr_2Cl$	0.3	0.1–0.8	0.12	0.06–0.23	0.09	0.04–0.19	0.08	0.02–0.16	0.05	0.02–0.14
$CHBrCl_2$	0.3	0.1–0.9	0.26	0.18–0.55	0.18	0.08–0.49	0.15	0.07–0.31	0.12	0.05–0.32
CH_3I	0.8	0.3–2.1	0.16	0.00–0.49	0.08	0.0–0.32	0.04	0.0–0.25	0.03	0.00–0.14
Total Cl	177	144–221	130	111–149	112	91–136	105	88–127	100 (92)[4]	83–117 (75–110)[4]
Anthrop. Cl[5]	150	122–189	109	93–126	98	75–127	93	73–118	88	69–108
Total Br	6.5	2.8–18.0	4.3	2.7–6.8	3.2	1.6–5.2	2.8	1.1–4.6	2.2	0.8–4.2
Total I	0.8	0.3–2.1	0.16	0.00–0.49	0.08	0.0–0.32	0.04	0.0–0.25	0.03	0.00–0.14

Notes:

[1] LZRH (z_0) corresponds to the level of zero clear-sky radiative heating (see Box 1-3 of Carpenter and Reimann et al. (2014)). As in the previous Assessment, this level is at about 15 km or 360 K, where there is a transition from clear-sky radiative cooling to clear-sky radiative heating. In general, air masses above this level are expected to enter the stratosphere.

[2] Abundances in the MBL are median values. MBL CH_2Cl_2, $CHCl_3$, CH_2ClCH_2Cl, C_2HCl_3, and C_2Cl_4 data are from the CAST and CONTRAST missions (Andrews et al., 2016; Pan et al., 2017). MBL $CHBr_3$, CH_2Br_2, and CH_3I data are from the compilation of Ziska et al. (2013). MBL CH_2BrCl, $CHBr_2Cl$, and $CHBrCl_2$ data are from the previous (Carpenter and Reimann et al., 2014) Assessment. In and above the TTL, abundances are mean values. For brominated VSLSs and CH_3I, data have been compiled from observations obtained during the Pre-AVE, CR-AVE, TC4, HIPPO, SHIVA, CONTRAST, and ATTREX aircraft campaigns (Navarro et al., 2015; Pan et al., 2017; Sala et al., 2014; Wofsy et al., 2011), and from balloon observations (Brinckmann et al., 2012). ATTREX values used here differ from those used in Wales et al. (2018), as they have been filtered by altitude instead of applying any tracer-tracer correlation. For chlorinated VSLSs, data are from the CONTRAST (2014) and ATTREX (2013/2014) missions in 2013/2014 only (Navarro et al., 2015), with the exception of CH_2ClCH_2Cl, which does not include data from ATTREX 2013. See below for definitions of field mission acronyms. Note that calibration scales for VSLSs may differ among different research groups (e.g. Hall et al., 2014; Jones et al., 2011).

[3] In the MBL the stated observed range is 10^{th} to 90^{th} percentile. Above the MBL, the stated observed range represents the smallest mean minus 1 standard deviation and the largest mean plus 1 standard deviation.

[4] Values for 2016 based on the model by (Hossaini et al., 2017), which are used to derive total stratospheric VSL SGI for chlorine, as explained in section 1.3.2.1, in order to reduce variability from individual campaigns in assessing total Cl input to the stratosphere.

[5] The anthropogenic fraction of VSLS (Anthrop. Cl) is approximate and has been calculated from the sum of 90% of CH_2Cl_2, 50% of $CHCl_3$, and 100% of other compounds.

Pre-AVE = Pre-Aura Validation Experiment (2004); CR-AVE = Costa Rica-Aura Validation Experiment (2006); TC4 = Tropical Composition, Cloud and Climate Coupling missions (2007); HIPPO = HIAPER (High-Performance Instrumented Airborne Platform for Environmental Research) Pole-to-Pole Observations (2009–2011); SHIVA = Stratospheric Ozone: Halogen Impacts in a Varying Atmosphere; ATTREX = Airborne Tropical Tropopause Experiment (2011, 2013, and 2014); CAST = Co-ordinated Airborne Studies in the Tropics (2014); CONTRAST = Convective Transport of Active Species in the Tropics (2014).

In contrast to CH_2Cl_2, global perchloroethylene (C_2Cl_4) emissions and mole fractions in background air have largely been in decline at least since the mid-1990s (**Figure 1-8**). C_2Cl_4 observations from AGAGE are only available from 2004, though relative (−44%) and absolute (−0.8 ppt) changes since then are comparable to NOAA trends over the same period (−32%, −0.6 ppt). The global mean C_2Cl_4 mole fraction was ~1 ppt in 2016 (**Table 1-3**).

For chloroform ($CHCl_3$), AGAGE measurements show stable global mean mole fractions in the range of 7.3–7.7 ppt over the 1997–2010 period, followed by a subsequent increase to 8.9 ppt in 2016. Emissions between 2011 and 2016 are estimated to have increased by ~20% (**Figure 1-8**). During this period, the IHD of surface $CHCl_3$ mole fractions increased from 4.3 ppt to 6.3 ppt, suggesting an increase in NH anthropogenic emissions.

No 1,2-dichloroethane (CH_2ClCH_2Cl) measurements are available from either AGAGE or NOAA, thus its budget and emissions are poorly constrained. Based on recent aircraft observations, boundary layer CH_2ClCH_2Cl mole fractions are of the order ~10–20 ppt in the NH (**Table 1-4**), with SH mole fractions a factor of ~6 lower (Hossaini et al., 2016a), indicative of dominant anthropogenic sources. Given these abundances, CH_2ClCH_2Cl is potentially an important source of chlorine to the troposphere (smaller than CH_2Cl_2 but comparable to $CHCl_3$). However, owing to its relatively short lifetime compared to other VSLSs **(Table A-1)**, its importance as a source of stratospheric chlorine is estimated to be lower.

Trichloroethene (C_2HCl_3) is a relatively minor tropospheric chlorine source. A limited set of AGAGE measurements show NH surface mole fractions of

~1.1 ppt in the early 2000s (Simmonds et al., 2006), with recent aircraft data confirming its low abundance (**Table 1-4**).

Short-lived halogenated unsaturated hydrocarbons (halogenated olefins) have recently been used to replace high-GWP HCFCs and HFCs. In this Assessment, hydrofluoroolefins (HFOs) are discussed in **Chapter 2**. Hydrochlorofluoroolefins (HCFOs) are also in use, and the only atmospheric record currently available is that for HCFO-1233zd(E) (trans-$CF_3CH{=}CHCl$) from central Europe (Vollmer et al., 2015a). While this compound was detectable in only 30% of the samples measured at Jungfraujoch in 2013, this increased to 100% by 2016, with a mean mole fraction of 0.03 ppt in that year (update from Vollmer et al., 2015a).

While measurements of VSLSs from NOAA and AGAGE largely reflect background concentrations (e.g. see Simmonds et al., 2006), regional emissions may lead to higher and more variable abundances. Elevated levels in urban air and at sites likely influenced by regional industrial/commercial processes are reported over the USA (Logue et al., 2010) and China, with the latter including up to several tens of ppt of C_2Cl_4 and several hundred ppt or more of CH_2Cl_2, $CHCl_3$ and CH_2ClCH_2Cl (Mao et al., 2009; M. Yang et al., 2016; Zhang et al., 2014). The regional sum of chlorine from CH_2Cl_2, $CHCl_3$, C_2Cl_4, and CH_2ClCH_2Cl can therefore exceed the background global mean (**Table 1-3**) by up to an order of magnitude, as observed, e.g., over Malaysia and the island of Taiwan and (see e.g. Oram et al., 2017)). Oram et al. (2017) estimated anthropogenic CH_2Cl_2 emissions from China to be 455 ± 46 Gg yr^{-1} in 2015 (i.e., ~40–50% of the top-down derived global emissions in **Table 1-3**. Similarly, CH_2ClCH_2Cl emissions from China of 203 (±20) Gg yr^{-1} were derived for 2015.

Natural $CHCl_3$ sources from marine (phytoplankton) and terrestrial (e.g., soils, peatlands, and plants) environments have been identified (e.g. Albers et al., 2017; Forczek et al., 2015; Khalil et al., 1999; Khan et al., 2011) and account for 50–90% of global emissions (McCulloch, 2003; Worton et al., 2006). For CH_2Cl_2, biomass burning may be a small (Lobert et al., 1999) or negligible global source (Leedham Elvidge et al., 2015a; Lawson et al., 2015; Simpson et al., 2011), though oceanic emissions may be more significant. Based on limited observational data, estimates of ocean CH_2Cl_2 emissions range from 124 ± 38 Gg yr^{-1} (Xiao, 2008) to 192 Gg yr^{-1} (Khalil et al., 1999). Natural CH_2Cl_2 sources are therefore uncertain but are likely small relative to industrial emissions, which are estimated to account for 90% of total CH_2Cl_2 emissions (Carpenter and Reimann et al., 2014; Montzka and Reimann et al., 2010). An increase in industrial emissions is the most probable cause of recent CH_2Cl_2 growth.

Global combined tropospheric chlorine from the three VSLSs measured by the NOAA and AGAGE

networks (CH_2Cl_2, $CHCl_3$ and C_2Cl_4) was 92–110 ppt Cl in 2016 (**Table 1-3**), with a 4.0 ± 1.5 ppt Cl yr^{-1} increase over the 5-year period 2012 to 2016. The given uncertainty range includes the differences in the NOAA and AGAGE calibration scales. In the NH tropical boundary layer, total tropospheric chlorine from VSLSs in 2014, including additional contributions from CH_2ClCH_2Cl and C_2HCl_3, is estimated from aircraft observations at 177 (144–221) ppt Cl (**Table 1-4**).

1.3.1.2 Bromine-Containing Very Short-Lived Source Gases

Bromoform ($CHBr_3$) and dibromomethane (methylene dibromide, CH_2Br_2) are the principal brominated VSL SGs. Along with bromochloromethane (CH_2BrCl), dibromochloromethane ($CHBr_2Cl$), and bromodichloromethane ($CHBrCl_2$), these VSL SGs are predominantly of natural marine origin, with ocean phytoplankton and macroalgae being the dominant sources (e.g. Carpenter et al., 2007; Leedham Elvidge et al., 2015b; Hamed et al., 2017; Quack et al., 2007)). Typical tropospheric mole fractions of the above brominated compounds are summarized in **Table 1-4**. Though poorly characterized, minor terrestrial sources include peatland and organic-rich soils (Albers et al., 2017; Carpenter et al., 2005) and production due to water chlorination processes (Worton et al., 2006). In coastal zones, industrial discharge of chlorinated effluents to seawater is also identified as a source of several brominated VSL SGs, in particular $CHBr_3$ (Boudjellaba et al., 2016; Hamed et al., 2017; Yang, 2001). The importance of this source on a global scale is not clear (Liu et al., 2011).

Since the last Assessment, brominated VSL SG emissions in several oceanic regions have been reported from ship cruises, including the Yellow, Sulu, and South China Seas (Nadzir et al., 2014; Yang et al., 2014), the tropical Atlantic (Hepach et al., 2015) Pacific Peruvian coastal waters (Fuhlbrugge et al., 2016a), and the west Indian Ocean (Fiehn et al., 2017). CH_2Br_2 emissions derived in these studies were in some cases significantly larger than those estimated from previous studies (Butler et al., 2007; 2015; Hepach et al., 2014; Tegtmeier et al., 2012) and confirm large spatiotemporal variability in sea–air VSL SG fluxes (e.g. Montzka and Reimann et al., 2010), varying by an order of magnitude or more during a given cruise. Many factors contribute to such variability, including subsurface biogeochemical processes, proximity to coastal sources, wind speed, and sea surface temperature, among others (Stemmler et al., 2015). The correlation between $CHBr_3$ and CH_2Br_2 concentrations in background air suggests the two compounds are largely derived from a common process at the global scale (Carpenter and Liss, 2000; Yokouchi et al., 2017).

While there is evidence for seasonal variations in oceanic VSL SG emissions from observations (Hughes et al., 2009; Yang et al., 2014; Yokouchi et al., 2017) and ocean biogeochemical models (Stemmler et al., 2015), much of the observed seasonality of background surface $CHBr_3$ and CH_2Br_2 is well explained by seasonal changes in OH and other chemical sinks (Hossaini et al., 2016b).

Recent bottom-up estimates of global $CHBr_3$ emissions are a factor of two lower than top-down estimates, most likely due to poor temporal and spatial data coverage, resulting in missing sources and emission hot spots (Stemmler et al., 2015; Ziska et al., 2013). There is no clear evidence for long-term changes in the atmospheric abundance of brominated VSLSs, although small increases in global emissions (~6–8% between 1979 and 2013 for CHBr3 and CH_2Br_2) are suggested to have occurred due predominantly to increases in surface wind speed (Ziska et al., 2017). For $CHBr_3$, the global source estimate of 120–820 Gg Br yr^{-1} given in the last Assessment is unchanged (Carpenter and Reimann et al., 2014). For CH_2Br_2, the range from the last Assessment (57–280 Gg Br yr^{-1}) is reduced to 57–100 Gg Br yr^{-1}, reflecting the most up-to-date emission climatologies (e.g. Lennartz et al., 2015; Ziska et al., 2013) and supported by the fact that global models reproduce tropospheric CH_2Br_2 observations well using emissions at the lower end (Hossaini et al., 2016b). Global CH_2BrCl, $CHBr_2Cl$, and $CHBrCl_2$ emissions are estimated at 4–6 Gg Br yr^{-1}, 15–43 Gg Br $yr^{-1,}$ and 8–11 Gg Br yr^{-1}, respectively (Brinckmann et al., 2012; Ordonez et al., 2012; Warwick et al., 2006; Yokouchi et al., 2005).

1.3.1.3 Iodine-Containing Very Short-Lived Source Gases

Methyl iodide (CH_3I), with mainly oceanic sources, is the main iodine-containing VSL SG. Since the last Assessment, further evidence for oceanic CH_3I

Box 1-2. Regional Variability and Modeling of VSLS Transport to the Stratosphere

Eleven global models participated in the first concerted VSLS multi-model intercomparison (Hossaini et al., 2016b), testing a range of prescribed emissions and using a common chemistry scheme. Despite differences in transport schemes, most of the models were capable of reproducing observed $CHBr_3$ and CH_2Br_2 mole fractions in the TTL, providing confidence in a proper representation of the average transport processes affecting VSLS stratospheric injection.

While the average transport is thus rather well represented, global and trajectory models have intrinsic limitations in properly representing very deep convection of air parcels from the boundary layer to the stratosphere (Feng et al., 2011; Hosking et al., 2010; Hoyle et al., 2011; Orbe et al., 2017), although increasing the model resolution has been found to improve the representation of the strength and location of convective events (Russo et al., 2015).

Modeled SG concentrations in the TTL do not depend only on total emissions, but in particular also on the geographical distribution of the sources. These are mainly natural oceanic sources for bromine; for the input of VSLS chlorine to the stratosphere on a regional scale, the transport of anthropogenic pollution plumes to the upper atmosphere plays a crucial role (Anderson et al., 2016; Ashfold et al., 2015; Chen et al., 2016; Oram et al., 2017). For brominated and iodinated species, which have mostly natural sources, the collocation of natural, mainly oceanic, sources and effective vertical transport is important. The Maritime Continent (Indonesia, Philippines, New Guinea, and other Southeast Asia islands) (Tegtmeier et al., 2012, 2015), the tropical Indian Ocean (Liang et al., 2014a), and the Tropical Western Pacific (Fernandez et al., 2014) have been suggested as particularly important source regions in this respect. The collocation of elevated emissions with the Asian monsoon circulation during boreal summer and with the tropical pacific warm pool during boreal winter also likely provides oceanic VSL SGs an efficient transport route to the stratosphere (Fiehn et al., 2017; Hossaini et al., 2016b; Liang et al., 2014a).

production via biotic (e.g., phytoplankton and cyanobacteria) and abiotic (e.g., photochemical breakdown of dissolved organic matter) processes has been provided by laboratory and field studies (e.g. Allard and Gallard, 2013; Hepach et al., 2015; Mendez-Diaz et al., 2014; Ooki et al., 2015; Shi et al., 2014; Yuan et al., 2016). Terrestrial CH_3I sources are poorly quantified, though include soils/vegetation, rice paddies, wetlands, salt marshes, and biomass burning (e.g. Akagi et al., 2011; Lawson et al., 2015; Lee-Taylor and Redeker, 2005; Manley et al., 2006; Sive et al., 2007), accounting for up to 30% of total CH_3I emissions in some inventories (Bell et al., 2002).

In the marine boundary layer (MBL), recently observed mean CH_3I mole fractions of 0.59 ± 0.30 ppt over the Tropical Western Pacific (Fuhlbrugge et al., 2016b) and 0.84 ± 0.12 ppt over the Indian Ocean (Fiehn et al., 2017) are generally consistent with previous observations (**Table 1-4**). Generally, larger mole fractions are observed at low latitudes than toward the poles (Hu et al., 2016b). No new information on long-term atmospheric CH_3I trends has been reported since the last Assessment (Carpenter and Reimann et al., 2014), when trends were shown to have varied over the past decades (Yokouchi et al., 2012). The best estimate of coastal plus open-oceans emissions is unchanged and is in the range of 157–550 Gg I yr^{-1} (Carpenter and Reimann et al., 2014).

Several other iodinated VSLSs have been detected in the MBL, including CH_2ICl, CH_2IBr, CH_2I_2 and C_2H_5I (Allan et al., 2015; Jones et al., 2010; Shimizu et al., 2017). Owing to their short lifetimes (minutes to hours at the surface) these VSL SGs are not expected to reach the upper troposphere. However, their photolysis is a significant source of tropospheric inorganic iodine (Carpenter et al., 2013; Saiz-Lopez et al., 2014; Sherwen et al., 2016) and may contribute to particulate iodine (Sherwen et al., 2016) observed in the upper troposphere and stratosphere (Murphy et al., 2014; Murphy and Thomson, 2000).

1.3.2 Input of VSLS Halogen to the Stratosphere

VSL SGs can be chemically broken down during transport to the stratosphere. We differentiate between stratospheric halogen input arising from halogen atoms crossing the tropopause in the form of the emitted source gases (source gas injection, SGI) and in the form of product gases released from source gas photodecomposition (product gas injection, PGI). Since the last Assessment, new observations of brominated, chlorinated, and iodinated SGs have been obtained in the tropical troposphere, including the near-tropopause region, allowing constraints on SGI especially from chlorinated and brominated SGs. New measurements of brominated PGs have also been reported from several aircraft campaigns, and global models with a more explicit treatment of PG chemistry have reported PGI estimates. In situ measurements of chlorinated and iodinated PGs remain sparse. Transport processes relevant to the input of VSLSs to the stratosphere show a large regional and seasonal variability, which is discussed in **Box 1-2.** In this subsection, we assess the magnitude of both SGI and PGI for the different halogens.

Dynamical processes relevant to the transport of VSLSs from the marine boundary layer (MBL) to the tropical tropopause layer (TTL) and from the TTL to the stratosphere have been discussed in detail in previous Assessments (see Section 1.3.2 in Montzka and Reimann et al., 2010; see also Carpenter and Reimann et al., 2014). Briefly, the TTL is the region between the lapse rate minimum (~12 km / θ = 345 K) and the cold point tropopause (CPT; ~17 km, θ = 380 K) (see Fueglistaler et al., 2009). The level of zero radiative heating (LZRH; ≈ 15 km / θ = 360 K) marks the transition from clear-sky radiative cooling (below) to clear-sky radiative heating (above). Once a tropospheric air parcel crosses the LZRH, it is expected to reach the lower tropical stratosphere.

1.3.2.1 Source Gas Injection (SGI)

SGI describes the stratospheric input of halogenated SGs in the same form as they were emitted at the surface. The efficiency of SGI is different for each compound and depends on its tropospheric loss rate (mainly through reaction with OH or photolysis) and the timescales for troposphere-to-stratosphere transport (Aschmann and Sinnhuber, 2013; Schofield et al., 2011). SGI—the global average halogen mixing ratio

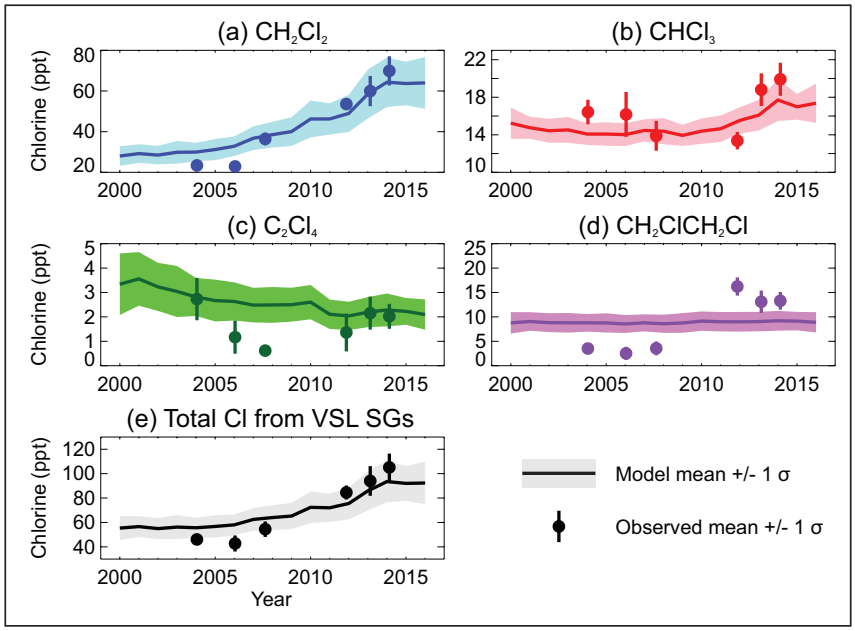

Figure 1-9. Modeled and observed stratospheric chlorine SGI (ppt Cl) evaluated at the tropical tropopause from (a) CH_2Cl_2, (b) $CHCl_3$, (c) C_2Cl_4, (d) CH_2ClCH_2Cl, and (e) total. Update of Hossaini et al. (2015).

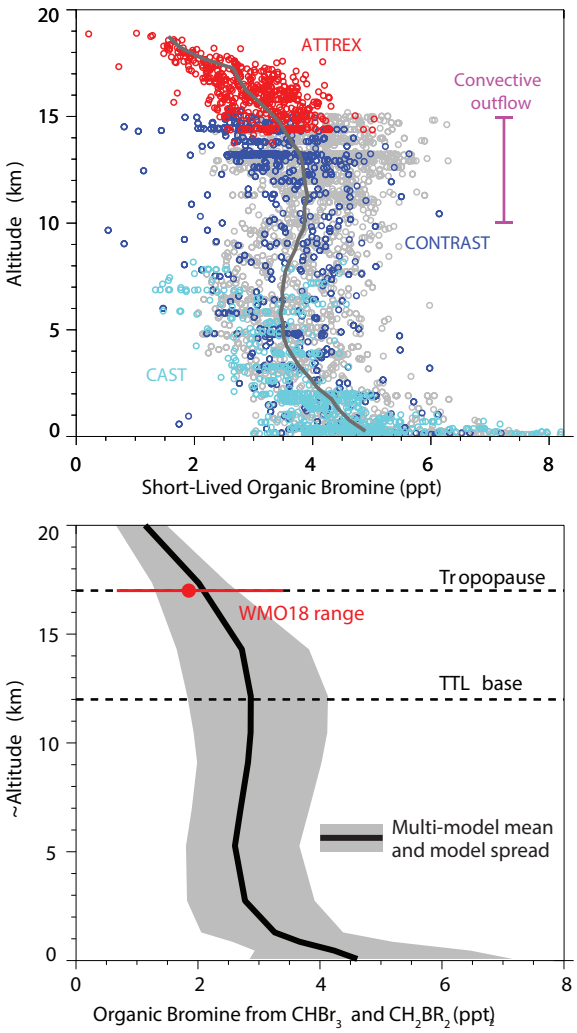

Figure 1-10. *Top panel:* Vertical profile of total organic bromine (ppt Br) from brominated VSL SGs ($CHBr_3$, CH_2Br_2, $CHBr_2Cl$, CH_2BrCl, and $CHBrCl_2$) observed during 2014 CAST, CONTRAST, and ATTREX missions over the Tropical Western Pacific (modified from Pan et al., 2017). *Bottom panel:* Organic bromine from the two main source gases $CHBr_3$ and CH_2Br_2 (ppt Br) from the TransCom-VSLS model intercomparison. The multi-model mean (black line) and model spread (gray shading) are shown, along with the best estimate (red circle) and range (red line) from this Assessment (**Table 1-4**). Modified from Hossaini et al. (2016b).

transported into the stratosphere—can be quantified from SG measurements around the tropical tropopause (~17 km) or from global models.

Since the last Assessment, new aircraft measurements of chlorinated, brominated, and iodinated SGs in the tropical upper troposphere have been reported. These are from the 2013 and 2014 NASA Airborne Tropical TRopopause EXperiment (ATTREX) in the Eastern and Western Pacific (Jensen et al., 2017; Jensen et al., 2013), the 2014 CONTRAST (Convective Transport of Active Species in the Tropics) mission, located in the Western Pacific (Pan et al., 2017), and the 2014 CAST (Coordinated Airborne Studies in the Tropics) mission, also in the Western Pacific (Harris et al., 2017). These campaigns provide new information on the abundance of VSL SGs from the MBL to the TTL and around the tropical tropopause (**Table 1-4**).

SGI from Chlorinated VSLs

Observation-based chlorine SGI from VSLSs is 100 (83–117) ppt Cl based on recent ATTREX measurements only (**Table 1-4**), due to the recent increases of mainly anthropogenic chlorinated VSLSs (see **Section 1.3.1.1**). CH_2Cl_2, $CHCl_3$, and CH_2ClCH_2Cl account for ~65%, ~20%, and ~13% of this total, respectively; the remaining ~2% is from C_2Cl_4 and C_2HCl_3. This chlorine SGI estimate is ~40% larger than the 72 (50–95) ppt Cl derived in the last Assessment and predominantly reflects larger observed mole fractions of CH_2Cl_2 and CH_2ClCH_2Cl around the tropical tropopause during ATTREX compared to the previous measurement compilation. Local upper tropospheric (10–12 km) enhancements of CH_2Cl_2, $CHCl_3$, C_2Cl_4, and CH_2ClCH_2Cl over Southeast Asia have been observed (Oram et al., 2017), with a sum of chlorine in these VSLSs of up to 330 ppt Cl (compared to the average 111–149 ppt Cl from **Table 1-4** in the lower TTL).

An estimate of chlorine SGI (2000 to 2016) from the TOMCAT chemical transport model is shown in **Figure 1-9** (update of Hossaini et al., 2015). The model is constrained by time-dependent, latitudinal-varying boundary conditions, based on NOAA and AGAGE surface measurements (except CH_2ClCH_2Cl, whose emissions were assumed to remain constant). The model reproduces observed CH_2Cl_2 mole fractions around the tropical tropopause reasonably well and shows that chlorine SGI from CH_2Cl_2 increased from 28 (23–33) ppt Cl to 64 (52–76) ppt Cl between 2000 and 2014. Total modeled chlorine SGI is 94 (77–110) ppt Cl in 2014 and is thus in reasonable agreement with the measurement-derived 100 (83–117) ppt Cl

assessed here (**Table 1-4**). Due to the high variability of VSLS observations in the TTL and near the tropical tropopause (see **Figure 1-9e**), the use of SG observations from individual campaigns will lead to large year-to-year variability, which may not be representative of the global mean input to the stratosphere and may not be a good basis for trend estimates. For this Assessment, we therefore use the model data constrained by surface boundary conditions, as the model is able to reproduce the observations from various campaigns reasonably well (see **Figure 1-9**) but at the same time eliminates the variability from the individual campaigns. Based on this model, the total VSL SG injection to the stratosphere is thus assessed to be 92 (75–110) ppt for the year 2016.

SGI from Brominated VSLSs

Total organic bromine from $CHBr_3$, CH_2Br_2, $CHBr_2Cl$, CH_2BrCl, and $CHBrCl_2$ observed during the CAST, CONTRAST, and ATTREX campaigns is shown in **Figure 1-10**. These campaigns were conducted around the Tropical Western Pacific warm pool, a region characterized by strong convective activity where the troposphere-to-stratosphere transport of brominated VSLSs is particularly rapid (e.g. Fernandez et al., 2014; Hosking et al., 2010; Tegtmeier et al., 2015). Intercalibration of standards during CAST, CONTRAST, and ATTREX revealed generally good agreement between VSLS measurements performed by different instruments (relative standard deviation of <10%) (Andrews et al., 2016). CONTRAST measurements show a total of ~4.3 (2.1–7.7) ppt Br in the lower TTL for the five VSL SGs noted above, similar to previous estimates obtained over Southeast Asia (Sala et al., 2014; Wisher et al., 2014). At the LZRH, the CONTRAST mean is ~3.6 (2.0–5.9) ppt Br, ~30% larger than that reported by Carpenter and Reimann et al., (2014). Similarly, both 2013 and 2014 ATTREX data (Navarro et al., 2015) showed roughly equal SGI for bromine over the Western (~3.3 ± 0.5 ppt Br) and Eastern Pacific (~3.0 ± 0.4 ppt Br), which lie around the upper limit of the previously assessed range. These higher values most likely reflect spatiotemporal variability of VSLS sources and transport and should not be taken as an indicator of long-term growth in abundance.

Incorporating the new ATTREX measurements (Navarro et al., 2015) with previously compiled data (Carpenter and Reimann et al., 2014), our best estimate of SGI from brominated VSLSs has increased from 1.4 (0.7–3.4) ppt Br to 2.2 (0.8–4.2) ppt Br. $CHBr_3$ and CH_2Br_2 dominate this supply, accounting for ~84% of the total (**Table 1-4**). The factor of ~5 uncertainty (of similar magnitude to the last Assessment) likely reflects spatiotemporal variability in VSL SG surface emissions (Fiehn et al., 2017; Tegtmeier et al., 2012), tropospheric VSL SG sinks (Aschmann and Sinnhuber, 2013; Rex et al., 2014), and transport processes (Ashfold et al., 2012; Kruger et al., 2008), all of which influence the amount of VSLSs reaching the tropical tropopause.

The revised bromine SGI estimate of 2.2 (0.8–4.2) ppt Br is in broad agreement with a ~2.0 ppt Br estimate from recent global modeling (Fernandez et al., 2014) and the 2.9 ± 0.6 ppt Br derived from recent tracer-tracer correlation of stratospheric VSLS and CFC-11 observations (Wales et al., 2018). For $CHBr_3$ and CH_2Br_2, it is also in good agreement with the climatological multi-model mean of 2.0 (1.2–2.5) ppt Br from the TransCom-VSLS model intercomparison (**Figure 1-10b**; Hossaini et al., 2016b).

SGI from Iodinated VSLSs

With the exception of CH_3I, there is no evidence that significant levels of iodinated VSLSs are present in the TTL (Carpenter and Reimann et al., 2014). From **Table 1-4**, mean CH_3I mole fractions are below 0.1 ppt at 15 km, decreasing to below 0.05 ppt around the tropical tropopause. Iodine SGI is assessed to be in the range of 0 to 0.1 ppt, in agreement with modeling (Saiz-Lopez et al., 2015; Tegtmeier et al., 2013).

1.3.2.2 Product Gas Injection (PGI)

A variable fraction of the halogenated PGs, which arise from the degradation of source gases (SGs), experience efficient dry and wet scavenging during transit to the stratosphere. In principle, PGs can be produced from any halocarbon, but VSL SGs are the main source of PGs. Recent aircraft campaigns have provided new information regarding the vertical distribution of halogenated PGs; these are complemented by box- and global-modeling studies to provide new constraints on stratospheric PGI.

PGI from Chlorinated VSLSs

Product gases arising from chlorinated SGs include phosgene ($COCl_2$) and hydrogen chloride (HCl) and

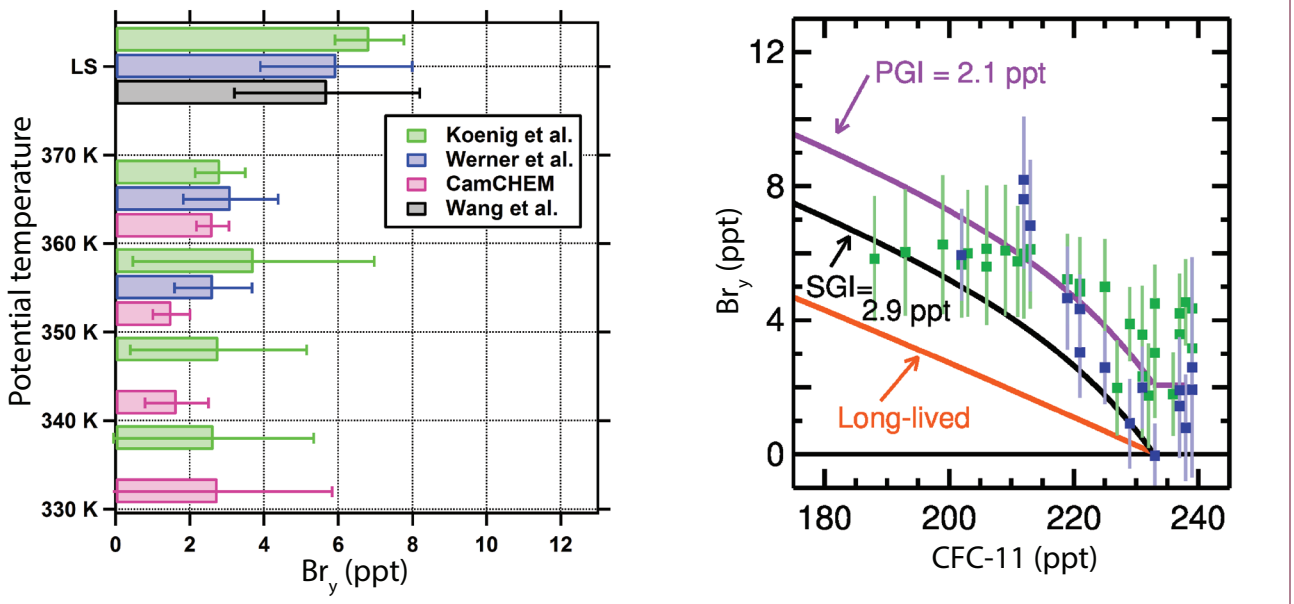

Figure 1-11. *Left panel:* Vertical variation of inferred inorganic bromine (Br_y) from VSLSs within the TTL during the CONTRAST and ATTREX missions (adapted from Koenig et al., 2017). *Right panel:* SGI and PGI inferred from the correlation between stratospheric VSLSs and CFC-11 measured in the Tropical Western Pacific. Inferred Br_y from DOAS (green) and CIMS (blue) instruments are shown, together with the tracer-tracer correlation for VSL SGs (black line) and the SGI + PGI best estimation (purple line). Modified from Wales et al. (2018).

may contribute to PGI. In the last two Assessments, PGI was estimated from $COCl_2$ (up to 32 ppt Cl) and HCl (up to 20 ppt Cl) observations around the LZRH (Brown et al., 2011; Marcy et al., 2007; Mébarki et al., 2010). Since both $COCl_2$ and HCl are also produced from degradation of long-lived ODSs, an unknown amount of these products could be recirculated from the stratosphere into the troposphere. VSLS-derived products were estimated to contribute 0–100%, or ~25 (0–50) ppt, to the observed chlorine PGI (Carpenter and Reimann et al., 2014).

Using a chemical transport model, Hossaini et al. (2015) derived a total VSLS PGI of ~18 (±8) ppt Cl in 2013, with equivalent contributions from $COCl_2$ and HCl and a small contribution from other chlorinated organic PGs that have yet to be observed (~2 ± 0.8 ppt Cl). Simulated chlorinated PGI increased by ~50% between 2005 and 2013, owing to surface trends in SGs, notably CH_2Cl_2, during this period (see **Section 1.3.1.1**, **Figure 1-8**).

All recent studies estimate a non-zero PGI contribution from chlorinated VSLSs. We have therefore increased the lower limit of total chlorine PGI from VSLSs but maintained the upper limit with respect to previous Assessments, giving a best estimate of 25 (8–50) ppt Cl PGI from VSLSs. The lower limit reflects the lower limit from the above modeling work (Hossaini et al., 2015), considering $COCl_2$ and HCl only. This estimate does not include a possible additional chlorine input from ClO or $ClONO_2$, both of which can be strongly influenced by heterogeneous chlorine activation in the upper troposphere and lower stratosphere (Solomon et al., 2016; von Hobe et al., 2011).

PGI from Brominated VSLSs

Several aircraft campaigns targeting brominated PGs in the tropical free troposphere and TTL have been performed since the last Assessment (Chen et al., 2016; Koenig et al., 2017; Le Breton et al., 2017; Volkamer et al., 2015; Wang et al., 2015a; Werner et al., 2017). Bromine monoxide (BrO) and total inorganic bromine (Br_y) mole fractions rapidly increased with altitude, doubling from ~2.5 ppt at the bottom of the TTL to ~5 ppt above the CPT. PGI inferred from BrO (**Figure 1-11**) ranged from 3.4 ± 1.2 ppt within the Tropical Eastern Pacific during ATTREX (Werner et

al. (2017) to 2.7 (2.4–3.0) ppt in the Tropical Western Pacific during CONTRAST (Koenig et al., 2017). Based on the relationship between inferred stratospheric Br_y and CFC-11, measurements obtained during CONTRAST and ATTREX (Wales et al., 2018) estimated a global PGI from brominated VSLSs of 2.1 ± 2.1 ppt (**Figure 1-11**). This is well reproduced by a wide range of Chemistry Climate Models (CCMs), mostly from those considering an explicit treatment of tropospheric chemistry and sources of VSLSs (**Figure 1-11**).

The previous Assessment (Carpenter and Reimann et al., 2014) estimated a global PGI contribution between 1.1 and 4.3 ppt Br, based mainly on global modeling studies that considered only the two major VSL SGs ($CHBr_3$ and CH_2Br_2) and a simplified treatment of gas-phase Br_y speciation and washout (Aschmann and Sinnhuber, 2013; Hossaini et al., 2012; Liang et al., 2014a). New model developments, including a comprehensive heterogeneous recycling scheme on upper-tropospheric ice crystals (**Box 1-3**), suggest a Br_y injection of 3.0 (±1.9) ppt Br in the Eastern Pacific and 2.0 (±0.2) ppt Br in the Western Pacific (Navarro et al., 2015). The contribution from minor VSLSs ($CHBr_2Cl$, $CHBrCl_2$, CH_2BrCl, and CH_2BrI) to PGI was modeled to be ~0.3 ppt Br (Fernandez et al., 2014), which matches the upper limit of previous estimates (Carpenter and Reimann et. al., 2014; Montzka and Reimann et al. (2010).

In summary, there is now consistent observational evidence confirming the prevalence of gas-phase inorganic bromine throughout the free troposphere and TTL. This finding is consistent with previous PGI model estimates and with the amount of bromine required to reconcile Br_y inferred from stratospheric BrO retrievals with the input from long-lived brominated source gases to the stratosphere (see **Section 1.4**). Based on both modeling and measurement studies, our current best estimate of total PGI is thus ~2.7 (1.7–4.2) ppt Br.

PGI from Iodinated VSLSs

The possible injection of significant amounts of inorganic iodine to the stratosphere is under debate. New daytime iodine monoxide (IO) aircraft observations at low solar zenith angles (SZA <45°) within the tropical upper troposphere and lower TTL suggest that significant levels of total reactive iodine (between 0.25 and 0.7 ppt I_y) could be injected to the stratosphere (Saiz-Lopez et al., 2015). This value is 2 to 5 times larger than the recommended PGI upper limit given in the previous Assessment (PGI <0.1 ppt I_y), which was based on balloon-borne solar occultation (SZA ≈ 90°) measurements performed in the tropical lower stratosphere (Bösch et al., 2003; Butz et al., 2009). The discrepancy between the new and previous studies lies in the different chemical scheme used to derive I_y (particularly the treatment of higher-order iodine

Table 1-5. Summary of estimated VSL source gas injection (SGI) and product gas injection (PGI) contributions to stratospheric halogens (based on observations and model results).

VSLS Best Estimate (ppt)	SGI[1]	PGI[2]	Total (SGI + PGI)[3]
Chlorine	92 (75–110)	25 (8–50)	**115 (75–160)**
Bromine	2.2 (0.8–4.2)	2.7 (1.7–4.2)	**5 (3–7)**
Iodine	0–0.1	0–0.7	**0–0.8**

Notes:

[1] Due mainly to the increasing trend in chlorinated compounds, the SGI estimate for chlorinated VSL SGs is representative of year 2016 based on model data (see **Table 1.4**). SGI for bromine and iodine represent the global mean from 2004 onwards as there are no reports of long-term trends.

[2] PGI for chlorine has been estimated based on HCl and $COCl_2$ only (additional input from ClO and $ClONO_2$ has not been considered). PGI for bromine and iodine has been estimated by box- and global-modeling studies based on BrO and IO measurements, respectively.

[3] The SGI and PGI lower/upper limits are not strictly additive because whenever SGI increases (for example due to rapid lifting), the correspondent PGI arising from SG photodecomposition decreases (and vice-versa).

Box 1-3. Heterogeneous Chemistry of Very Short-Lived Product Gases

Atmospheric particles (such as cloud droplets, ice crystals, and aerosols) can affect the tropospheric burden of inorganic product gases (PGs) arising from the degradation of halogenated very short-lived source gases (SGs). The competition, fate, and efficiency of heterogeneous reactions occurring on these particles are still some of the largest uncertainties affecting the stratospheric halogen burden from PGI (Aschmann and Sinnhuber, 2013; Fernandez et al., 2014; Koenig et al., 2017; Liang et al., 2014a; Saiz-Lopez et al., 2015; Schmidt et al., 2016; Wang et al., 2015a).

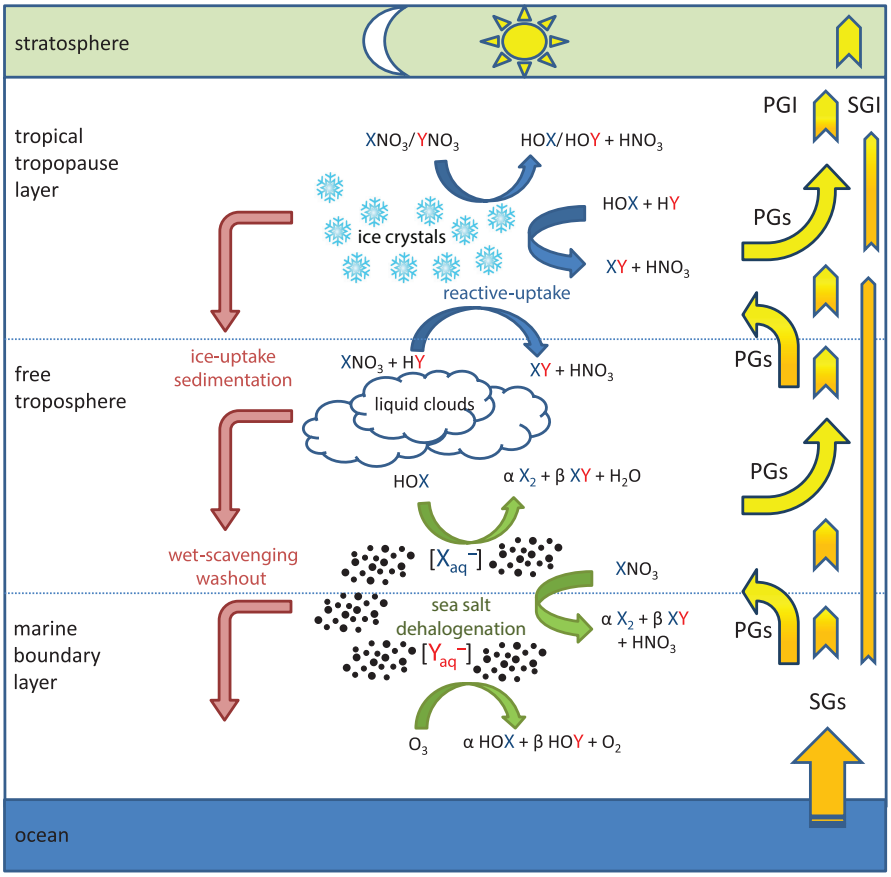

Box 1-3 Figure 1. Schematic representation of tropospheric heterogeneous recycling processes affecting PGI. The upward arrows on the right represent the vertical ascent of halogenated inorganic PGs (yellow) arising from VSL SGs (orange) decomposition. The different transport regimes within each region (e.g., convective lifting and large-scale ascent) are shown by different arrow lengths, while the color gradient indicates the relative SG/PG partitioning. Green arrows indicate the occurrence of sea salt dehalogenation, which constitute an additional source of inorganic PGs (α and β denote the variability in the aerosol enrichment for each halogen family, specified by X and Y). Red downward arrows represent the net sinks of soluble PGs occurring through uptake on liquid/ice clouds followed by precipitation/sedimentation. Blue arrows represent the ice/aerosol mediated repartitioning of inorganic reservoirs, which do not necessarily represent either a net sink or a source of PGs. Note that the distinction of the height at which each heterogeneous process occurs is qualitative, and all processes can occur during the day and night.

Box 1-3, continued.

Oceanic halides comprising the bulk of sea-salt aerosols can be released to the atmosphere as an additional inorganic halogen source through heterogeneous oxidation (**Box 1-3, Figure 1**) (Vogt et al., 1996). The efficiency of this process, usually referred to as sea-salt aerosol dehalogenation, depends on the total halogen fraction prevailing in the aerosol (the so-called enrichment factor), the net rate of gas-phase halogen adsorption and reactive uptake, and the concurrence/collocation of significant sea-salt production and convective transport throughout the troposphere (Yang et al., 2005). Sea-salt recycling has been estimated to provide an additional tropospheric chlorine source of ~5–6 Tg Cl yr^{-1} (Hossaini et al., 2016a; Schmidt et al., 2016) and between 1.4 to 3.5 Tg Br yr^{-1} for the case of bromine (Chen et al., 2017; Fernandez et al., 2014; Parrella et al., 2012; Schmidt et al., 2016; Yang et al., 2005). In the case of bromine, this source has been estimated to be between two and four times larger than the global tropospheric emissions from brominated VSL SGs (Schmidt et al., 2016; Yang et al., 2005). Inclusion of this source in models has helped to reduce differences between models and observations of tropospheric BrO columns densities (Koenig et al., 2017; Schmidt et al., 2016; Wang et al., 2015a).

The processes involved in heterogeneous processing of halogen species are complex. The adsorption followed by effective washout of hydrophilic reservoir species depends on the aqueous/gas-phase partial pressure equilibrium of each individual halogen species (Sander, 2015). However, if the adsorption of reservoirs occurs on top of ice crystals or sulfate/nitrate aerosols, many heterogeneous reactions can proceed (**Box 1-3 Figure 1**), reducing the washout efficiency by transforming the soluble reservoir species into more volatile and photolabile compounds. Inclusion of heterogeneous recycling on ice crystals and upper-tropospheric aerosols has been reported as a necessary process to be considered in box and chemistry-climate models in order to reconcile satellite tropospheric columns with model tropospheric abundances (Parrella et al., 2012; Schmidt et al., 2016), as well as to reproduce the inorganic bromine (Fernandez et al., 2014; Koenig et al., 2017) and iodine (Dix et al., 2013; Saiz-Lopez et al., 2015) vertical profiles throughout the tropical upper troposphere and TTL. Concurrent estimation of gas-phase inorganic PGs and aerosol halide content at high altitudes is required to close the halogen budget in the TTL and lower stratosphere and thus to improve the assessment of PGI. However, as many of the heterogeneous processes are poorly constrained and the uncertainty involved in their parameterization is very large, the evaluation of the overall effect of heterogeneous chemistry on VSLS halogen input to the stratosphere is currently difficult to be quantified.

oxides) as well as on the different temporal field of view (i.e., SZA range) of the measurement technique deployed on each field campaign.

In light of the new results, we cannot provide a central value for iodinated PGI but only a wide interval ranging from zero to an upper limit (0–0.7 ppt I_y). If the maximum PGI value is considered, the impact of iodine on the lower tropical stratosphere could be as large as that of brominated VSLSs.

1.3.2.3 Total Halogen Input into the Stratosphere from VSLSs

Table 1-5 presents the current best estimate of the total injection to the stratosphere from halogenated VSLSs, discriminating SGI and PGI contributions. The relative importance of PGI to SGI depends on the chemical transformation processes during transport from the sources to the stratosphere. The fraction of PGI to total VSLS halogen derived here is higher for bromine than it is for chlorine. While the uncertainty associated with iodine PGI has increased since the previous Assessment, the uncertainty range for the stratospheric flux of organic and inorganic bromine and chlorine has in general been reduced with respect to the previous Assessment.

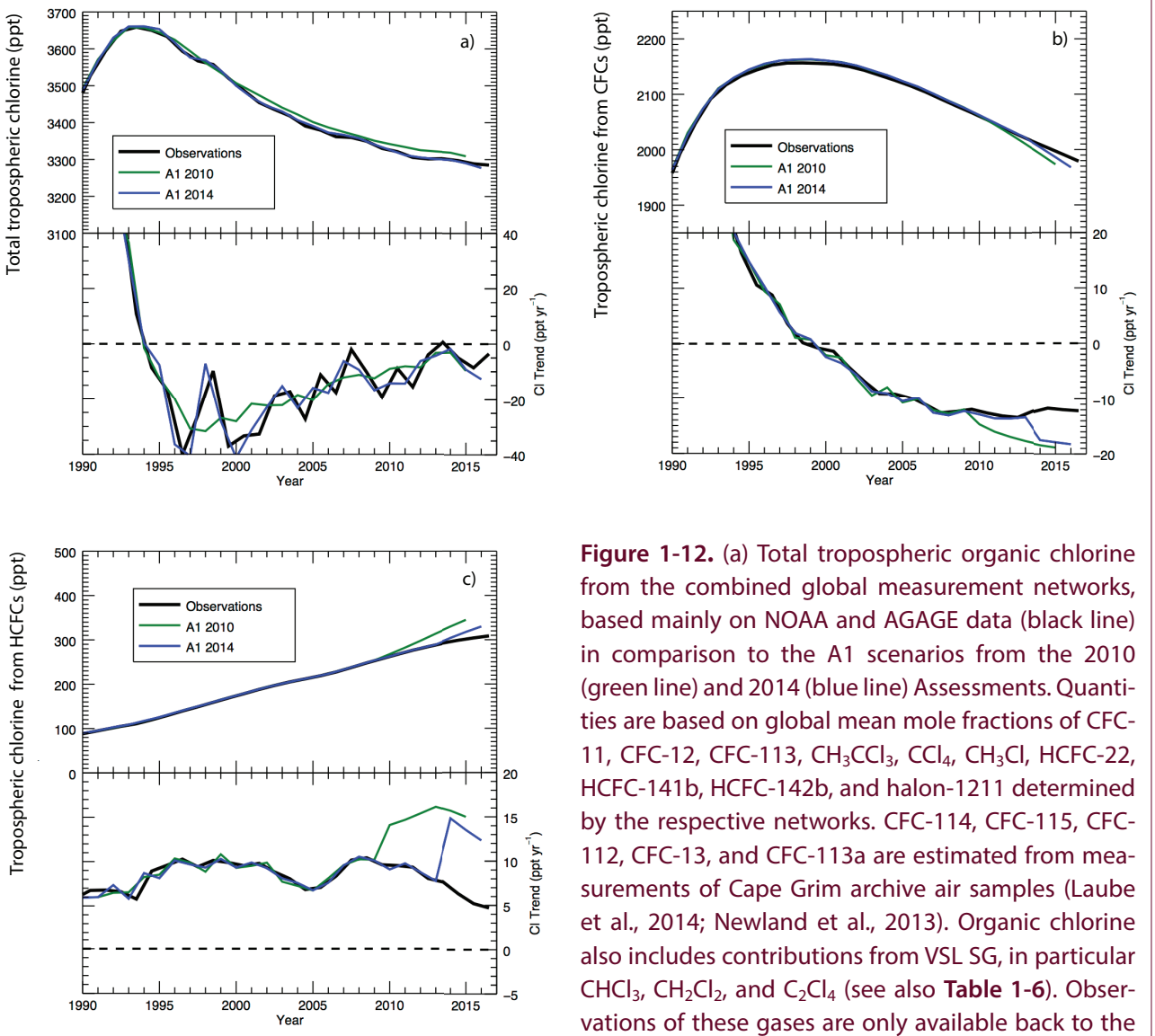

Figure 1-12. (a) Total tropospheric organic chlorine from the combined global measurement networks, based mainly on NOAA and AGAGE data (black line) in comparison to the A1 scenarios from the 2010 (green line) and 2014 (blue line) Assessments. Quantities are based on global mean mole fractions of CFC-11, CFC-12, CFC-113, CH_3CCl_3, CCl_4, CH_3Cl, HCFC-22, HCFC-141b, HCFC-142b, and halon-1211 determined by the respective networks. CFC-114, CFC-115, CFC-112, CFC-13, and CFC-113a are estimated from measurements of Cape Grim archive air samples (Laube et al., 2014; Newland et al., 2013). Organic chlorine also includes contributions from VSL SG, in particular $CHCl_3$, CH_2Cl_2, and C_2Cl_4 (see also **Table 1-6**). Observations of these gases are only available back to the mid-1990s. Before that, constant mixing ratios are assumed. For species which are not included in the scenarios (some minor CFCs and VSLSs), the observed values were included here in order to provide a comparison based on the same set of compounds. (b) and (c) Show the same as panel a for the sum of the tropospheric chlorine contents of the CFCs and the tropospheric chlorine content of all HCFCs, respectively.

Total Input from Chlorinated VSLSs

A "best estimate" of total chlorine (SGI + PGI) from VSLSs reaching the stratosphere is obtained by summing the contribution from individual SGs around the tropopause (**Table 1-4** and **Section 1.3.2.1**) and adding the estimated PG contribution from $COCl_2$ and HCl (see **Section 1.3.2.2).** As explained in **Section 1.3.2.1**, we use model data of SGI, constrained by surface observations (update of Hossaini et al., 2015) here rather than individual campaign observations, since campaign-based estimates are subject to seasonal and regional variability. This yields total Cl from VSLSs entering the stratosphere of 115 (75–160) ppt Cl for 2016 **(Table 1-5)**. This value is very similar to the global average of chlorine VSLSs of 110 ppt derived in **Section 1.4.1.** Around the tropopause, the anthropogenic contribution to the total stratospheric chlorine injection is estimated to be ~85% (**Table 1-4**). The overall

contribution of chlorine from VSLSs has increased to about 3.5% (see discussion in **Section 1.4**).

Total Input from Brominated VSLSs

Various lines of evidence show that brominated VSLSs may provide ~2.2 (0.4–4.2) ppt Br to the stratosphere via SGI and ~2.7 (1.7–4.2) ppt Br via PGI. The best estimate of global stratospheric bromine from VSLSs is ~5 (3–7) ppt Br (see **Table 1.5**), with approximately half due to SGI and half due to PGI. While the central value is unchanged with respect to previous reports, the uncertainty range is reduced based on recent observations and modeling studies. The overall SGI and PGI partitioning is well reproduced by a wide range of Chemistry Climate Models (CCMs), mostly from those considering an explicit treatment of VSL tropospheric chemistry and sources (Wales et al., 2018). Although many of the new aircraft campaigns yielded a total VSLS bromine injection lying in the upper half of the assessed range (Navarro et al., 2015; Werner et al., 2017), this should not be taken as an indication of a positive trend in the contribution from VSLSs to stratospheric Br_y in recent years: Most measurements were performed within regions where the source strength is larger and the vertical transportation of VSLSs is faster. The 5 (3–7) ppt Br global mean also matches the indirect estimate derived from total stratospheric bromine abundances as described in **Section 1.4.** Due to the decline in the abundance of regulated long-lived bromine compounds, the relative contribution of VSLSs to total stratospheric bromine has continued to increase, reaching ~26% by year 2016 (see **Figure 1-17**).

Total Input from Iodinated VSLSs

While the SGI of iodine in the form of CH_3I is expected to be very low (<0.1 ppt), there is a new debate regarding the possible injection of iodine from VSLSs to the stratosphere through PGI. New measurements of IO confirm rather low IO levels, but model calculations suggest an additional impact of higher iodine oxides to the total I_y fraction (Saiz-Lopez et al., 2015). The revised upper limit of total iodine input from VSLSs is therefore extended to 0.8 ppt (0.1 ppt SGI + 0.7 ppt PGI, see **Table 1.5**), which is considerably larger than the upper limit given in previous Assessments (total iodine injection < 0.15 ppt, PGI < 0.1 ppt) (Carpenter and Reimann et al., 2014; Montzka and Reimann et al., 2010).

1.4 CHANGES IN ATMOSPHERIC HALOGENS

In this section we discuss the total halogen loading in the atmosphere and its changes. These are discussed separately for chlorine, bromine, and iodine in **Sections 1.4.1–1.4.3** for the troposphere based on organic sources (ODSs and VSL SGs) and for the stratosphere based on inorganic halogen observations. The total chlorine and bromine input to the stratosphere, including contributions from VSLSs, is then discussed in **Section 1.4.4.** This input should be reflected in inorganic halogen levels, especially in the upper stratosphere, where virtually all halogen has been transferred to the inorganic form. **Section 1.4.4** also discusses equivalent effective stratospheric chlorine (EESC), which is used as a proxy to describe the halogen impact on stratospheric ozone (see **Box 1-4**). EESC does not include contributions from VSLSs. Finally, fluorine, while not contributing to ozone depletion, is discussed in **Section 1.4.5**.

Estimates of tropospheric halogen loading primarily originate from the global surface networks, which are averaged together when mole fractions from multiple networks are available. In general, a simple average is used; however, where data from one network are available for some years but not others, existing network data are scaled to remain consistent with the two-network average (consistent with previous Assessments).

1.4.1 Tropospheric and Stratospheric Chlorine Changes

1.4.1.1 Tropospheric Chlorine Changes

As stated in previous Assessments (e.g., Carpenter and Reimann et. al., 2014; Montzka and Reimann et al., 2010), the total tropospheric chlorine has been decreasing continuously since its peak abundance observed during the years 1993–1994 (**Figure 1-12a**). The maximum annual average total chlorine observed was about 3,660 ppt in 1993. The maximum rate of decrease in total tropospheric organic chlorine was close to 40 ppt yr^{-1} in the years 1995 and 1996, mainly driven by the decrease of the rather short-lived CH_3CCl_3 (lifetime of about 5 years). As expected, the rate of decrease has since slowed and has continued to slow down since the last Assessment. Total chlorine from controlled ODSs declined at an average rate of 12.7 ppt yr^{-1} between early 2012 and late 2016 (**Table 1-6**).

Table 1-6. Contributions of long-lived ODSs and VSL SGs to total chlorine in the troposphere.

	Total Cl (ppt)[1]			Contribution to Total (%)			Average Rate of Change of Total Cl_2 (ppt yr^{-1})		
	2008	2012	2016	2008	2012	2016	2004–2008	2008–2012	2012–2016
All CFCs	2079	2027	1979	62.1	61.4	60.2	–11.6 (1.5)	–12.9 (0.7)	–12.0 (0.4)
CCl_4	359	340	322	10.7	10.3	9.8	–4.4 (0.4)	–4.7 (0.3)	–4.5 (0.2)
HCFCs	248	285	309	7.4	8.6	9.4	9.1 (1.6)	9.2 (0.7)	5.9 (1.3)
CH_3CCl_3	32	16	7.8	1.0	0.5	0.2	–8.3 (2.0)	–4.1 (0.8)	–2.0 (0.5)
halon-1211	4.25	3.96	3.55	0.13	0.12	0.11	–0.02 (0.03)	–0.07 (0.01)	–0.1 (0.01)
Total Controlled Chlorine	2722	2672	2621	81.3	80.9	79.7	–15.2 (1.9)	–12.6 (0.3)	–12.7 (0.9)
CH_3Cl	545	539	556	16.3	16.3	16.9	2.7 (5.2)	–1.8 (4.7)	4.0 (3.6)
VSLSs	82	91	110	2.4	2.8	3.3	2.5 (1.1)	2.6 (3.1)	4.3 (4.9)
Total Chlorine	3349	3302	3287				–10.0 (6.7) (–0.29% yr^{-1})	–11.8 (6.9) (–0.35% yr^{-1})	–4.4 (4.1) (–0.13% yr^{-1})

[1] Chlorine mid-year mole fractions were derived using AGAGE, NOAA, and archive data.

[2] Total and relative Cl changes over 5-year periods, as indicated. The values in parentheses represent the standard deviation of the annual growth rates during the respective period, which reflects the observed variability. Relative changes in total chlorine (in percent per year) were calculated relative to values at the beginning of each period (3,390 ppt total chlorine in 2004). We refer to these periods as 5-year periods, as they are based on annual average values, e.g., from the beginning of 2012 to the end of 2016.

Values for past years differ slightly from previous Assessments because of updated calibration information, different methods for determining global mean mole fractions, rounding errors, and the inclusion of CFC-112 (Kloss et al., 2014) and CFC-113a (Adcock et al., 2018). Total Cl also includes 82, 91, and 110 ppt as VSLSs in 2008, 2012, and 2016, respectively.

This recent decrease of chlorine from controlled substances has been partly offset by an increase in substances not controlled under the Montreal Protocol (e.g., CH_3Cl and VSLSs). In addition to the mainly natural CH_3Cl (which increased at 4.0 ppt yr^{-1}), chlorine from chlorine-containing VSLSs also increased at an average rate of 4.3 ppt yr^{-1} between 2012 and 2016. While chlorine from controlled substances has decreased by 12.7 ppt yr^{-1}, these increases in chlorine from compounds not controlled under the Montreal Protocol have partly offset this decrease, leading to a decrease of total chlorine of only 4.4 ppt yr^{-1} (0.13% yr^{-1}) during this 5-year period. Overall, the fractional contribution of substances not controlled under the Montreal Protocol to total tropospheric chlorine has increased and is now above 20%, mainly due to CH_3Cl (16.9%).

Figure 1-12a compares the observed decrease in total chlorine with the projected trend based on the A1 scenarios from the 2010 and 2014 Assessments. Total chlorine from controlled substances is decreasing at close to the expected overall rate. However, this is partially due to the offsetting effects of a slower than projected increase in HCFCs (**Figure 1-12c**; note that the A1 scenarios for the HCFCs in previous Assessments assumed that Article 5 countries would produce the maximum amount allowed under the Montreal Protocol) and a slower than projected decrease in CFCs (**Figure 1-12b**). This slower than expected decrease in chlorine from CFCs is dominated by CFC-11 but CFC-12 and CFC-113 have also recently contributed to this difference.

1.4.1.2 Stratospheric Chlorine Changes

As mentioned above, total organic chlorine in the troposphere peaked in the early 1990s and has since been declining, although the rate of decline is not constant in time. One would expect a similar global long-term response in stratospheric inorganic chlorine, shifted

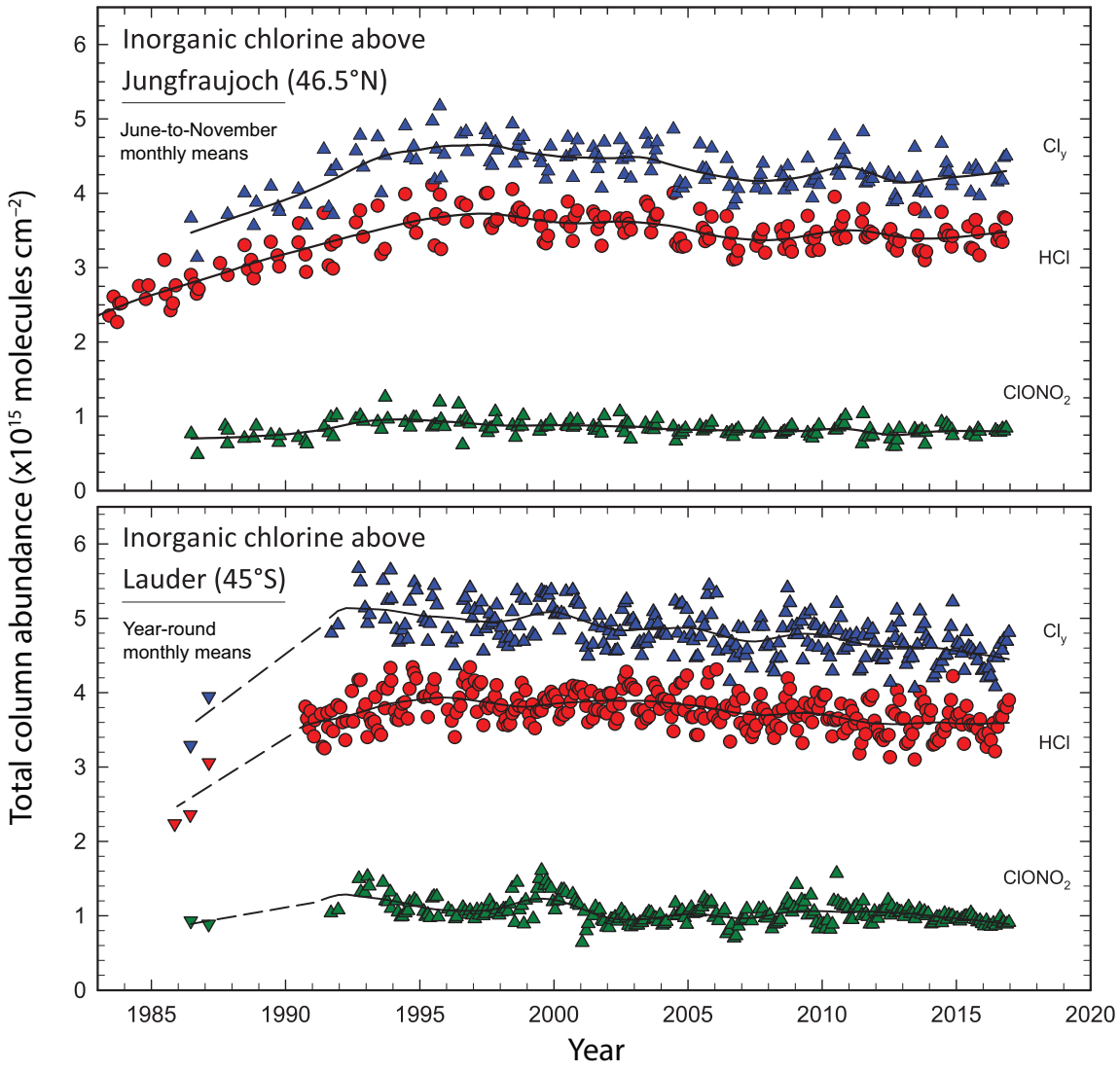

Figure 1-13. Multi-decadal monthly mean total column time series of the two main chlorine reservoirs, HCl and $ClONO_2$, and their summation, as monitored at the Jungfraujoch station (Swiss Alps, 46.5°N, 3,580 m altitude) and the Lauder station (New Zealand, 45.0°S, 370 m altitude), in the framework of the NDACC network. For the Jungfraujoch, in contrast to the data shown in Figure 1-2, the datasets are restricted to the June to November months in an effort to limit the variability caused by atmospheric transport and subsidence during winter and spring. The continuous lines come from non-parametric least-squares fits involving an integration time of about 3 years and help to visualize the non-monotonic and non-linear changes in stratospheric chlorine after the peak from 1996 to 1997.

by a timescale relating to transport into that region (age of air) and photochemical conversion. Significant short-term temporal and latitudinal variability in inorganic chlorine was noted in the lower stratosphere, based on HCl measured from ground-based column data (mostly sensitive to the lower stratosphere) and satellites (Mahieu et al., 2014a). Based on the latter work, increases were observed in total column and lower-stratospheric northern mid-latitude HCl from about 2005 to 2011. These increases were attributed

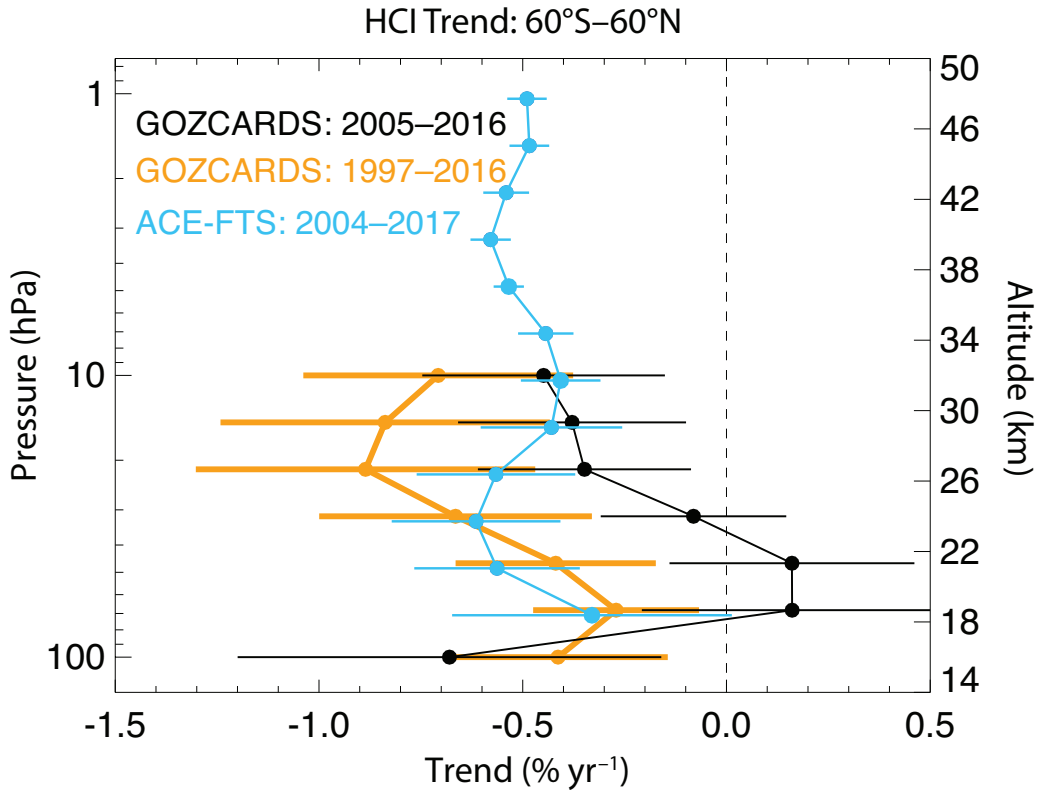

Figure 1-14. Trends (% yr^{-1}) in near-global (60°S to 60°N) HCl abundances, based on different satellite-based datasets and time periods. The longer-term (1997–2016) average linear trend profile (orange dots) is obtained from GOZCARDS merged HCl lower-stratospheric data (updated from Froidevaux et al. (2015), using additional Aura MLS data through 2016). The same dataset is also analyzed for 2005–2016 (black dots). The GOZCARDS trends are derived using a multi-linear regression model that includes seasonal and shorter period cycles, as well as QBO-type variations. The blue dots arise from a linear trend calculation (Bernath and Fernando, 2018) for a seasonally-averaged (and de-seasonalized) ACE-FTS time series (60°S to 60°N, 2005 through 2017) based on version 3.5/3.6 data; these trends do not change appreciably if the 2005–2016 period is used instead. The ACE-FTS trend errors are 2-sigma estimates, taking into account the auto-correlation of the residuals. The GOZCARDS error bars provided here are 2-sigma estimates, based on a bootstrap resampling method (using 20,000 resampling cases from blocks of data).

to variability in the circulation affecting the Northern Hemisphere. **Figure 1-13** shows an update to the long-term total column data for HCl and $ClONO_2$ and their sum, which represents most of the inorganic chlorine in the stratosphere, at Jungfraujoch (46.5°N) and at Lauder (45°S), through the end of 2016. At the Jungfraujoch station, statistically significant decreases are observed for both species for the period from 1997 through 2016: –0.42±0.23% yr^{-1} for HCl and –0.60±0.39% yr^{-1} for $ClONO_2$ (based on June to November data; updated from Mahieu et al., 2014a). The trend over the past decade is, however, not significant. Similar trends have been reported for the mid-latitudes of the Northern Hemisphere from other NDACC (Network for the Detection of Atmospheric Composition Change) stations (Kohlhepp et al. (2012). For the same period (1997–2016), slightly larger negative trends are derived from the Lauder data (including all months) for the Southern Hemisphere, with a decrease of –0.51 ± 0.12% yr^{-1} for HCl and –0.74 ± 0.59% yr^{-1} for $ClONO_2$. HCl from the Global Ozone Chemistry And Related trace gas Data records for the Stratosphere (GOZCARDS), based on the HALOE, ACE-FTS, and Aura MLS satellite instruments (Froidevaux et al., 2015), shows similar trends (1997–2016) for Northern Hemisphere mid-latitudes.

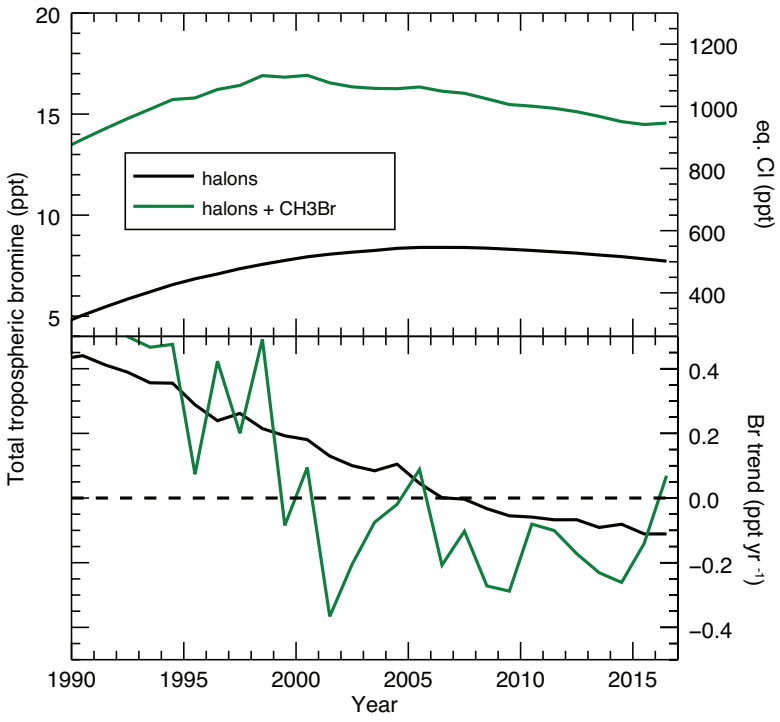

Figure 1-15. Tropospheric bromine time series and annual changes from long-lived gases, separated by contributions due to halons and CH_3Br. No contribution from VSLS species is included here. The values are also shown expressed in equivalent chlorine (right-hand axis of upper panel), adapting a value of α=65 to account for the higher efficiency of bromine in catalyzing ozone destruction. All values are derived from a merged dataset based on NOAA, AGAGE, and UEA data.

GOZCARDS also shows latitude-dependent, short-term lower-stratospheric HCl changes (for different 6- to 8-year periods), with steadier/larger decreases at southern latitudes contrasting with increases at northern mid-latitudes.

Near-global (60°S–60°N) trends of HCl from GOZCARDS and ACE-FTS are compared for the 12-year period 2005–2016 in **Figure 1-14**. While GOZCARDS is dominated by MLS results, as a merged satellite product it also contains some information from ACE-FTS, so the two estimates are not completely independent. ACE-FTS shows a decrease in the uppermost stratosphere at a rate of about –0.48 ± 0.02% yr^{-1} (Bernath and Fernando, 2018) and good agreement with the GOZCARDS result near 10 hPa. Taking into account the time shift between the troposphere and the upper stratosphere of about 5 years, this rate of decrease is in good agreement with the average rate of decrease in tropospheric chlorine over the time period from 2000–2010. There is increasing divergence between these two satellite-based datasets at the lower altitudes, although not significant at the 2-sigma level. In the ACE-FTS trend calculation, dynamical variability has been removed based on a regression model using N_2O time series (Stolarski et al., 2018). Such a procedure was not applied to the GOZCARDS results in **Figure 1-14**, but it would likely reduce the differences in lower-stratospheric trends versus the ACE-FTS result. Sampling differences between MLS and ACE-FTS, and instrument or retrieval issues, could also play a role in explaining these differences. Long-term changes in HCl could also be influenced by changes in stratospheric dynamics and chlorine partitioning, especially in the ratio between $ClONO_2$ and HCl. There is also evidence for significant latitudinal differences in the trends obtained from various FTIR column $ClONO_2$ time series (Kohlhepp et al., 2012), although the ratio between HCl and $ClONO_2$ at Jungfraujoch does not show any significant trend within the 95% confidence interval. Variability in atmospheric circulation has been suggested as a reason for the lack of a significant trend at Northern Hemisphere mid-latitude HCl over the past decade (Mahieu et al., 2014a). This is corroborated by observed changes in the mean age of air in Northern Hemisphere mid-latitudes over the same time period (Haenel et al., 2015; Stiller et al., 2012) and smaller

than expected trends in source gases (Chirkov et al., 2016; Nedoluha et al., 2015).

We conclude that, despite some complications in the lower-stratospheric HCl measurement comparisons, there is continuing evidence for locally non-monotonic latitude-dependent HCl changes in this region, with a slowdown in the decrease of lower-stratospheric HCl since the initial period (about 1997–2005) after its peak concentrations. Upper-stratospheric HCl (close to the abundance of inorganic chlorine, Cl_y) is continuing to decrease steadily, based on ACE-FTS HCl data.

Other evidence for continuing decreases in stratospheric inorganic chlorine comes from ground-based and satellite ClO measurements over Antarctica (Nedoluha et al., 2016). ClO trend detection in this region is complicated by large, meteorologically driven, interannual variability. Temperature-adjusted ClO (as a rough proxy for Cl_y) over that region shows a trend from the Scott Base data of –0.6 ± 0.8 (2 sigma) % yr^{-1} for 1996–2015 and –0.5 ± 0.4% yr^{-1} for 2004–2015 as measured zonally by Aura MLS at the Scott Base latitudes. Based on millimeter-wave emission measurements at Mauna Kea, Hawai'i, ClO near 33–37 km continued to show decreases (Connor et al., 2013). Updated ClO trends (from day-minus-night data) are as follows: –1.08 ± 0.40% yr^{-1} for the early period from 1995 to 2004 (unchanged from the above reference), –0.49 ± 0.12% yr^{-1} for 1995–2015, and –0.32 ± 0.26% yr^{-1} for the 2005–2015 period, 2-sigma uncertainties. To first order at least (since upper-stratospheric ClO is not an exact proxy for Cl_y), these results suggest broad agreement, with other evidence pointing to a continuing decrease with a gradual slowdown in the rate of decrease in stratospheric (and tropospheric) chlorine.

1.4.2 Tropospheric and Stratospheric Bromine Changes

1.4.2.1 Tropospheric Bromine Changes

As stated in previous Assessments, total tropospheric bromine from CH_3Br and halons, the brominated substances controlled under the Montreal Protocol, reached a maximum in 1998 with an annual average value of 16.9 ppt. Since 1998, its abundance has been decreasing at an average rate of 0.15 ± 0.1 ppt yr^{-1} (1% yr^{-1}) over the period from 2000 to 2016 (**Figure 1-15**), reaching a value of 14.6 ppt by mid-2016. This value does not include bromine from VSLSs, such as CH_2Br_2 and $CHBr_3$, which are not regulated under the Montreal Protocol. While bromine from CH_3Br has been decreasing since the late 1990s, bromine from halons did not start to decrease until 2006. For the period from 2008 to 2012, total bromine decreased at a rate of 0.16 ppt yr^{-1}. Halons contributed ~38% to this decline, while CH_3Br contributed ~62%. In the more recent period from 2012 to 2016, total bromine declined at a rate of 0.15 ± 0.04 ppt yr^{-1} (1% yr^{-1}). However, the contributions of halons and CH_3Br were nearly reversed compared to the previous period: halons contributed ~70% (–0.10 ppt yr^{-1}), while CH_3Br contributed ~30% (–0.04 ppt yr^{-1}). For the first time, the decrease in total bromine over the past 5-year period was thus not dominated by a decrease in CH_3Br but rather by a decrease in halons. The reduced contribution of CH_3Br to the decline in total bromine was caused by an as-yet-unexplained increase in CH_3Br in 2016 (see **Section 1.2.7**). The observed decrease in halons is in overall good agreement with the decrease projected by the A1 scenarios from the 2014 Assessment (Harris and Wuebbles et al., 2014).

1.4.2.2 Stratospheric Bromine Changes

Bromine is transported to the stratosphere in the form of long-lived ODSs, mainly the halons and CH_3Br as well as from VSLSs, both in organic and inorganic forms. In general, the amount of bromine in the stratosphere can either be determined by summing up the long-lived ODSs and VSLSs (Brinckmann et al., 2012; Navarro et al., 2015; Pfeilsticker et al., 2000; Sala et al., 2014; Wamsley et al., 1998) or by combining measurements of BrO with a modeled ratio of BrO/Br_y (Dorf et al., 2006; Dorf et al., 2008; Höpfner et al., 2009; Kreycy et al., 2013; Millán et al., 2012; Stachnik et al., 2013; Werner et al., 2017). Br_y is the sum of all inorganic bromine species. The BrO-based method will also yield an estimate of total bromine if the measurements are performed in the upper stratosphere, where all organic long-lived ODSs and VSL SGs are broken down and all bromine is thus in the inorganic form. If this method is applied in the lower stratosphere, additional measurements of the remaining long-lived ODSs and VSL SGs are needed to determine total bromine (Wales et al., 2018; Werner et al., 2017).

In the case of the source gas-based technique, the determination of the contribution from the long-lived

ODSs is straightforward, as they are sufficiently long-lived to be transported into the stratosphere and their stratospheric entry mole fraction can thus be estimated using the global mean from the observational networks (see **Sections 1.2** and **1.4.2.1**). For the contribution from the VSLS gases, both organic (SGI) and inorganic (PGI) forms need to be considered. The sum of these two was assessed to be 5 (3–7) ppt in **Section 1.3** (see **Table 1-5**). As there is no indication of a long-term change in this value, total organic bromine input to the stratosphere is thus derived by adding 5 ppt to the respective sum of the long-lived source gases.

Figure 1-16 compares studies that have used the BrO-based technique, based on total column and vertically resolved measurements, with source gas observations of CH_3Br and halons. **Figure 1-16** is an update

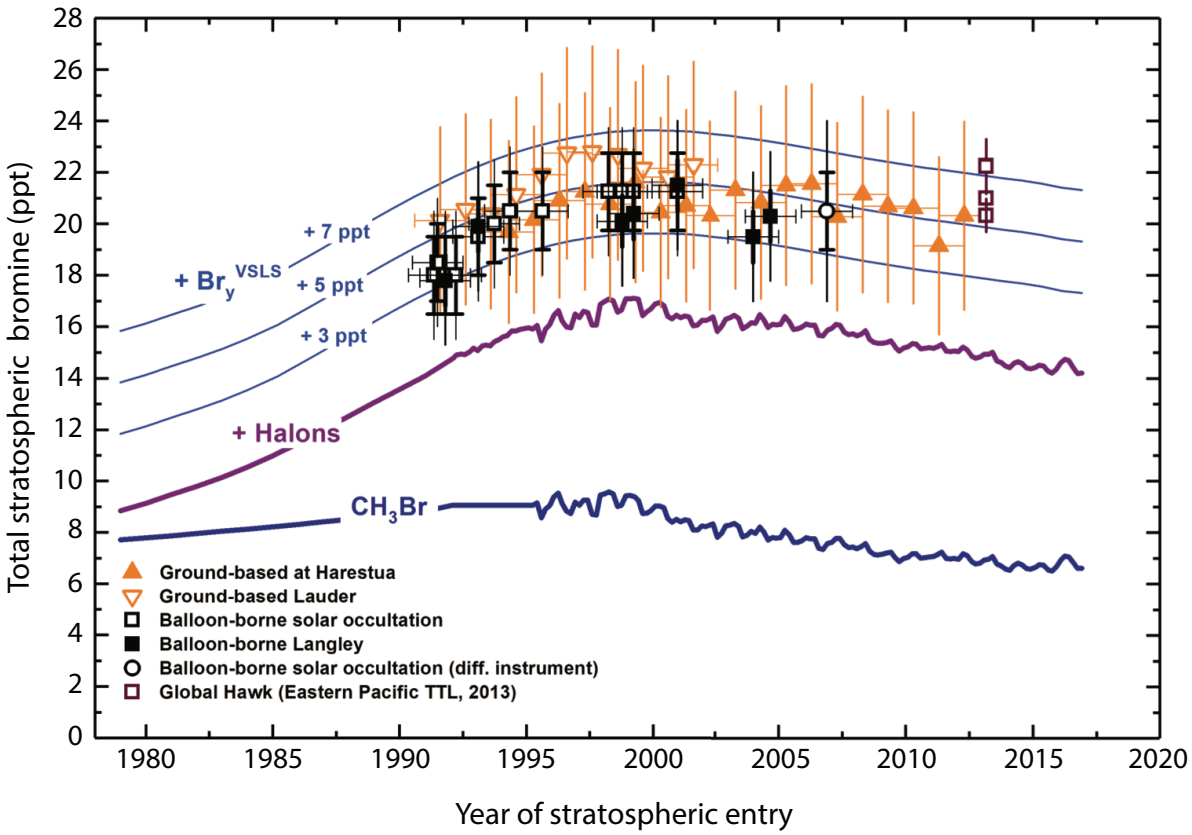

Figure 1-16. Changes in total stratospheric Br_y (ppt) derived from balloon-borne (black squares) (update of Dorf et al., 2006) and airborne (purple open squares) (Werner et al., 2017) BrO observations and annual mean mole fractions calculated from ground-based UV-visible measurements of stratospheric BrO made at Harestua (60°N) and Lauder (45°S) stations (filled and open orange triangles, respectively (adapted from Hendrick et al., 2007 and Hendrick et al., 2008). All UV-visible measurements of stratospheric BrO were evaluated using a common BrO absorption cross section (based on Wahner et al., 1988), frequency-shifted to match the wavelength scale (Wilmouth et al., 1999). For the balloon-borne observations, bold/faint error bars correspond to the precision/accuracy of the estimates, respectively. For the ground-based measurements (triangles), the error bars correspond to the total uncertainties in the Br_y estimates. For stratospheric data, the date corresponds to the time when the air was last in the troposphere, i.e., sampling date minus estimated mean age of the stratospheric air parcel. Time series of CH_3Br and halons have been updated (see Carpenter and Reimann et al. (2014) for details). The blue lines show the expected stratospheric Br_y, assuming an additional input of 3, 5, and 7 ppt of brominated VSLSs, respectively. For tropospheric data, the date corresponds to the sampling time. This figure updates Figure 1-20 from the previous Assessment (Carpenter and Reimann et al., 2014).

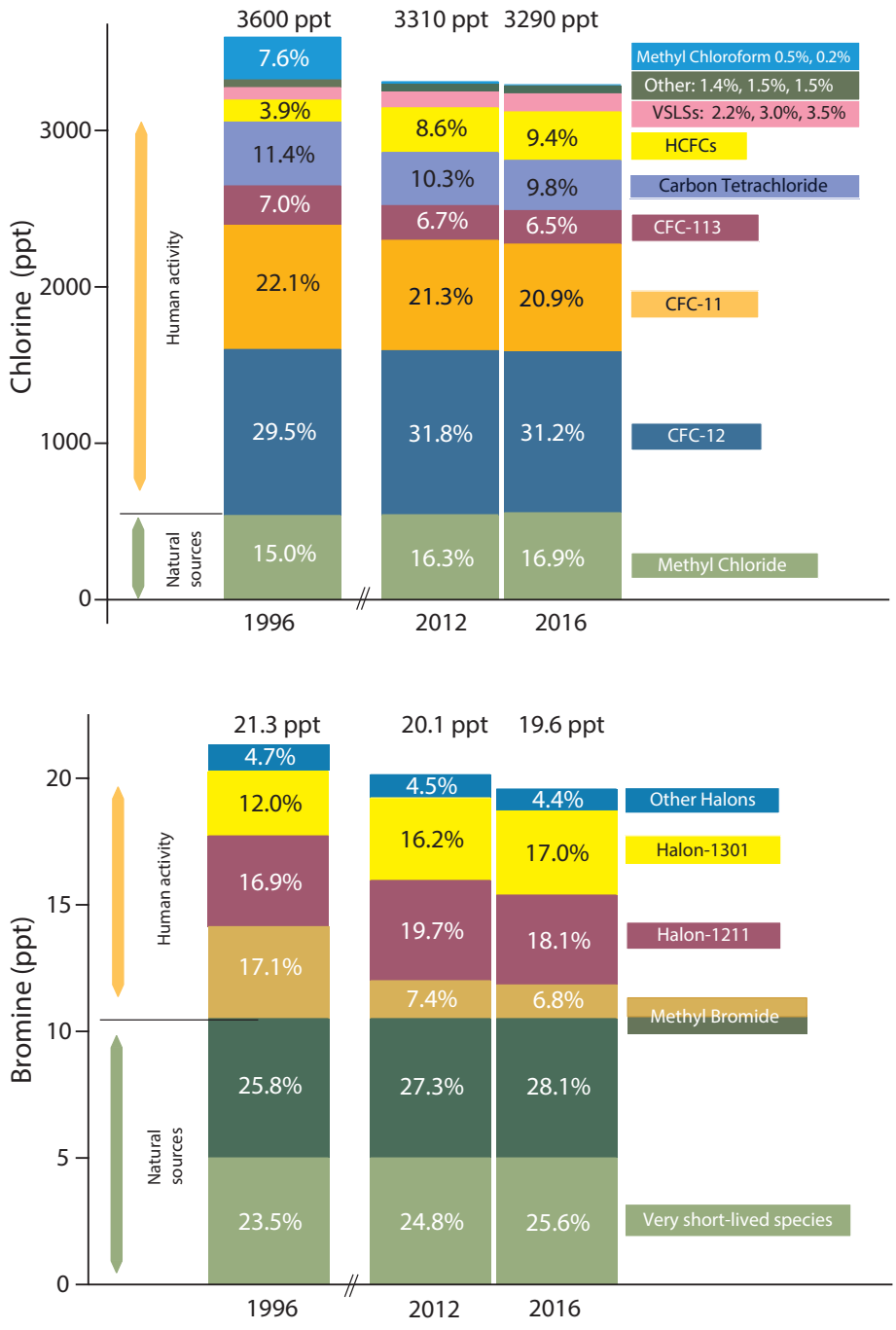

Figure 1-17. Chlorine and bromine input to the stratosphere for 1996, 2012, and 2016 for different species and classes of compounds. The year 1996 represents a reference which is close to the maximum of both chlorine and bromine loading of the troposphere. Mole fractions of long-lived gases are derived from surface observations (global networks). VSLS contributions for bromine are included as a constant 5 ppt, as discussed in **Section 1.3** and summarized in **Table 1-5.** The VSLS chlorine contribution is based on the VSL SG input from a model constrained by observed surface boundary conditions (update of Hossaini et al., 2015), see discussion in **Section 1.3.2.1**). Total VSLS Cl input derived in this way is 80 ppt, 100 ppt, and 115 ppt for years 1996, 2012, and 2016, respectively. For chlorine, "other" includes minor CFCs and halon-1211. For bromine, "other halons" is the sum of bromine contained in halon-1202 and halon-2402. Methyl chloride is counted as having purely natural sources, despite some indications of anthropogenic contributions (see **Section 1.2.6**).

of data presented in the last Assessment (Carpenter and Reimann et. al, 2014; Dorf et al., 2006; Hendrick et al., 2008; Hendrick et al., 2007) and includes new data from the ATTREX campaign (Werner et al., 2017). The stratospheric data are plotted against the "year of stratospheric entry" (respective air mass age) in order to take into account the time to transport air upward in the stratosphere, as characterized by the mean age of air. From these data, a long-term decrease of stratospheric bromine of –0.16 ± 0.07 ppt yr^{-1} is derived for the period from 2004 to 2014, in excellent agreement with the trend in tropospheric bromine derived for the same time period. A value of 19–20 ppt for total bromine in the stratosphere is deduced for the year 2016, in good agreement with the bottom-up method if an input of about 5 ppt from VSLSs (sum of PGI and SGI) is added to the long-lived ODSs. This good agreement enhances the confidence in our overall understanding of bromine input to the stratosphere due to VSLSs. It should also be noted that due to the decline in the compounds regulated under the Montreal Protocol, less than 50% of bromine entering the stratosphere is now due to anthropogenic emissions.

1.4.3 Tropospheric and Stratospheric Iodine Changes

The main organic source gas for iodine is CH_3I. There are no updated data on tropospheric trends since those published by Yokouchi et al. (2012), and there is consensus that the direct input of CH_3I to the stratosphere is small, i.e., below 0.1 ppt (Carpenter and Reimann et al., 2014; Tegtmeier et al., 2013). Observations also agree on the amount of IO in the TTL, which is on the order of 0.15 ppt or less (Bösch et al., 2003; Butz et al., 2009; Dix et al., 2013; Saiz-Lopez et al., 2015). The recent debate about the possibility of a higher PGI to the stratosphere of up to 0.7 ppt (Saiz-Lopez et al., 2015) (see Section 1.3) does not concern a long-term change but rather a different partitioning of total iodine to IO. If the mechanism suggested by Saiz-Lopez et al. (2015), involving higher oxides of iodine, is effective, this would imply a higher iodine content of the stratosphere but not necessarily a long-term change.

1.4.4 Changes in Ozone-Depleting Halogen Abundance in the Stratosphere

Chlorine and Bromine Input to the Stratosphere

Due to the regulations of the Montreal Protocol, many long-lived ODSs that contribute chlorine and bromine to the stratosphere are now decreasing in the atmosphere. Aside from some minor CFCs (**Table 1-1**), the exception to this are HCFCs, which are still increasing, though the rates of increase are slowing down (see **Section 1.2**). On the other hand, chlorinated VSL SGs have shown significant increases during the past decade. This has resulted in changes in the total burden and the relative contributions of different species to total chlorine and bromine in the troposphere and thus to the input of halogens to the stratosphere. **Figure 1-17** shows the changes in total bromine and total chlorine input to the stratosphere. This input is derived by assuming that the global average values derived for long-lived compounds are representative of the amount transported to the stratosphere. For chlorine and bromine from short-lived substances, VSLS input is included from measurements and modeling at the tropical tropopause, as discussed in **Section 1.3** and shown in **Table 1-5**, considering both source gas injection (SGI) and product gas injection (PGI). For bromine, the absolute contribution from VSL SGs is constant, but the relative contribution is increasing, reaching about 25% in 2016. For chlorine, both the absolute and relative contribution of VSL SGs is increasing, although the relative contribution remains small compared to bromine, at 3.9% in 2016. For both bromine and chlorine, there have been no signs of significant long-term changes in the natural sources, so the absolute contributions of natural sources to stratospheric chlorine and bromine remain constant, but their relative contribution is increasing. In the case of bromine, it is now estimated that more than half of the stratospheric bromine input is due to natural sources.

Equivalent Effective Stratospheric Chlorine (EESC)

While the total amount of chlorine and bromine transported to the stratosphere is important, the most relevant metric for the impact on stratospheric ozone is the inorganic halogen loading. The inorganic halogen loading depends not only on the amount of

Box 1-4. Equivalent Effective Stratospheric Chlorine (EESC) and Fractional Release Factors

EESC is a metric used to describe the combined impact of chlorine and bromine on stratospheric ozone and the temporal development of this effect due to tropospheric trends. The basic concept of EESC, as well as that of fractional release factors, which are needed for the calculation of EESC, has been presented and discussed in previous Assessments (Daniel and Velders et al., 2011; Harris and Wuebbles et al., 2014). EESC is expressed as an equivalent chlorine and is commonly defined as "the sum of the time-dependent chlorine and bromine derived from ODSs tropospheric abundances, weighted to reflect their potential influence on ozone" (Harris and Wuebbles et al., 2014). EESC is derived from observed or projected tropospheric mole fractions of ODSs. The calculation of EESC does not take into account changes in stratospheric transport or photochemistry. Therefore, it is important to emphasize that any discussion of EESC changes and

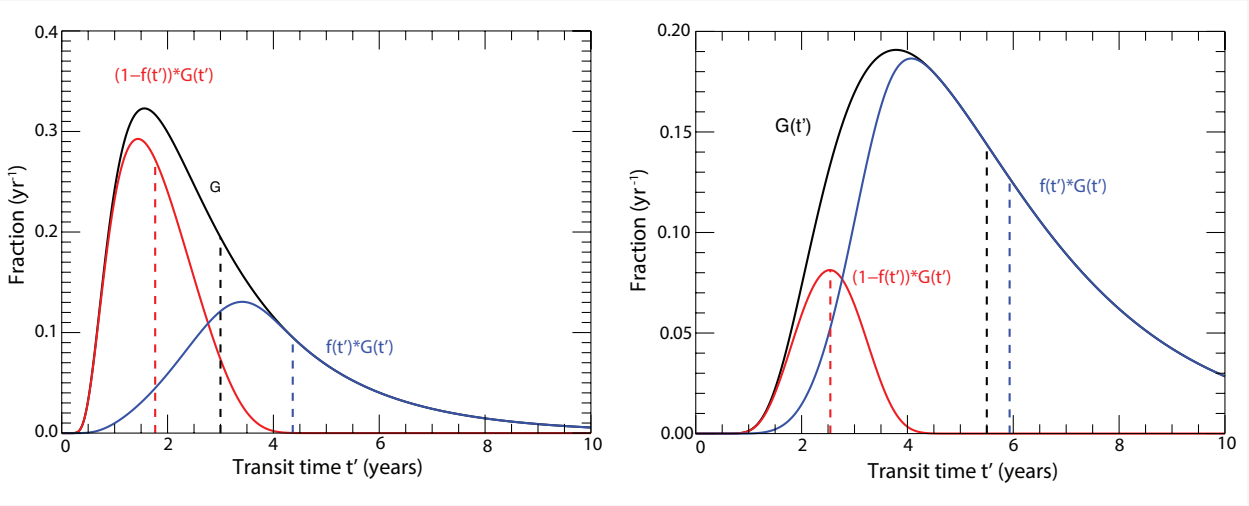

Box 1-4 Figure 1. Age spectra G (black line) for an inert tracer compared to the transit time distributions weighted with chemical loss (red and blue line) for a mean age of 3 years (a), and 5.5 years (b). The red line represents the transit time distribution for the remaining organic fraction of a source gas; the blue line represents the fraction which has been released and is thus in the inorganic form. The loss function has been approximated as a function of transit time in order to represent a tracer similar to CFC-11 (Engel et al., 2018). The first moments of the three functions differ substantially: the first moment of the red curve (representing the remaining organic fraction) is younger, and that of the blue curve (describing the inorganic halogen released from the source gas) is older than the mean age value. Note that this figure is purely for illustrative purposes, as the loss function has been approximated.

percentage reductions of EESC does not imply a similar response of ozone. Such a relationship between EESC and ozone would only be expected in the absence of any other factors influencing ozone. The formulation used in the previous Assessments to calculate EESC was based on Newman et al. (2007), which takes into account the time delay and mixing during transport in the stratosphere by adapting an age spectrum. For polar winter conditions, a mean age value of 5.5 years is used, and a value of 3 years is adapted for mid-latitudes, in line with previous Assessments. The efficiency with which each chlorine or bromine compound releases their halogen content is taken into account using age-of-air-dependent fractional release factors in the calculation of EESC. These fractional release factors describe the fraction of a halogen-carrying source gas that is photochemically lost as a function of mean age. Fractional release factors are higher for 5.5 years of mean age, leading to overall higher values of EESC under polar winter conditions in comparison to mid-latitude conditions.

Box 1-4, continued.

Fractional release factors are mostly derived from observations, again taking into account the age spectrum to compensate for the time-lag between the troposphere and the stratosphere and the tropospheric trends. Fractional release factors should be constant in time as long as stratospheric transport and chemistry do not change, thus representing a molecular property for a given atmospheric state. In particular, they should be independent of the tropospheric trend of a trace gas; i.e., fractional release factors derived during different periods should be very similar, as atmospheric transport is expected to change much less rapidly than tropospheric trends of the source gases. It has recently been shown by Ostermöller et al. (2017) that this is not the case for the current formulation used to calculate fractional release factors (Newman et al., 2007), because the age spectrum used to calculate fractional release is that of an inert tracer and does not take into account chemical loss. Based on the work of Plumb et al. (1999), Ostermöller et al. (2017) suggested that a different transit time distribution should be used to better take into account the interaction of tropospheric trends, chemical breakdown, and stratospheric transport. They presented a new method to calculate fractional release based on a different age spectrum, which is weighted by the chemical loss. As discussed by Engel et al. (2018), the actual loss function will depend on both transit time and the transport pathway of the individual fluid elements of an air parcel, with transport pathways that reached higher altitudes generally showing larger fractional loss. Nevertheless, it has been shown (Engel et al., 2018) that when describing the loss only as a function of transit time, a much better agreement between EESC calculated from model-derived fractional release factors and inorganic halogen loading from model calculations can be achieved. **Box 1-4 Figure 1** shows age spectra for mean ages of 3 and 5.5 years for a compound with a loss function $f(t')$ approximated as function of transit time t' which is approximately representative of CFC-11. As chemical loss is more pronounced in the fraction having long transit times, the transit time distribution describing the remaining organic fraction is weighted more strongly at shorter transit times and thus has a lower mean value. The mean value of this distribution has been termed the "mean arrival time" (Plumb et al., 1999); and the distribution itself, the "arrival time distribution." Using this formulation, fractional release factors can be derived that are largely independent of the tropospheric trend (Ostermöller et al., 2017).

Based on the same concept that the age spectrum is weighted with chemical loss, Engel et al. (2018) showed that the calculation method for EESC could also be improved. While the arrival time distribution used to describe the remaining organic fraction is weighted with the remaining fraction $(1–f(t'))$ (red curve in **Box 1-4 Figure 1**), the fraction describing the released inorganic halogen fraction is weighted with the loss function $f(t')$ (blue curve in **Box 1-4 Figure 1**). The transit time distribution describing the released inorganic halogen has been termed the "release time distribution," in analogy to the arrival time distribution, and its first moment has been termed the "mean release time." The mean release time will always be longer than the mean age.

In this Assessment we present results for EESC from the method presented by Newman et al. (2007) and the method suggested by Engel et al. (2018).

source gases transported into the stratosphere but also on the efficacy with which halogens are released from the source gases. Furthermore, both transport from the troposphere to the stratosphere and transport and mixing in the stratosphere need to be considered, with timescales for the latter being on the order of several years. The different efficiencies with which ODSs and VSLSs release their halogen content are described by *fractional release factors*. Stratospheric transport and mixing are described by an *age-of-air spectrum*. While mean age is the average time it takes for an air parcel to be transported from the troposphere to a certain location in the stratosphere, this age spectrum describes the probability distribution for different transit times. Furthermore, it has to be taken into account that bromine is a much more effective

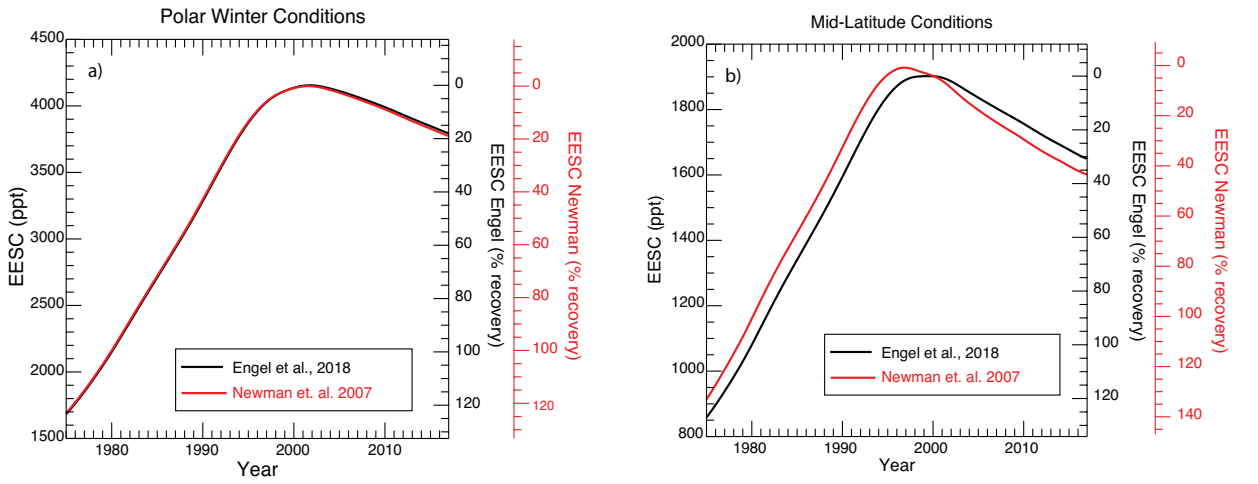

Figure 1-18. Level of EESC recovery towards 1980 benchmark values comparing the EESC calculation as used in the 2014 Assessment (Carpenter and Reimann et al., 2014; Newman et al., 2007) to the new method suggested by Engel et al. (2018). Plot (a) is for 3 years of mean age, representative of mid-latitude conditions, while plot (b) is for 5.5 years of mean age, representative of polar winter conditions. In all cases, the different age spectra (see **Box 1-2**) were parameterized as suggested by Newman et al. (2007) using half of the mean age as width of the age spectrum and an inverse Gaussian function as the shape of the age spectrum. The age spectrum has been integrated over a time period of 20 years. Fractional release factors were used as in the last Assessment report and in Velders and Daniel (2014) for the formulation according to Newman et al. (2007). In the calculation using the formulation suggested by Engel et al. (2018), the same fractional release factors were used, but these were modified to be consistent with the formulation of fractional release suggested by Ostermöller et al. (2017), as explained in Engel et al. (2018). The same tropospheric data were used as in **Section 1.4.1.1** and **Section 1.4.2.1**. VSLS contributions to EESC are not included in this calculation. In the calculation of EESC, the higher efficiency of bromine to destroy stratospheric ozone is taken into account. As in previous Assessments, we adopt a factor of 60 for mid-latitude conditions and a factor of 65 for polar winter conditions.

Table 1-7. EESC values for early 1980 and early 2017 as well as the value when EESC was at its maximum. Values are given for 3 and 5.5 years of mean age and for the two calculation methods discussed (see text in **Section 1.4** for details). Also shown are decreases achieved by early 2017 with respect to the maximum and the percent recovery with respect to the 1980 values. The calculated decreases and recovery rates for 3 years of mean age are significantly smaller using the new method of Engel et al. (2018) than when using the Newman et al. (2007) method.

3 Years of Mean Age; Mid-Latitude Conditions					
	EESC 1980	EESC maximum	EESC early 2017	% decrease from maximum	% Recovery to 1980
Newman et al. (2007)	1161	1928	1601	–17%	43%
Engel et al. (2018)	1080	1902	1649	–13%	31%
5.5 Years of Mean Age; Polar Winter Conditions					
	EESC 1980	EESC maximum	EESC early 2017	% decrease from maximum	% Recovery to 1980
Newman et al. (2007)	2161	4148	3774	–9%	19%
Engel et al. (2018)	2151	4154	3794	–9%	18%

ozone destruction catalyst than chlorine. As in previous Assessments, we adopt a factor of 60 for mid-latitudes and 65 for high-latitude polar winter conditions for the relative efficiency of bromine versus chlorine with respect to ozone destruction. These factors are combined in the metric of equivalent effective stratospheric chlorine (EESC). New formulations to derive fractional release factors (Ostermöller et al., 2017) and EESC (Engel et al., 2018) have recently been proposed (see **Box 1-4**), with a refined treatment of the interaction between chemistry and transport. In the past, different fractional release factors have also been used, mainly based on work by Newman et al. (2007) and Laube et al. (2013). The work by Laube et al. (2013) has recently been re-evaluated using a new method (Ostermöller et al., 2017) and taking into account possible offsets in mean age of air in this work due to the use of SF_6-derived mean age (Leedham Elvidge et al., 2018). With this there is much better agreement with the fractional release values used in (Engel et al., 2018; Newman et al., 2007; Velders and Daniel, 2014) and recent WMO reports.

A refinement in the method to calculate EESC has recently been suggested by Engel et al. (2018). The concept of EESC, the methods of calculation, and the changes in the concept suggested by Engel et al. (2018) are explained in **Box 1-4**. Here, we will present results from both methods. Significant differences in these methods are derived for mid-latitude conditions only, while for polar winter conditions both methods yield very similar results. We have retained the same parameterization of the age spectrum as in previous Assessments; i.e., the width of the distribution is taken as half the value of the mean age. Here, we integrate the age spectrum over 20 years instead of 10 years, as was done in the previous Assessment. As can be seen in **Box 1-4 Figure 1**, a significant fraction of air has transit times greater than 10 years for a mean age of 5.5 years. We use a 20-year integration period to better account for all contributing air parcels.

The different methods in how EESC is calculated, and the integration periods considered, result in slightly different maximum EESC values as well as different benchmark values calculated for the year 1980. EESC in 1980 has been used as a benchmark in many previous Assessments, although this is certainly somewhat arbitrary, as ozone loss occurred prior to 1980. We also note that a return to 1980 EESC levels does not imply a recovery of the ozone layer to the 1980 state, as ozone is influenced by additional parameters like changes in stratospheric dynamics and chemistry. Independent of the formulation used to calculate EESC and the time

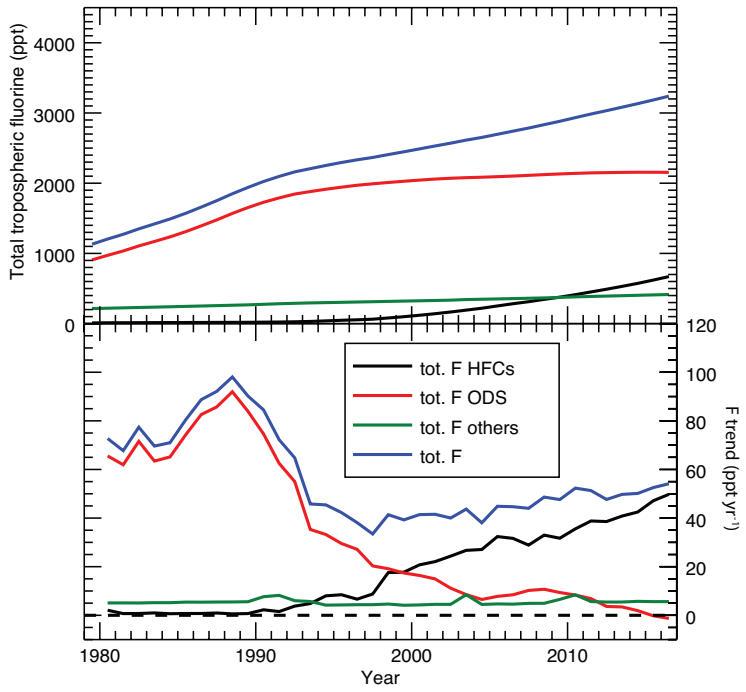

Figure 1-19. Tropospheric total fluorine time series and annual changes from long-lived gases, separated by contributions due to ODS, HFCs (see **Chapter 2**), and other fluorinated gases (such as SF_6, NF_3, and CF_4). ODS mole fractions were derived from a merged dataset based on NOAA, AGAGE, and UEA data. HFC mole fractions were derived from AGAGE and NOAA data. HFC records prior to regular global measurements were supplemented with estimates from Miller et al. (2010); Mühle et al. (2010); O'Doherty et al. (2009); Oram et al. (1996); Simmonds et al. (1998); Vollmer et al. (2011); and Weiss et al. (2008).

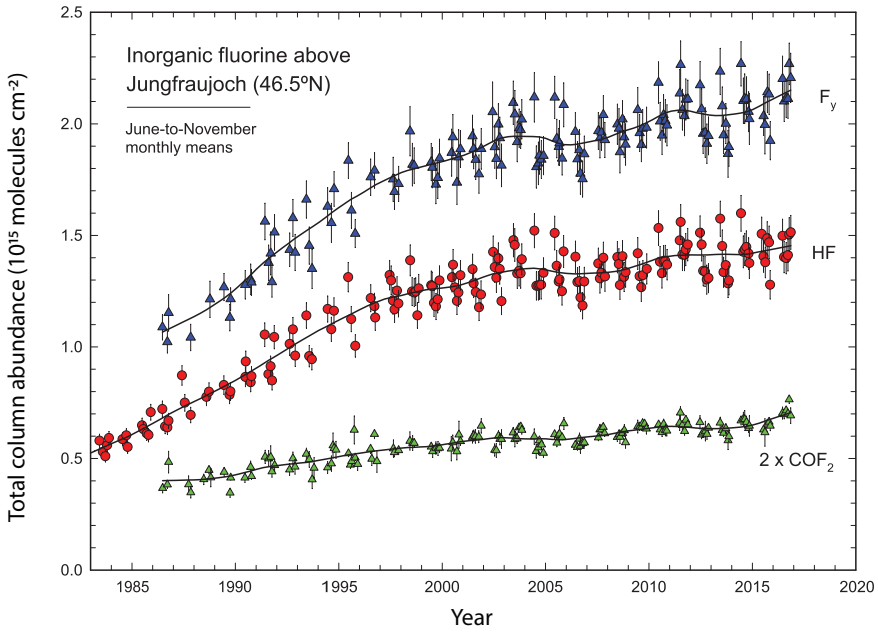

Figure 1-20. Multi-decadal monthly mean total column time series of the two main fluorine reservoirs, HF and COF_2, and their summation (F_y), as monitored at the Jungfraujoch station (Swiss Alps, 46.5°N, 3,580 m altitude), in the framework of the NDACC network. The datasets are restricted to the June to November months, so as to reduce the variability caused by atmospheric transport and subsidence during winter and spring. The continuous lines come from non-parametric least-squares fits involving an integration time of about 3 years and help to visualize the non-monotonic and non-linear changes in stratospheric chlorine after the peak in 1996–1997.

over which the spectrum is integrated, a continuous decline of EESC is derived. For a mean age of 5.5 years, as used for typical polar winter conditions, fractional release is nearly complete, and both formulations of EESC converge. However, in the case of a 3-year mean age, which is typically used for mid-latitude conditions, there are significant differences. Applying the new formulation, inorganic chlorine is expected to lag the tropospheric source gases more than expected based on a mean age representation of an inert tracer (see discussion in **Box 1-4**). One consequence of this is that a lower EESC is derived for the 1980 benchmark. Using the formulation for EESC from Newman et al. (2007) as in the last Assessment, but with a 20-year integration time, an early-1980 benchmark value of 1,160 ppt is calculated for a 3-year mean age, while 1,080 ppt is calculated using the new formulation of EESC suggested by Engel et al. (2018) (**Figure 1-18**, **Table 1-7**). This lower EESC value implies that it will take longer for EESC to decline to 1980 benchmark values. Accordingly, the percentage rate of recovery already achieved is also lower. For a mean age of 5.5 years, very similar values are derived with both methods (see **Table 1-7**). Using the new method, by 2017 we derive recovery of 31% towards 1980 values of EESC for mid-latitudes and of 18% for polar winter conditions; using the formulation by Newman et al. (2007) as in the previous Assessment, but with a 20-year integration time, by early 2017 we derive recovery of 43% for mid-latitude conditions and 19% for polar winter conditions.

Changes in EESC over the past 5 years (early 2012 to early 2017) are very similar for both methods, with maximum differences of 0.1%. The average change derived from both methods is given here. EESC, excluding contributions from short-lived substances, declined 4.3% from early 2012 to late 2016 in mid-latitudes and by 3.6% in high latitudes. The main driver of the decrease in EESC between early 2012 and early 2017 were the CFCs, which contributed 1.3% and 1.4% to this decline for mid-latitude and polar conditions,

respectively. CH_3Br was the second-most important contributor to changes in EESC, reducing EESC by 1.2% and 1% for mid-latitude and polar conditions, respectively. The impact of decreases in CH_3CCl_3 has now decreased to 0.8% (it was an important contributor during the period 2008–2012, with a decrease of about 1.5% for both polar winter conditions and mid-latitudes). EESC from halons decreased by 0.9% and 0.3% for mid-latitude and polar conditions, respectively. This is the first time that a decrease in EESC from halons is now also calculated for polar winter conditions. The decrease in tropospheric CCl_4 has resulted in a decrease of 0.8% in EESC at mid-latitudes and 0.6% in polar latitudes. The continuing increase in HCFCs has offset the total decrease by 0.4% at mid-latitudes and 0.6% for polar winter conditions.

1.4.5 Tropospheric and Stratospheric Fluorine Changes

Fluorine is not an efficient catalyst for stratospheric ozone depletion, due to the stability of the inorganic reservoir gases HF and COF_2, which are breakdown products of fluorine-containing source gases. However, many fluorinated source gases have a high radiative efficiency and are thus strong greenhouse gases, and most important fluorine gases are regulated under the Montreal Protocol. This regulation under the Montreal Protocol for chlorine- and fluorine-containing CFCs and HCFCs was motivated by the chlorine content. The regulation of HFCs, which are also included in the Kyoto Protocol, has only recently been added to the Montreal Protocol (see details in **Chapter 2**) in the framework of the Kigali Amendment, as these gases are replacement compounds for substances already regulated under the Montreal Protocol.

Figure 1-19 shows the time series of tropospheric fluorine in organic and some inorganic (SF_6 and NF_3, see **Section 1.5**) gases, separated by compound classes. In contrast to chlorine, a continuing increase in tropospheric fluorine is observed. A trend in total fluorine of 51.6 ± 2.3 ppt yr^{-1}, or 1.7 ± 0.07% yr^{-1}, is derived for the time period 2012–2016, which is comparable to the trend of 50.1 (±1.9) ppt yr^{-1}, or 1.7 (±0.07) % yr^{-1}, for the period 2008–2012. However, the drivers of this trend have changed. From 2008 to 2012, this increase was due to increases in ODSs (CFCs and HCFCs; 7.8 ppt yr^{-1}), HFCs (36.4 ppt yr^{-1}), and other fluorinated gases (6.6 ppt yr^{-1}). For the most recent 5-year period (2012–2016), it is more strongly dominated by HFCs (45 ppt yr^{-1}). Total fluorine input from ODSs has decreased to an average of 0.9 ± 1.9 ppt yr^{-1}, and the contribution from other fluorinated gases has been relatively stable at 5 ppt yr^{-1}. Total tropospheric fluorine and total tropospheric chlorine do not follow the same trajectory, largely because the largest contribution to a decrease in total Cl since ~1988 results from changes in CH_3CCl_3, which does not contain fluorine. However, the contribution to total tropospheric fluorine from all ODSs has been declining since the late 1980s, and the trend went from positive to negative in the last year (**Figure 1-19**, lower panel).

As can be seen from **Figure 1-19**, the contributions of different compounds and classes of compounds to the total tropospheric fluorine have changed significantly over time. As different gases release their fluorine with different efficiency, this implies that a direct reflection of tropospheric trends of fluorinated compounds in the inorganic fluorine content of the stratosphere is not necessarily expected.

A good proxy for the total inorganic fluorine (F_y) in the stratosphere is obtained by the weighted combination of the two most abundant fluorinated reservoirs, i.e., hydrogen fluoride (HF) and two times carbonyl fluoride (COF_2); this can thus be used as an independent check of the fluorine budget. **Figure 1-20** shows the multi-decadal monthly mean total column time series of inorganic fluorine above the Jungfraujoch station (Swiss Alps, 46.5°N, 3,580 m altitude), restricted to the June-to-November months, when atmospheric variability is at a minimum. A non-parametric least-squares fit to the time series helps to identify fluctuations in the rise of the fluorine loading in the Northern Hemisphere, fluctuations which are related to short-term variability in the atmospheric circulation and dynamics. The total column of HF increased at an average rate of 0.89 ± 0.17% yr^{-1} and that of COF_2 at 1.07 ± 0.14% yr^{-1} (update from Duchatelet et al., 2010; Duchatelet et al., 2009), as calculated using a bootstrap method (Gardiner et al., 2008). Total inorganic fluorine (F_y) has increased at a rate of 0.98 ± 0.15% yr^{-1} between 2007 and 2016.

Based on datasets from HALOE and ACE-FTS and a merged dataset from GOZCARDS, (Harrison et al., 2016) found a substantial slowdown in the rate of

Table 1-8. Measured mole fractions of selected fluorinated compounds (PFCs, SF_6, NF_3, SO_2F_2, SF_5CF_3) and other gases of interest.

Chemical Formula	Common or Industrial Name	Annual Mean Mole Fraction (ppt) 2012	2015	2016	Change (2015–2016) ppt yr^{-1}	% yr^{-1}	Network, Method
Perfluorocarbons (PFCs)							
CF_4	PFC-14	**79.7**	**81.9**	**82.7**	**0.8**	**1.0**	AGAGE in situ (Global)
C_2F_6	PFC-116	**4.2** *3.7*	**4.5** *3.9*	**4.6** *4.0*	**0.1** **0.1**	**2.1** **1.9**	AGAGE in situ (Global) *UEA, Cape Grim*[1]
C_3F_8	PFC-218	**0.57** **0.54**	**0.62** **0.60**	**0.63** **0.60**	**0.02** **0.00**	**2.6** **0.7**	AGAGE in situ (Global) UEA, Cape Grim
c-C_4F_8	PFC-c318	*1.26*	*1.39*	*1.44*	*0.05*	*3.6*	*UEA, Cape Grim*
n-C_5F_{12}	PFC-41-12	*0.142*	*0.149*	*0.148*	*–0.001*	*–0.7*	*UEA, Cape Grim*[1]
Other fluorinated compounds							
SF_6	sulfur hexafluoride	**7.6** **7.6**	**8.6** **8.6**	**8.9** **8.9**	**0.3** **0.3**	**3.8** **3.9**	AGAGE, flask and in situ (Global) NOAA, flask and in situ (Global)
NF_3	nitrogen trifluoride	**0.9**	**1.3**	**1.5**	**0.1**	**11.5**	AGAGE in situ (Global)
SO_2F_2	sulfuryl fluoride	**1.8**	**2.1**	**2.3**	**0.1**	**6.2**	AGAGE in situ (Global)
SF_5CF_3		*0.153*	*0.154*	*0.153*	*-0.001*	*-0.65*	*UEA, Cape Grim*
Other compounds							
CH_4 (ppb)	methane	**1809** **1808** **1808** **1806** **1819**	**1834** **1834** **1830** **1833** **1844**	**1842** **1843** **1840** **1841** **1853**	**8** **9** **10** **8** **9**	**0.4** **0.5** **0.5** **0.4** **0.5**	AGAGE in situ (Global) NOAA, flask and in situ (Global) UCI, flask (Global) CSIRO, flask (Global) WMO/GAW (Global)
N_2O (ppb)	nitrous oxide	**325.6** **325.0** **324.9** **325.1**	**328.5** **328.1** **327.8** **328.1**	**329.3** **328.9** **328.6** **328.9**	**0.8** **0.8** **0.8** **0.8**	**0.2** **0.2** **0.2** **0.2**	AGAGE in situ (Global) NOAA, flask and in situ (Global) CSIRO, flask (Global) WMO/GAW (Global)
COS (ppt)	carbonyl sulfide	**501**	**499**	**505**	**6**	**1.2**	NOAA, flask and in situ (Global)

Mole fractions in this table are from various monitoring networks that measure long-term trends in these gases. Results in bold text are estimates of global surface mean mole fractions. Values in italics represent observations from only one site and therefore do not represent a global mean. AGAGE (Advanced Global Atmospheric Gases Experiment, https://agage.mit.edu/) data are described in Arnold et al. (2013), Cunnold et al. (2002), Mühle et al. (2010), Mühle et al. (2009), Prinn et al. (2018) and Rigby et al. (2010), and global averages are calculated using data from five baseline AGAGE stations, assimilated into an atmospheric box model (extension of Rigby et al., 2014). NOAA (National Oceanic and Atmospheric Administration, USA, http://www.esrl.noaa.gov/gmd/dv/site/) data are described in Dlugokencky et al. (2011), Hall et al. (2011), and Montzka et al. (2007), global means are calculated as area-weighted means from observations at 12 sites for SF_6, and 45 sites for CH_4 (including shipboard sampling). UCI (University of California, Irvine, USA, http://ps.uci.edu/~rowlandblake/research_atmos.html) data are described in Simpson et al. (2012). UEA (University of East Anglia, United Kingdom, http://www.uea.ac.uk/environmental-sciences/research/marine-and-atmospheric-sciences-group) data are described in Laube et al. (2012); Leedham Elvidge et al. (2017), Oram et al. (2012), and Sturges et al. (2012). CSIRO data (Commonwealth Scientific and Industrial Research Organisation) are described in Francey et al. (2003). Cape Grim refers to the Cape Grim Baseline Air Pollution Station, Australia; WMO/GAW, World Meteorological Organization, Global Atmosphere Watch, World Data Centre for Greenhouse Gases, (http://ds.data.jma.go.jp/gmd/wdcgg and https://public.wmo.int/en/resources/library/wmo-greenhouse-gas-bulletin). Differences between each network are due to calibration scales, differences in spatial and temporal sampling strategies, and the different methods for estimating global means.

Note:

[1] Mole fractions for 2016 represent averages from January to July for UEA data for these compounds.

increase of global stratospheric HF. Trends of 0.52 ± 0.03% yr^{-1} were obtained from 2004–2012, in comparison to 1.12 ± 0.08% yr^{-1} for 1998–2005 and 4.97 ± 0.12% yr^{-1} for 1991–1997. The observed trends and the slowdown are in good overall agreement with results from modeled HF time series, although the model calculated a slightly lower increase for the 1991–1997 period. Significant short-term and latitudinal variability was observed in the trends of HF, which is attributed to dynamical variability in the stratosphere.

Overall, these data show a continuing increase in total fluorine. The magnitudes of the total tropospheric fluorine and stratospheric inorganic fluorine trends are somewhat different. As explained above, this may be due to the changing relative importance of different fluorinated gases, with different efficiencies of fluorine release in the stratosphere. The tropospheric increase is now mainly driven by increases in HFCs (**Chapter 2**).

1.5 CHANGES IN OTHER TRACE GASES THAT INFLUENCE OZONE AND CLIMATE

This section describes recent trends in gases that are not covered by the Montreal Protocol but that indirectly affect ozone. The gases nitrous oxide (N_2O) and methane (CH_4) play a role in stratospheric ozone chemistry and contribute to climate change and are discussed in **Sections 1.5.1** and **1.5.2**. **Section 1.5.3** addresses the sulfur-containing gases carbonyl sulfide (COS) and sulfur dioxide (SO_2), which are transported to the stratosphere where they contribute to stratospheric sulfuric acid aerosol. Finally, changes in some fluorine-containing greenhouse gases (GHGs), which indirectly influence ozone through their contribution to global warming (**Chapter 5**), are discussed in **Section 1.5.4**. Carbon dioxide (CO_2) is not discussed here, as it is described in detail elsewhere (e.g., Ciais and Sabine et al., 2013; Le Quéré et al., 2018). In contrast to previous Assessments, HFCs are no longer covered in this section, as they are now the subject of **Chapter 2**.

1.5.1 Nitrous Oxide (N_2O)

N_2O is the dominant source of reactive nitrogen to the stratosphere, which can lead to depletion of stratospheric ozone. Currently, natural and anthropogenic emissions of N_2O make a larger contribution to stratospheric ozone depletion than emissions of any of the individual ODSs discussed in **Section 1.2** (Ravishankara et al., 2009). While it is likely to remain a major contributor to ozone depletion throughout the 21st century, due to changes in stratospheric chemistry and dynamics brought about by increasing GHG concentrations, there remains some uncertainty about its long-term impact on ozone (Revell et al., 2015). Owing to its relatively high GWP, N_2O is the third-most important long-lived GHG after CO_2 and CH_4 (Myhre and Shindell et al., 2013; Ravishankara et al., 2009). The previous Assessment noted that N_2O had been growing relatively steadily, at a rate of around 0.8 ppb yr^{-1}. This trend has continued through 2016, for which an annual surface global mean mole fraction of around 329 ppb was reached (**Table 1-8**). As a result of this growth, the contribution of N_2O to radiative forcing has continued to rise, reaching 0.19 W m^{-2} in 2016 (**Figure 1-3**), approximately 10% that of CO_2.

Recent studies have attempted to better constrain N_2O sources and sinks. The previous Assessment summarized the findings of the SPARC Lifetimes Assessment, which estimated the N_2O lifetime to be 123 (104–152) years (2-sigma "most likely" range, SPARC (2013)). Based on observations from the Microwave Limb Sounder (MLS) and a radiative transfer model, Prather et al. (2015) recommend a lifetime of 116 ± 9 years, which is lower than the maximum likelihood SPARC estimate but within their uncertainties. Emissions of N_2O originate primarily from natural and agricultural soils and the ocean, with approximately one-third of emissions from anthropogenic sources (Ciais and Sabine et al., 2013). Thompson et al. (2014) produced top-down estimates of N_2O emissions using four different chemical transport models. Their estimate of global annual emissions of between 16.1 and 18.7 TgN yr^{-1} was broadly in agreement with IPCC AR5 (Ciais and Sabine et al., 2013) and therefore does not substantially alter our previous understanding of the global budget. More recently, Wagner-Riddle et al. (2017) proposed a 1.07 ± 0.59 TgN yr^{-1} source of N_2O induced by freeze-thaw cycles over croplands, which has not been included in previous budgets.

1.5.2 Methane (CH_4)

Methane, the second-most important anthropogenic GHG, is a source of water vapor and HO_x (OH and HO_2) radicals to the stratosphere and thereby also influences stratospheric ozone. Methane has continued to grow between 2012 and 2016, with the global mean mole fraction increasing between 32 and 35 ppb during this period (**Table 1-8**). The radiative forcing due to CH_4 was 0.5 W m^{-2} in 2016 (**Figure 1-3**), 25% the value of CO_2.

A recent study re-evaluated the global CH_4 budget from 2000–2012 and concluded that around 60% of global emissions are anthropogenic, although there remains a mismatch between emissions estimated using bottom-up and top-down methods (Saunois et al., 2016). Major sources of uncertainty in the CH_4 budget were found to be due to wetland CH_4 emissions and the magnitude and variability of the global hydroxyl radical (OH) concentration. Several recent studies have focused on the causes of the pause in CH_4 growth that occurred between 2000 and 2007, and the subsequent renewed rise. Nisbet et al. (2016) and Schaefer et al. (2016) used data from CH_4 isotopologues to conclude that the renewed growth was likely being driven by an increase in tropical

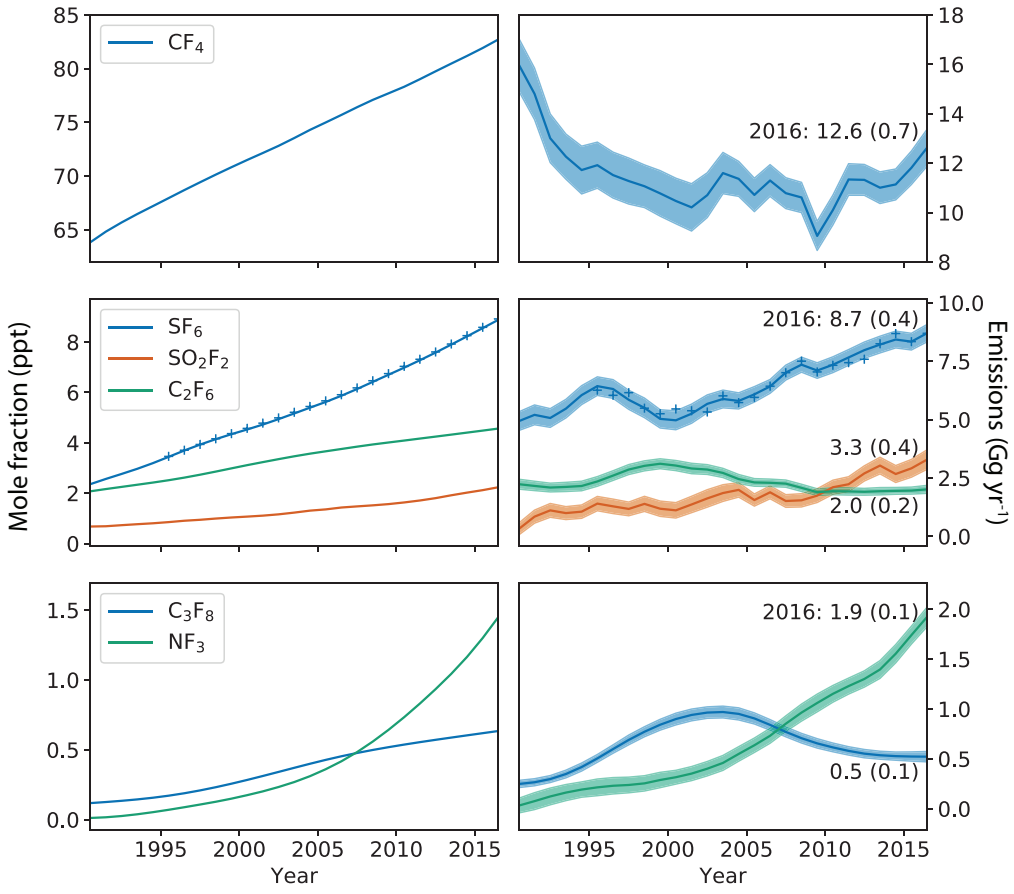

Figure 1-21. Global mean mole fractions (*left panels*) and emissions (*right panels*) for fluorinated greenhouse gases (excluding CFCs, HCFCs, and HFCs). Mole fractions are output from the AGAGE 12-box model (Cunnold et al., 1983; Rigby et al., 2013) and constrained using AGAGE data described in Arnold et al. (2013); Mühle et al. (2010); Mühle et al. (2009); Prinn et al. (2018); and Rigby et al. (2010). For SF_6, pluses represent data from NOAA (Hall et al., 2011, extended). Emissions were estimated using the Bayesian method described above **(Figure 1-4),** with atmospheric lifetimes as summarized in **Table A-1.**

wetland or agricultural (primarily ruminant animal) emissions, respectively. By analyzing global livestock populations and revising emissions factors, Wolf et al. (2017) also proposed that growing emissions from animals could be a significant contributor to the rise. Hausmann et al. (2016) pointed to the coincident growth in atmospheric ethane (C_2H_6) to infer an increase in CH_4 emissions related to oil and gas extraction since 2008, while Dalsoren et al. (2016) proposed an increase in anthropogenic emissions from East Asia. Schwietzke et al. (2016) used new estimates of isotopic source signatures to revise upwards the contribution of fossil fuel to the global CH_4 budget, compared to bottom-up inventories. They inferred a gradual decline in fossil fuel emission since the early 2000s, coincident with a gradual rise in emissions from microbial sources. In contrast, Worden et al. (2017) proposed that recent trends are consistent with a decline in biomass burning emissions and increase in fossil fuel emissions. McNorton et al. (2016), Rigby et al. (2017), and Turner et al. (2017) inferred global OH concentrations using AGAGE and NOAA methyl chloroform (CH_3CCl_3) data. They found an increase in OH in the 1990s and early 2000s, followed by a decline in OH that could explain much of the pause and renewed growth, although the uncertainties were found to be large compared to the magnitude of the inferred change. Overall, the uncertainty in the global CH_4 budget remains considerable, and there is no consensus on the drivers of recent trends.

1.5.3 Aerosol Precursors: Carbonyl Sulfide (COS) and Sulfur Dioxide (SO_2)

The sulfur-containing gases COS and SO_2, which are transported to the stratosphere, can be oxidized to yield sulfuric acid, which can condense on preexisting particles or nucleate to form new particles. Injection of sulfur gases occurs sporadically during volcanic eruptions, as well as more continuously through the atmospheric transport of tropospheric sulfur-containing gases to the stratosphere. As particles can interact with solar and terrestrial radiation, this has an influence on both tropospheric and stratospheric temperatures. In addition, heterogeneous reactions on aerosol surfaces in liquid aerosol particles can influence stratospheric chemistry. A review of stratospheric aerosols and their precursor gases has recently been published by Kremser et al. (2016).

Carbonyl sulfide (COS) is the most important substance responsible for transporting sulfur into the stratosphere. Recent modeling estimates of the sulfur fluxes from COS suggest that this accounts for 56% (Sheng et al., 2015) to 70% (Brühl et al., 2012) of the stratospheric aerosol burden. The magnitude of the sulfur fluxes calculated in the models is in agreement with sulfur fluxes from COS derived from observations (Barkley et al., 2008; Krysztofiak et al., 2015). There are large uncertainties in the global sources and sinks of carbonyl sulfide, with current sink estimates surpassing the source assessments, due to a recent factor-of-two upward revision in the global surface sink estimate (Kremser et al., 2016). While Berry et al. (2013) and Launois et al. (2015) suggested that missing sources may be due to oceanic emissions, this was not confirmed by Lennartz et al. (2017). Therefore, there are currently remaining uncertainties concerning the sinks and sources of COS. The main anthropogenic source of COS is thought to be CS_2 emissions from rayon production, which are rapidly oxidized to form COS in the atmosphere (Campbell et al., 2015). The main source region for these emissions is thought to have shifted to China during the past decades (Campbell et al., 2015).

Recent atmospheric observations of COS confirm that there is currently no or only a very small long-term trend in tropospheric COS (Lejeune et al., 2017). Between 2015 and 2016, tropospheric background values of COS increased by about 6 ppt (**Table 1-8**), but this is more likely a short-term variability than a sign of a long-term increase. Preindustrial levels of COS are confirmed to have been significantly lower than this based on ice core and firn air measurements (Aydin et al., 2014; Campbell et al., 2017). Comprehensive observations of COS in the stratosphere have recently become available from the MIPAS instrument onboard Envisat for June 2002 to April 2012. These observations also do not show a significant trend in the stratosphere (Glatthor et al., 2017). Balloon measurements reveal less than 5% change in stratospheric COS over the past 25 years (Toon et al., 2017).

Following volcanic eruptions, it has been shown that stratospheric sulfur loading from the upper troposphere to the upper stratosphere is enhanced (Höpfner et al., 2015; Höpfner et al., 2013). A large fraction of the SO_2 observed in the stratosphere in the absence of recent volcanic emission is from oxidation of COS in

the stratosphere. The relevance of the direct transport of SO_2 to the stratosphere remains unclear, with large variations between different models (Kremser et al., 2016; Sheng et al., 2015); however, an analysis of model results combining in situ measurements with MIPAS data indicates that it is near negligible (Rollins et al., 2017). Consequently, the impact of changes in tropospheric emissions—for example, the recent reduction in Chinese emissions of SO_2 (van der A et al., 2017)—remains unclear.

1.5.4 Other Fluorine-Containing Gases (SF_6, PFCs, NF_3, SO_2F_2, SF_5CF_3, HFEs)

Sulfur Hexafluoride (SF_6)

Sulfur hexafluoride, which was regulated under the Kyoto Protocol, is used primarily for electrical insulation (e.g. Ko et al., 1993). Its atmospheric global surface mean mole fraction increased from 7.6 to 8.9 ppt between 2012 and 2016, contributing 5.1 mW m^{-2} to global radiative forcing in 2016 (**Table 1-8, Figure 1-3, Figure 1-21**). During the period from 2010 to 2016, FTIR measurements above Jungfraujoch showed an increase in the atmospheric column mean mole fraction of 4.34 ± 0.19% yr^{-1}, which is slightly higher than the corresponding increase in the lower troposphere of 3.90 ± 0.06% yr^{-1} based on ground-based measurements (see **Table 1-2**). Emissions inferred from AGAGE and NOAA observations show that SF_6 global emissions have increased during this period, reaching 8.7 ± 0.4 Gg yr^{-1}, equivalent to 205 ± 9 Mt CO_2 yr^{-1}, in 2016 (**Figure 1-21**). These emissions are now 72% higher than a minimum inferred around the year 2000 (Levin et al., 2010; Rigby et al., 2010).

Using atmospheric SF_6 observations, Fang et al. (2014) estimated increasing emissions from East Asia, from 2.4 Gg in 2006 to 4.1 Gg in 2012, which is on average ~50% of the global emissions for this period. Recent studies have suggested a significant downward revision of the SF_6 lifetime, for which a value of 3,200 years has been widely used (Ravishankara et al., 1993). Using a 3-D model with updated atmospheric electron density, Kovacs et al. (2017) estimated an average lifetime of 1,278 years, with a range 1,120 to 1,475 years. From observations of SF_6 in the Arctic polar vortex, Ray et al. (2017) estimated a lifetime of 850 (580–1,400) years. Since the lifetime remains very long, these estimates will not significantly influence SF_6 emissions derived using observed atmospheric trends, or GWPs over a 100-year time horizon or shorter. However, climate impacts over longer timescales will be influenced.

Perfluorocarbons (PFCs)

Perfluorocarbons are compounds that consist of only carbon and fluorine and typically have very long lifetimes and high radiative efficiencies. The major PFCs are primarily emitted during aluminum and semiconductor production, and they were regulated under the Kyoto Protocol (e.g. Mühle et al., 2010). Since the previous Assessment, atmospheric abundances of all major PFCs have continued to increase (**Table 1-8, Figure 1-21**). CF_4 (PFC-14; lifetime greater than 50,000 years) increased by 0.8 ppt yr^{-1} between 2015 and 2016, reaching 82.7 ppt in 2016; C_2F_6 (PFC-116; lifetime greater than 10,000 years), at 0.1 ppt yr^{-1} to 4.6 ppt; and C_3F_8 (PFC-218; lifetime 2,600 years), at ~0.02 ppt yr^{-1} to 0.63 ppt. *c*-C_4F_8 (PFC-c318; lifetime 3,200 years) has reached 1.44 ppt at Cape Grim (update to Oram et al., 2012). Collectively, the PFCs contributed 6.3 mW m^{-2} to global radiative forcing in 2016 **(Figure 1-3)**. FTIR-based remote sensing observations at Jungfraujoch showed an increase of 1.11 ± 0.09% yr^{-1} for CF_4, which is slightly higher than the rate of 0.94 ± 0.01% yr^{-1} over the period from 2010 to 2016 derived from ground-based measurements (see **Table 1-2**). Emissions of the major PFCs have remained relatively stable since 2012 **(Figure 1-21)**. In 2016, emissions of CF_4, C_2F_6, and C_3F_8 were 12.6 ± 0.7, 2.0 ± 0.2, and 0.52 ± 0.05 Gg yr^{-1}, respectively, equivalent to CO_2 emissions of 84 ± 5, 22 ± 2, 4.6 ± 0.5 Mt yr^{-1}.

Trudinger et al. (2016) used measurements of CF_4, C_2F_6, and C_3F_8 from ice cores, firn, archived air samples, and field stations to reconstruct atmospheric abundances since 1800. They inferred an increase in emissions during the 20th century for these compounds until the early 1980s (CF_4) or early 2000s (C_2F_6 and C_3F_8), after which emissions declined. The growth in emissions of CF_4 and C_2F_6 was found not to have kept pace with global aluminum production (the major source of these gases), suggesting a decrease in the emissions factor from this industry. Apart from an apparent drop in emissions in 2009, attributed to

the global financial crisis, aggregate emissions of these compounds were found to be relatively stable from the late 2000s onwards (also shown in **Figure 1-21**).

Nitrogen Trifluoride (NF_3)

Since the previous Assessment, NF_3 (lifetime 569 years, GWP_{100} 15,750), which is primarily used in semiconductor manufacture and was included in the Kyoto Protocol (Arnold et al., 2013), has grown by more than 10% yr^{-1}, to 1.5 ppt in 2016 (**Table 1-8, Figure 1-21**). Its contribution to radiative forcing remained relatively small in 2016 at 0.3 mW m^{-2} (**Figure 1-3**). Emissions of NF_3 inferred for 2016 reached 1.9 ± 0.1 Gg yr^{-1}, equivalent to 30 ± 2 Mt CO_2 yr^{-1} (**Figure 1-21**). The compound is primarily used in the electronics industry as a source of reactive fluorine, in place of C_2F_6. Arnold et al. (2013) estimated a considerable climate benefit of this transition, due to the higher efficiency at which reactive fluorine can be extracted from NF_3, compared to C_2F_6. However, they also estimated global emissions that were significantly larger than expected under industrial "best practices." Both the atmospheric abundance and inferred emissions reported here for 2016 are more than 60% higher than the values for 2011 in Arnold et al. (2013).

Sulfuryl Fluoride (SO_2F_2)

SO_2F_2 is used as a fumigant for structural and post-harvest agricultural fumigation. It is increasingly being used in place of the ozone-depleting methyl bromide. The first atmospheric observations of SO_2F_2 were reported by Mühle et al. (2009), who estimated a lifetime of 36 ± 11 years, primarily due to loss to the oceans. The rate of growth of SO_2F_2 has increased since the previous Assessment. The 2016 atmospheric abundance was 2.25 ppt, 25% higher than in 2012 (**Table 1-8**, **Figure 1-21**). In 2016, sulfur fluoride contributed 0.45 mW m^{-2} to radiative forcing of climate (**Figure 1-3**). Inferred emissions increased by 35% between 2012 and 2016, from 2.7 ± 0.3 Gg yr^{-1} to 3.6 ± 0.4 Gg yr^{-1}, which is equivalent to 14 ± 2 Mt CO_2 yr^{-1} (**Figure 1-21**).

(Trifluoromethyl) Sulfur Pentafluoride (SF_5CF_3)

This compound has a long lifetime (650–950 years), a very high radiative efficiency (0.59 W m^{-2} ppb^{-1}), and may have been emitted to the atmosphere during the production of perfluorooctanyl sulfonate (Sturges et al., 2012). Data from the Southern Hemisphere show that SF_5CF_3 has remained at 0.153 ppt for the last four years (**Table 1-8)**, contributing around 0.09 mW m^{-2} to radiative forcing. This observed abundance is similar to that given by Sturges et al. (2012), who showed that growth, and therefore emissions, ceased around the late 1990s.

Halogenated Ethers (HFEs)

Information on atmospheric halogenated ethers (HFEs) is sparse. The first atmospheric observations of three inhalation anesthetics—desflurane (HFE-236ea2, $CHF_2OCHFCF_3$), isoflurane (HCFE-235da2, $CHF_2OCHClCF_3$), and sevoflurane (HFE-347 isomer, $(CF_3)_2CHOCH_2F$)—were published by Vollmer et al. (2015c). Using flask samples from the Northern Hemisphere and Antarctica, combined with in situ measurements from Jungfraujoch, 15-year records showed an increase in global mean abundances to levels in 2014 of 0.097 ppt, 0.30 ppt, and 0.13 ppt for isoflurane, desflurane, and sevoflurane. Using radiative efficiencies in **Table A-1**, these mole fractions equate to radiative forcings of 0.04, 0.14, and 0.04 mW m^{-2}, respectively. Using a box model and updated lifetimes from Sulbaek Andersen et al. (2010) and Sulbaek Andersen et al. (2012), global emissions for 2014 were estimated at 0.88 Gg yr^{-1}, 0.96 Gg yr^{-1}, and 1.2 Gg yr^{-1} for the three anesthetics, respectively, equivalent to approximately 3 Mt CO_2 yr^{-1} in total.

REFERENCES

Adcock, K.E., C.E. Reeves, L.J. Gooch, E.C. Leedham Elvidge, M.J. Ashfold, C.A.M. Brenninkmeijer, C. Chou, P.J. Fraser, R.L. Langenfelds, N. Mohd Hanif, S. O'Doherty, D.E. Oram, C.F. Ou-Yang, S.M. Phang, A.A. Samah, T. Röckmann, W.T. Sturges, and J.C. Laube, Continued increase of CFC-113a (CCl_3CF_3) mixing ratios in the global atmosphere: emissions, occurrence and potential sources, *Atmos. Chem. Phys.*, *18*(7), 4737–4751, doi:10.5194/acp-18-4737-2018, 2018.

Akagi, S.K., R.J. Yokelson, C. Wiedinmyer, M.J. Alvarado, J.S. Reid, T. Karl, J.D. Crounse, and P.O. Wennberg, Emission factors for open and domestic biomass burning for use in atmospheric models, *Atmos. Chem. Phys.*, *11*(9), 4039–4072, doi:10.5194/acp-11-4039-2011, 2011.

Albers, C.N., O.S. Jacobsen, E.M.M. Flores, and A.R. Johnsen, Arctic and subarctic natural soils emit chloroform and brominated analogues by alkaline hydrolysis of trihaloacetyl compounds, *Environ. Sci. Technol.*, *51*(11), 6131–6138, doi:10.1021/acs.est7b00144, 2017.

Allan, J.D., P.I. Williams, J. Najera, J.D. Whitehead, M.J. Flynn, J.W. Taylor, D. Liu, E. Darbyshire, L.J. Carpenter, R. Chance, S.J. Andrews, S.C. Hackenberg, and G. McFiggans, Iodine observed in new particle formation events in the Arctic atmosphere during ACCACIA, *Atmos. Chem. Phys.*, *15*(10), 5599–5609, doi:10.5194/acp-15-5599-2015, 2015.

Allard, S., and H. Gallard, Abiotic formation of methyl iodide on synthetic birnessite: A mechanistic study, *Sci. Total Environ.*, 463, 169–175, doi:10.1016/j.scitotenv.2013.05.079, 2013.

Anderson, D.C., J.M. Nicely, R.J. Salawitch, T.P. Canty, R.R. Dickerson, T.F. Hanisco, G.M. Wolfe, E.C. Apel, E. Atlas, T. Bannan, S. Bauguitte, N.J. Blake, J.F. Bresch, T.L. Campos, L.J. Carpenter, M.D. Cohen, M. Evans, R.P. Fernandez, B.H. Kahn, D.E. Kinnison, S.R. Hall, N.R.P. Harris, R.S. Hornbrook, J.-F. Lamarque, M. Le Breton, J.D. Lee, C. Percival, L. Pfister, R.B. Pierce, D.D. Riemer, A. Saiz-Lopez, B.J.B. Stunder, A.M. Thompson, K. Ullmann, A. Vaughan, and A.J. Weinheimer, A pervasive role for biomass burning in tropical high ozone/low water structures, *Nat. Commun.*, 10267, doi:10.1038/ncomms10267, 2016.

Andrews, S.J., L.J. Carpenter, E.C. Apel, E. Atlas, V. Donets, J.R. Hopkins, R.S. Hornbrook, A.C. Lewis, R.T. Lidster, R. Lueb, J. Minaeian, M. Navarro, S. Punjabi, D. Riemer, and S. Schauffler, A comparison of very short lived halocarbon (VSLS) and DMS aircraft measurements in the tropical west Pacific from CAST, ATTREX and CONTRAST, *Atmos. Meas. Tech.*, *9*(10), 5213–5225, doi:10.5194/amt-9-5213-2016, 2016.

Arnold, T., C.M. Harth, J. Mühle, A.J. Manning, P.K. Salameh, J. Kim, D.J. Ivy, L.P. Steele, V.V. Petrenko, J.P. Severinghaus, D. Baggenstos, and R.F. Weiss, Nitrogen trifluoride global emissions estimated from updated atmospheric measurements, *Proc. Natl. Acad. Sci.*, *110*(6), 2029–2034, doi:10.1073/pnas.1212346110, 2013.

Aschmann, J., and B.M. Sinnhuber, Contribution of very short-lived substances to stratospheric bromine loading: uncertainties and constraints, *Atmos. Chem. Phys.*, *13*(3), 1203–1219, doi:10.5194/acp-13-1203-2013, 2013.

Ashfold, M.J., N.R.P. Harris, E.L. Atlas, A.J. Manning, and J.A. Pyle, Transport of short-lived species into the Tropical Tropopause Layer, *Atmos. Chem. Phys.*, *12*(14), 6309–6322, doi:10.5194/acp-12-6309-2012, 2012.

Ashfold, M.J., J.A. Pyle, A.D. Robinson, E. Meneguz, M.S.M. Nadzir, S.M. Phang, A.A. Samah, S. Ong, H.E. Ung, L.K. Peng, S.E. Yong, and N.R.P. Harris, Rapid transport of East Asian pollution to the deep tropics, *Atmos. Chem. Phys.*, *15*(6), 3565–3573, doi:10.5194/acp-15-3565-2015, 2015.

Ashford, P., A. Ambrose, M. Jeffs, B. Johnson, S. Kocchi, S. Lee, D. Nott, P. Vodianitskaia, and J. Wu, Foams, Chapter 7 in *IPCC/TEAP Special Report on Safeguarding the Ozone Layer and the Global Climate System: Issues Related to Hydrofluorocarbons and Perfluorocarbons*, Cambridge University Press, Cambridge, United Kingdom, 2005.

Aydin, M., T.J. Fudge, K.R. Verhulst, M.R. Nicewonger, E.D. Waddington, and E.S. Saltzman, Carbonyl sulfide hydrolysis in Antarctic ice cores and an atmospheric history for the last 8000 years, *J. Geophys. Res. Atmos.*, *119*(13), 8500–8514, doi:10.1002/2014JD021618, 2014.

Barkley, M.P., P.I. Palmer, C.D. Boone, P.F. Bernath, and P. Suntharalingam, Global distributions of carbonyl sulfide in the upper troposphere and stratosphere, *Geophys. Res. Lett.*, *35*(14),

doi:10.1029/2008GL034270, 2008.

Bell, N., L. Hsu, D.J. Jacob, M.G. Schultz, D.R. Blake, J.H. Butler, D.B. King, J.M. Lobert, and E. Maier-Reimer, Methyl iodide: Atmospheric budget and use as a tracer of marine convection in global models, *J. Geophys. Res. Atmos.*, *107*(D17), doi:10.1029/2001JD001151, 2002.

Bernath, P., and A.M. Fernando, Trends in stratospheric HCl from the ACE satellite mission, *J. Quant. Spectrosc.* Radiat. Trans., 217, 126–129, doi:10.1016/j.jqsrt.2018.05.027, 2018.

Berry, J., A. Wolf, J.E. Campbell, I. Baker, N. Blake, D. Blake, A.S. Denning, S.R. Kawa, S.A. Montzka, U. Seibt, K. Stimler, D. Yakir, and Z. Zhu, A coupled model of the global cycles of carbonyl sulfide and CO_2: A possible new window on the carbon cycle, *J. Geophys. Res. Biogeosci.*, *118*(2), 842–852, doi:10.1002/jgrg.20068, 2013.

Bie, P.J., X.K. Fang, Z.F. Li, Z.Y. Wang, and J.X. Hu, Emissions estimates of carbon tetrachloride for 1992-2014 in *China, Environ. Pollut.*, *224*, 670–678, doi:10.1016/j.envpol.2017.02.051, 2017.

Bösch, H., C. Camy-Peyret, M.P. Chipperfield, R. Fitzenberger, H. Harder, U. Platt, and K. Pfeilsticker, Upper limits of stratospheric IO and OIO inferred from center-to-limb-darkening-corrected balloon-borne solar occultation visible spectra: Implications for total gaseous iodine and stratospheric ozone, *J. Geophys. Res.*, *108*(D15), doi:10.1029/2002JD003078, 2003.

Boudjellaba, D., J. Dron, G. Revenko, C. Demelas, and J.L. Boudenne, Chlorination by-product concentration levels in seawater and fish of an industrialised bay (Gulf of Fos, France) exposed to multiple chlorinated effluents, *Sci. Total Environ., 541*, 391–399, doi:10.1016/j.scitotenv.2015.09.046, 2016.

Brinckmann, S., A. Engel, H. Bonisch, B. Quack, and E. Atlas, Short-lived brominated hydrocarbons - observations in the source regions and the tropical tropopause layer, *Atmos. Chem. Phys.*, *12*(3), 1213-1228, doi:10.5194/acp-12-1213-2012, 2012.

Brown, A.T., M.P. Chipperfield, C. Boone, C. Wilson, K.A. Walker, and P.F. Bernath, Trends in atmospheric halogen containing gases since 2004, *J. Quant. Spectrosc. Radiat. Trans.*, *112*(16), 2552–2566, doi:10.1016/j.jqsrt.2011.07.005, 2011.

Brühl, C., J. Lelieveld, P.J. Crutzen, and H. Tost, The role of carbonyl sulphide as a source of stratospheric sulphate aerosol and its impact on climate, *Atmos. Chem. Phys.*, *12*(3), 1239–1253, doi:10.5194/acp-12-1239-2012, 2012.

Burkholder, J.B., S.P. Sander, J. Abbat, J.R. Barker, R.E. Huie, C.E. Kolb, M.J. Kurylo, V.L. Orkin, D. Wilmouth, and P.H. Wine, Chemical Kinetics and Photochemical Data for Use in Atmospheric Studies – Evaluation Number 18, edited by J.B. Burkholder, 1392 pp, JPL Publication, Pasadena, California, 2015.

Butler, J.H., S.A. Montzka, A.D. Clarke, J.M. Lobert, and J.W. Elkins, Growth and distribution of halons in the atmosphere, *J. Geophys. Res. Atmos.*, *103*(D1), 1503–1511, doi:10.1029/97JD02853, 1998.

Butler, J.H., D.B. King, J.M. Lobert, S.A. Montzka, S.A. Yvon-Lewis, B.D. Hall, N.J. Warwick, D.J. Mondeel, M. Aydin, and J.W. Elkins, Oceanic distributions and emissions of short-lived halocarbons, *Global Biogeochem. Cycles*, *21*(1), doi:10.1029/2006gb002732, 2007.

Butler, J.H., S.A. Yvon-Lewis, J.M. Lobert, D.B. King, S.A. Montzka, J.L. Bullister, V. Koropalov, J.W. Elkins, B.D. Hall, L. Hu, and Y.N. Liu, A comprehensive estimate for loss of atmospheric carbon tetrachloride (CCl_4) to the ocean, *Atmos. Chem. Phys.*, *16*(17), 10899-10910, doi:10.5194/acp-16-10899–2016, 2016.

Butz, A., H. Bösch, C. Camy-Peyret, M.P. Chipperfield, M. Dorf, S. Kreycy, L. Kritten, C. Prados-Román, J. Schwärzle, and K. Pfeilsticker, Constraints on inorganic gaseous iodine in the tropical upper troposphere and stratosphere inferred from balloon-borne solar occultation observations, *Atmos. Chem. Phys.*, *9*(18), 7229–7242, doi:10.5194/acp-9-7229-2009, 2009.

Campbell, J.E., M.E. Whelan, U. Seibt, S.J. Smith, J.A. Berry, and T.W. Hilton, Atmospheric carbonyl sulfide sources from anthropogenic activity: Implications for carbon cycle constraints, *Geophys. Res. Lett.*, *42*(8), 3004–3010, doi:10.1002/2015GL063445, 2015.

Campbell, J.E., J.A. Berry, U. Seibt, S.J. Smith, S.A. Montzka, T. Launois, S. Belviso, L. Bopp, and M. Laine, Large historical growth in global terrestrial gross primary production, *Nature*, *544*, 84, doi:10.1038/nature22030, 2017.

Carpenter, L.J., and P.S. Liss, On temperate sources of bromoform and other reactive organic bromine gases, *J. Geophys. Res. Atmos.*, *105*(D16), 20539–20547, doi:10.1029/2000JD900242, 2000.

Carpenter, L.J., D.J. Wevill, S. O'Doherty, G. Spain, and P.G. Simmonds, Atmospheric bromoform at Mace Head, Ireland: seasonality and evidence for a peatland source, *Atmos. Chem. Phys.*, *5*, 2927–2934, 2005.

Carpenter, L.J., D.J. Wevill, J.R. Hopkins, R.M. Dunk, C.E. Jones, K.E. Hornsby, and J.B. McQuaid, Bromoform in tropical Atlantic air from 25 degrees N to 25 degrees S, *Geophys. Res. Lett.*, *34*(11), doi:10.1029/2007GL029893, 2007.

Carpenter, L.J., S.M. MacDonald, M.D. Shaw, R. Kumar, R.W. Saunders, R. Parthipan, J. Wilson, and J.M.C. Plane, Atmospheric iodine levels influenced by sea surface emissions of inorganic iodine, *Nat. Geosci.*, *6*(2), 108–111, doi:10.1038/ngeo1687, 2013.

Carpenter, L.J., and S. Reimann (Lead Authors), J.B. Burkholder, C. Clerbaux, B.D. Hall, R. Hossaini, J.C. Laube, and S.A. Yvon-Lewis, Update on Ozone-Depleting Substances (ODSs) and Other Gases of Interest to the Montreal Protocol, Chapter 1 in *Scientific Assessment of Ozone Depletion: 2014*, Global Ozone Research and Monitoring Project–Report No. 55, World Meteorological Organization, Geneva, Switzerland, 2014.

Chen, D., L.G. Huey, D.J. Tanner, R.J. Salawitch, D.C. Anderson, P.A. Wales, L.L. Pan, E.L. Atlas, R.S. Hornbrook, E.C. Apel, N.J. Blake, T.L. Campos, V. Donets, F.M. Flocke, S.R. Hall, T.F. Hanisco, A.J. Hills, S.B. Honomichl, J.B. Jensen, L. Kaser, D.D. Montzka, J.M. Nicely, J.M. Reeves, D.D. Riemer, S.M. Schauffler, K. Ullmann, A.J. Weinheimer, and G.M. Wolfe, Airborne measurements of BrO and the sum of HOBr and Br_2 over the Tropical West Pacific from 1 to 15km during the CONvective TRansport of Active Species in the Tropics (CONTRAST) experiment, *J. Geophys. Res.*, *121*(12560–12578), doi:10.1002/2016JD025561.

Chen, Q., J.A. Schmidt, V. Shah, L. Jaeglé, T. Sherwen, and B. Alexander, Sulfate production by reactive bromine: Implications for the global sulfur and reactive bromine budgets, *Geophys. Res. Lett.*, *44*, 7069–7078, doi:10.1002/2017GL073812, 2017.

Chipperfield, M.P., Q. Liang, M. Rigby, R. Hossaini, S.A. Montzka, S. Dhomse, W.H. Feng, R.G. Prinn, R.F. Weiss, C.M. Harth, P.K. Salameh, J. Mühle, S. O'Doherty, D. Young, P.G. Simmonds, P.B. Krummel, P.J. Fraser, L.P. Steele, J.D. Happell, R.C. Rhew, J. Butler, S.A. Yvon-Lewis, B. Hall, D. Nance, F. Moore, B.R. Miller, J. Elkins, J.J. Harrison, C.D. Boone, E.L. Atlas, and E. Mahieu, Model sensitivity studies of the decrease in atmospheric carbon tetrachloride, *Atmos. Chem. Phys.*, *16*(24), 15741–15754, doi:10.5194/acp-16-15741-2016, 2016.

Chirkov, M., G.P. Stiller, A. Laeng, S. Kellmann, T. von Clarmann, C.D. Boone, J.W. Elkins, A. Engel, N. Glatthor, U. Grabowski, C.M. Harth, M. Kiefer, F. Kolonjari, P.B. Krummel, A. Linden, C.R. Lunder, B.R. Miller, S.A. Montzka, J. Mühle, S. O'Doherty, J. Orphal, R.G. Prinn, G. Toon, M.K. Vollmer, K.A. Walker, R.F. Weiss, A. Wiegele, and D. Young, Global HCFC-22 measurements with MIPAS: retrieval, validation, global distribution and its evolution over 2005–2012, *Atmos. Chem. Phys.*, *16*(5), 3345–3368, doi:10.5194/acp-16-3345-2016, 2016.

Ciais, P., C. Sabine (Coordinating Lead Authors), G. Bala, L. Bopp, V. Brovkin, J. Canadell, A. Chhabra, R. DeFries, J. Galloway, M. Heimann, C. Jones, C.L. Quéré, R.B. Myneni, S. Piao, and P. Thornton, Carbon and Other Biogeochemical Cycles, Chapter 6 in *Climate Change 2013: The Physical Science Basis. Contribution of Working Group I to the Fifth Assessment Report of the Intergovernmental Panel on Climate Change*, edited by T.F. Stocker, D. Qin, G.K. Plattner, M. Tignor, S.K. Allen, J. Boschung, A. Nauels, Y. Xia, V. Bex, and P.M. Midgley, 465–570, Cambridge University Press, Cambridge, United Kingdom, 2013.

Connor, B.J., T. Mooney, G.E. Nedoluha, J.W. Barrett, A. Parrish, J. Koda, M.L. Santee, and R.M. Gomez, Re-analysis of ground-based microwave ClO measurements from Mauna Kea, 1992 to early 2012, *Atmos. Chem. Phys.*, *13*(17), 8643–8650, doi:10.5194/acp-13-8643-2013, 2013.

Culbertson, J.A., J.M. Prins, E.P. Grimsrud, R.A. Rasmussen, M.A.K. Khalil, and M.J. Shearer, Observed trends for CF_3-containing compounds in background air at Cape Meares, Oregon, Point Barrow, Alaska, and Palmer Station, Antarctica, *Chemosphere*, *55*(8), 1109–1119, doi:10.1016/j.chemosphere.2003.11.002, 2004.

Cunnold, D.M., R.G. Prinn, R.A. Rasmussen, P.G. Simmonds, F.N. Alyea, C.A. Cardelino, A.J. Crawford, P.J. Fraser, and R.D. Rosen, The atmospheric lifetime experiment: 3. lifetime methodology and application to 3 years of $CFCl_3$ data, *J. Geo-*

phys. Res. Oceans, *88*, 8379–8400, doi:10.1029/JC088iC13p08379, 1983.

Cunnold, D.M., P.J. Fraser, R.F. Weiss, R.G. Prinn, P.G. Simmonds, B.R. Miller, F.N. Alyea, and A.J. Crawford, Global trends and annual releases of CCl_3F and CCl_2F_2 estimated from ALE/GAGE and other measurements from July 1978 to June 1991, *J. Geophys. Res. Atmos.*, *99*(D1), 1107–1126, doi:10.1029/93JD02715, 1994.

Cunnold, D.M., L.P. Steele, P.J. Fraser, P.G. Simmonds, R.G. Prinn, R.F. Weiss, L.W. Porter, S. O'Doherty, R.L. Langenfelds, P.B. Krummel, H.J. Wang, L. Emmons, X.X. Tie, and E.J. Dlugokencky, In situ measurements of atmospheric methane at GAGE/AGAGE sites during 1985-2000 and resulting source inferences, *J. Geophys. Res. Atmos.*, *107*(D14), doi:10.1029/2001JD001226, 2002.

Dalsoren, S.B., C.L. Myhre, G. Myhre, A.J. Gomez-Pelaez, O.A. Sovde, I.S.A. Isaksen, R.F. Weiss, and C.M. Harth, Atmospheric methane evolution the last 40 years, *Atmos. Chem. Phys.*, *16*(5), 3099–3126, doi:10.5194/acp-16-3099-2016, 2016.

Daniel, J.S., S. Solomon, and D.L. Albritton, On the evaluation of halocarbon radiative forcing and global warming potentials, *J. Geophys. Res. Atmos.*, *100*(D1), 1271–1285, doi:10.1029/94JD02516, 1995.

Daniel, J.S., G.J.M. Velders (Lead Authors), O. Morgenstern, D.W. Toohey, T.J. Wallington, and D.J. Wuebbles, A Focus on Information and Options for Policymakers, Chapter 5 in *Scientific Assessment of Ozone Depletion: 2010*, Global Ozone Research and Monitoring Project–Report No. 52, World Meteorological Organization, Geneva, Switzerland, 2011.

Dix, B., S. Baidar, J.F. Bresch, S.R. Hall, K.S. Schmidt, S. Wang, and R. Volkamer, Detection of iodine monoxide in the tropical free troposphere, *Proc. Natl. Acad. Sci.*, *110*(6), 2035–2040, doi:10.1073/pnas.1212386110, 2013.

Dlugokencky, E.J., E.G. Nisbet, R. Fisher, and D. Lowry, Global atmospheric methane: Budget, changes and dangers, *Philos. Trans. Roy. Soc. A*, *369*(1943), 2058–2072, doi:10.1098/rsta.2010.0341, 2011.

Dorf, M., J.H. Butler, A. Butz, C. Camy-Peyret, M.P. Chipperfield, L. Kritten, S.A. Montzka, B. Simmes, F. Weidner, and K. Pfeilsticker, Long-term observations of stratospheric bromine reveal slow down in growth, *Geophys. Res. Lett.*, *33*(24), L24803, doi:10.1029/2006GL027714, 2006.

Dorf, M., A. Butz, C. Camy-Peyret, M.P. Chipperfield, L. Kritten, and K. Pfeilsticker, Bromine in the tropical troposphere and stratosphere as derived from balloon-borne BrO observations, *Atmos. Chem. Phys.*, *8*(23), 7265–7271, doi:10.5194/acp-8-7265-2008, 2008.

Duchatelet, P., E. Mahieu, R. Ruhnke, W. Feng, M. Chipperfield, P. Demoulin, P. Bernath, C.D. Boone, K.A. Walker, C. Servais, and O. Flock, An approach to retrieve information on the carbonyl fluoride (COF_2) vertical distributions above Jungfraujoch by FTIR multi-spectrum multi-window fitting, *Atmos. Chem. Phys.*, *9*(22), 9027–9042, doi:10.5194/acp-9-9027-2009, 2009.

Duchatelet, P., P. Demoulin, F. Hase, R. Ruhnke, W. Feng, M.P. Chipperfield, P.F. Bernath, C.D. Boone, K.A. Walker, and E. Mahieu, Hydrogen fluoride total and partial column time series above the Jungfraujoch from long-term FTIR measurements: Impact of the line-shape model, characterization of the error budget and seasonal cycle, and comparison with satellite and model data, *J. Geophys. Res. Atmos.*, *115*, doi:10.1029/2010JD014677, 2010.

Eckert, E., T. von Clarmann, A. Laeng, G.P. Stiller, B. Funke, N. Glatthor, U. Grabowski, S. Kellmann, M. Kiefer, A. Linden, A. Babenhauserheide, G. Wetzel, C. Boone, A. Engel, J.J. Harrison, P.E. Sheese, K.A. Walker, and P.F. Bernath, MIPAS IMK/IAA carbon tetrachloride (CCl_4) retrieval and first comparison with other instruments, *Atmos. Meas. Tech.*, *10*(7), 2727–2743, doi:10.5194/amt-10-2727-2017, 2017.

Engel, A., H. Bönisch, J. Ostermöller, M.P. Chipperfield, S. Dhomse, and P. Jöckel, A refined method for calculating equivalent effective stratospheric chlorine, *Atmos. Chem. Phys.*, *2018*, 601–609, doi:10.5194/acp-18-601-2018, 2018.

Fang, X., R.L. Thompson, T. Saito, Y. Yokouchi, J. Kim, S. Li, K.R. Kim, S. Park, F. Graziosi, and A. Stohl, Sulfur hexafluoride (SF_6) emissions in East Asia determined by inverse modeling, *Atmos. Chem. Phys.*, *14*(9), 4779–4791, doi:10.5194/acp-14-4779-2014, 2014.

Fang, X.K., J. Wu, S.S. Su, J.R. Han, Y.S. Wu, Y.H. Shi, D. Wan, X.Z. Sun, J.B. Zhang, and J.X. Hu, Estimates of major anthropogenic halocarbon emissions from China based on interspecies correla-

tions, *Atmos. Environ., 62*, 26–33, doi:10.1016/j.atmosenv.2012.08.010, 2012.

Feng, W., M.P. Chipperfield, S. Dhomse, B.M. Monge-Sanz, X. Yang, K. Zhang, and M. Ramonet, Evaluation of cloud convection and tracer transport in a three-dimensional chemical transport model, *Atmos. Chem. Phys.*, *11*(12), 5783–5803, doi:10.5194/acp-11-5783-2011, 2011.

Fernandez, R.P., R.J. Salawitch, D.E. Kinnison, J.F. Lamarque, and A. Saiz-Lopez, Bromine partitioning in the tropical tropopause layer: Implications for stratospheric injection, *Atmos. Chem. Phys.*, *14*(24), 13391–13410, doi:10.5194/acp-14-13391-2014, 2014.

Fiehn, A., B. Quack, H. Hepach, S. Fuhlbrügge, S. Tegtmeier, M. Toohey, E. Atlas, and K. Krüger, Delivery of halogenated very short-lived substances from the west Indian Ocean to the stratosphere during the Asian summer monsoon, *Atmos. Chem. Phys.*, *17*(11), 6723–6741, doi:10.5194/acp-17-6723-2017, 2017.

Forczek, S.T., F. Laturnus, J. Dolezalova, J. Holik, and Z. Wimmer, Emission of climate relevant volatile organochlorines by plants occurring in temperate forests, *Plant Soil Environ.*, *61*(3), 103–108, doi:10.17221/900/2014-pse, 2015.

Francey, R.J., L.P. Steele, D.A. Spencer, R.L. Langenfelds, R.M. Law, P.B. Krummel, P.J. Fraser, D.M. Etheridge, N. Derek, S.A. Coram, L.N. Cooper, C.E. Allison, L. Porter, and S. Baly, The CSIRO (Australia) measurement of greenhouse gases in the global atmosphere, in *Baseline Atmospheric Program Australia 1999-2000*, edited by N.W. Tindale, N. Derek, and P.J. Fraser, 42–53, Bureau of Meteorology and CSIRO Atmospheric Research, Melbourne, Australia, 2003.

Fraser, P., B. Dunse, A.J. Manning, R. Wang, P. Krummel, P. Steele, L. Porter, C. Allison, S. O'Doherty, P.G. Simmonds, J. Mühle, and R. Prinn, Australian carbon tetrachloride (CCl_4) emissions in a global context, *Environ. Chem.*, *11*, doi:10.1071/EN13171, 2014.

Froidevaux, L., J. Anderson, H.J. Wang, R.A. Fuller, M.J. Schwartz, M.L. Santee, N.J. Livesey, H.C. Pumphrey, P.F. Bernath, J.M. Russell, and M.P. McCormick, Global OZone Chemistry And Related trace gas Data records for the Stratosphere (GOZCARDS): Methodology and sample results with a focus on HCl, H_2O, and O_3, *Atmos. Chem. Phys.*, *15*(18), 10471–10507, doi:10.5194/acp-15-10471-2015, 2015.

Fueglistaler, S., A.E. Dessler, T.J. Dunkerton, I. Folkins, Q. Fu, and P.W. Mote, Tropical tropopause layer, *Rev. Geophys.*, *47*(1), doi:10.1029/2008rg000267, 2009.

Fuhlbrugge, S., B. Quack, E. Atlas, A. Fiehn, H. Hepach, and K. Kruger, Meteorological constraints on oceanic halocarbons above the Peruvian upwelling, *Atmos. Chem. Phys.*, *16*(18), 12205–12217, doi:10.5194/acp-16-12205-2016, 2016a.

Fuhlbrugge, S., B. Quack, S. Tegtmeier, E. Atlas, H. Hepach, Q. Shi, S. Raimund, and K. Kruger, The contribution of oceanic halocarbons to marine and free tropospheric air over the tropical West Pacific, *Atmos. Chem. Phys.*, *16*(12), 7569–7585, doi:10.5194/acp-16-7569-2016, 2016b.

Gardiner, T., A. Forbes, M. de Mazière, C. Vigouroux, E. Mahieu, P. Demoulin, V. Velazco, J. Notholt, T. Blumenstock, F. Hase, I. Kramer, R. Sussmann, W. Stremme, J. Mellqvist, A. Strandberg, K. Ellingsen, and M. Gauss, Trend analysis of greenhouse gases over Europe measured by a network of ground-based remote FTIR instruments, *Atmos. Chem. Phys.*, *8*(22), 6719–6727, doi:10.5194/acp-8-6719-2008, 2008.

Glatthor, N., M. Höpfner, A. Leyser, G.P. Stiller, T. von Clarmann, U. Grabowski, S. Kellmann, A. Linden, B.M. Sinnhuber, G. Krysztofiak, and K.A. Walker, Global carbonyl sulfide (OCS) measured by MIPAS/Envisat during 2002–2012, *Atmos. Chem. Phys.*, *17*(4), 2631–2652, doi:10.5194/acp-17-2631-2017, 2017.

Graziosi, F., J. Arduini, F. Furlani, U. Giostra, L.J.M. Kuijpers, S.A. Montzka, B.R. Miller, S.J. O'Doherty, A. Stohl, P. Bonasoni, and M. Maione, European emissions of HCFC-22 based on eleven years of high frequency atmospheric measurements and a Bayesian inversion method, *Atmos. Environ., 112*, 196–207, doi:10.1016/j.atmosenv.2015.04.042, 2015.

Graziosi, F., J. Arduini, P. Bonasoni, F. Furlani, U. Giostra, A.J. Manning, A. McCulloch, S. O'Doherty, P.G. Simmonds, S. Reimann, M.K. Vollmer, and M. Maione, Emissions of carbon tetrachloride from Europe, *Atmos. Chem. Phys.*, *16*(20), 12849–12859, doi:10.5194/acp-16-12849-2016, 2016.

Haenel, F.J., G.P. Stiller, T. von Clarmann, B. Funke, E. Eckert, N. Glatthor, U. Grabowski, S. Kellmann, M. Kiefer, A. Linden, and T. Reddmann,

Reassessment of MIPAS age of air trends and variability, *Atmos. Chem. Phys.*, *15*, 13161–13176, doi:10.5194/acp-15-13161-2015, 2015.

Hall, B.D., G.S. Dutton, D.J. Mondeel, J.D. Nance, M. Rigby, J.H. Butler, F.L. Moore, D.F. Hurst, and J.W. Elkins, Improving measurements of SF_6 for the study of atmospheric transport and emissions, *Atmos. Meas. Tech.*, *4*(11), 2441–2451, doi:10.5194/amt-4-2441-2011, 2011.

Hall, B.D., A. Engel, J. Mühle, J.W. Elkins, F. Artuso, E. Atlas, M. Aydin, D. Blake, E.G. Brunke, S. Chiavarini, P.J. Fraser, J. Happell, P.B. Krummel, I. Levin, M. Loewenstein, M. Maione, S.A. Montzka, S. O'Doherty, S. Reimann, G. Rhoderick, E.S. Saltzman, H.E. Scheel, L.P. Steele, M.K. Vollmer, R.F. Weiss, D. Worthy, and Y. Yokouchi, Results from the International Halocarbons in Air Comparison Experiment (IHALACE), *Atmos. Meas. Tech.*, *7*(2), 469-490, doi:10.5194/amt-7-469-2014, 2014.

Hamed, M.A., M.E. Moustafa, Y.A. Soliman, M.A. El-Sawy, and A.I. Khedr, Trihalomethanes formation in marine environment in front of Nuweibaa desalination plant as a result of effluents loaded by chlorine residual, *Egyptian J. Aquatic Res.*, *43*(1), 45–54, doi:10.1016/j.ejar.2017.01.001, 2017.

Han, J.R., L. Li, S.S. Su, J. Wu, X.K. Fang, S.L. Jia, J.B. Zhang, and J.X. Hu, Estimated HCFC-142b emissions in China: 2000-2050, *Chinese Sci. Bull.*, *59*(24), 3046–3053, doi:10.1007/s11434-014-0337-z, 2014.

Harris, N.R.P., and D. Wuebbles (Lead Authors), J.S. Daniel, J. Hu, LJ.M. Kuijpers, K.S. Law, M.J. Prather, and R. Schofield, Scenarios and information for policymakers, Chapter 5 in *Scientific Assessment of Ozone Depletion: 2014*, Global Ozone Research and Monitoring Project – Report No. 55, World Meteorological Organization, Geneva, Switzerland, 2014.

Harris, N.R.P., L.J. Carpenter, J.D. Lee, G. Vaughan, M.T. Filus, R.L. Jones, B. OuYang, J.A. Pyle, A.D. Robinson, S.J. Andrews, A.C. Lewis, J. Minaeian, A. Vaughan, J.R. Dorsey, M.W. Gallagher, M. Le Breton, R. Newton, C.J. Percival, H.M.A. Ricketts, S.J.B. Bauguitte, G.J. Nott, A. Wellpott, M.J. Ashfold, J. Flemming, R. Butler, P.I. Palmer, P.H. Kaye, C. Stopford, C. Chemel, H. Boesch, N. Humpage, A. Vick, A.R. MacKenzie, R. Hyde, P. Angelov, E. Meneguz, and A.J. Manning, Coordinated Airborne Studies in the Tropics (CAST), *Bull. Am. Meterol. Soc.*, *98*(1), 145–162, doi:10.1175/bams-d-14-00290.1, 2017.

Harrison, J.J., M.P. Chipperfield, C.D. Boone, S.S. Dhomse, P.F. Bernath, L. Froidevaux, J. Anderson, and J. Russell, Satellite observations of stratospheric hydrogen fluoride and comparisons with SLIMCAT calculations, *Atmos. Chem. Phys.*, *16*(16), 10501–10519, doi:10.5194/acp-16-10501-2016, 2016.

Hausmann, P., R. Sussmann, and D. Smale, Contribution of oil and natural gas production to renewed increase in atmospheric methane (2007–2014): Top-down estimate from ethane and methane column observations, *Atmos. Chem. Phys.*, *16*(5), 3227–3244, doi:10.5194/acp-16-3227-2016, 2016.

Hendrick, F., M. Van Roozendael, M.P. Chipperfield, M. Dorf, F. Goutail, X. Yang, C. Fayt, C. Hermans, K. Pfeilsticker, J.P. Pommereau, J.A. Pyle, N. Theys, and M. De Mazière, Retrieval of stratospheric and tropospheric BrO profiles and columns using ground-based zenith-sky DOAS observations at Harestua, 60° N, *Atmos. Chem. Phys.*, *7*(18), 4869–4885, doi:10.5194/acp-7-4869-2007, 2007.

Hendrick, F., P.V. Johnston, M. De Mazière, C. Fayt, C. Hermans, K. Kreher, N. Theys, A. Thomas, and M. Van Roozendael, One-decade trend analysis of stratospheric BrO over Harestua (60°N) and Lauder (45°S) reveals a decline, *Geophys. Res. Lett.*, *35*(14), L14801, doi:10.1029/2008GL034154, 2008.

Hepach, H., B. Quack, F. Ziska, S. Fuhlbrugge, E.L. Atlas, K. Kruger, I. Peeken, and D.W.R. Wallace, Drivers of diel and regional variations of halocarbon emissions from the tropical North East Atlantic, *Atmos. Chem. Phys.*, *14*(3), 1255–1275, doi:10.5194/acp-14-1255-2014, 2014.

Hepach, H., B. Quack, S. Raimund, T. Fischer, E.L. Atlas, and A. Bracher, Halocarbon emissions and sources in the equatorial Atlantic Cold Tongue, *Biogeosci.*, *12*(21), 6369-6387, doi:10.5194/bg-12-6369–2015, 2015.

Höpfner, M., J. Orphal, T. von Clarmann, G. Stiller, and H. Fischer, Stratospheric $BrONO_2$ observed by MIPAS, *Atmos. Chem. Phys.*, *9*(5), 1735–1746, doi:10.5194/acp-9-1735-2009, 2009.

Höpfner, M., N. Glatthor, U. Grabowski, S. Kellmann, M. Kiefer, A. Linden, J. Orphal, G. Stiller, T. von Clarmann, B. Funke, and C.D. Boone, Sulfur dioxide SO_2 as observed by MIPAS/Envisat: Tem-

poral development and spatial distribution at 15–45 km altitude, *Atmos. Chem. Phys.*, *13*(20), 10405–10423, doi:10.5194/acp-13-10405-2013, 2013.

Höpfner, M., C.D. Boone, B. Funke, N. Glatthor, U. Grabowski, A. Günther, S. Kellmann, M. Kiefer, A. Linden, S. Lossow, H.C. Pumphrey, W.G. Read, A. Roiger, G. Stiller, H. Schlager, T. von Clarmann, and K. Wissmüller, Sulfur dioxide SO_2 from MIPAS in the upper troposphere and lower stratosphere 2002–2012, *Atmos. Chem. Phys.*, *15*(12), 7017–7037, doi:10.5194/acp-15-7017-2015, 2015.

Hosking, J.S., M.R. Russo, P. Braesicke, and J.A. Pyle, Modelling deep convection and its impacts on the tropical tropopause layer, *Atmos. Chem. Phys.*, *10*(22), 11175–11188, doi:10.5194/acp-10-11175-2010, 2010.

Hossaini, R., M.P. Chipperfield, W. Feng, T.J. Breider, E. Atlas, S.A. Montzka, B.R. Miller, F. Moore, and J. Elkins, The contribution of natural and anthropogenic very short-lived species to stratospheric bromine, *Atmos. Chem. Phys.*, *12*(1), 371–380, doi:10.5194/acp-12-371-2012, 2012.

Hossaini, R., M.P. Chipperfield, A. Saiz-Lopez, J.J. Harrison, R. von Glasow, R. Sommariva, E. Atlas, M. Navarro, S.A. Montzka, W. Feng, S. Dhomse, C. Harth, J. Mühle, C. Lunder, S. O'Doherty, D. Young, S. Reimann, M.K. Vollmer, P.B. Krummel, and P.F. Bernath, Growth in stratospheric chlorine from short-lived chemicals not controlled by the Montreal Protocol, *Geophys. Res. Lett.*, *42*(11), 4573–4580, doi:10.1002/2015gl063783, 2015.

Hossaini, R., M.P. Chipperfield, A. Saiz-Lopez, R. Fernandez, S. Monks, W. Feng, P. Brauer, and R. von Glasow, A global model of tropospheric chlorine chemistry: Organic versus inorganic sources and impact on methane oxidation, *J. Geophys. Res. Atmos.*, *121*(23), 14,271–214,297, doi:10.1002/2016JD025756, 2016a.

Hossaini, R., P.K. Patra, A.A. Leeson, G. Krysztofiak, N.L. Abraham, S.J. Andrews, A.T. Archibald, J. Aschmann, E.L. Atlas, D.A. Belikov, H. Bönisch, L.J. Carpenter, S. Dhomse, M. Dorf, A. Engel, W. Feng, S. Fuhlbrügge, P.T. Griffiths, N.R.P. Harris, R. Hommel, T. Keber, K. Krüger, S.T. Lennartz, S. Maksyutov, H. Mantle, G.P. Mills, B. Miller, S.A. Montzka, F. Moore, M.A. Navarro, D.E. Oram, K. Pfeilsticker, J.A. Pyle, B. Quack, A.D. Robinson, E. Saikawa, A. Saiz-Lopez, S. Sala, B.M. Sinnhuber, S. Taguchi, S. Tegtmeier, R.T. Lidster, C. Wilson, and F. Ziska, A multi-model intercomparison of halogenated very short-lived substances (TransCom-VSLS): Linking oceanic emissions and tropospheric transport for a reconciled estimate of the stratospheric source gas injection of bromine, *Atmos. Chem. Phys.*, *16*(14), 9163–9187, doi:10.5194/acp-16-9163-2016, 2016b.

Hossaini, R., M.P. Chipperfield, S.A. Montzka, A.A. Leeson, S.S. Dhomse, and J.A. Pyle, The increasing threat to stratospheric ozone from dichloromethane, *Nat. Commun.*, *8*, doi:10.1038/ncomms15962, 2017.

Hoyle, C.R., V. Marécal, M.R. Russo, G. Allen, J. Arteta, C. Chemel, M.P. Chipperfield, F. D'Amato, O. Dessens, W. Feng, J.F. Hamilton, N.R.P. Harris, J.S. Hosking, A.C. Lewis, O. Morgenstern, T. Peter, J.A. Pyle, T. Reddmann, N.A.D. Richards, P.J. Telford, W. Tian, S. Viciani, A. Volz-Thomas, O. Wild, X. Yang, and G. Zeng, Representation of tropical deep convection in atmospheric models – Part 2: Tracer transport, *Atmos. Chem. Phys.*, *11*(15), 8103–8131, doi:10.5194/acp-11-8103-2011, 2011.

Hu, L., S.A. Montzka, B.R. Miller, A.E. Andrews, J.B. Miller, S.J. Lehman, C. Sweeney, S.M. Miller, K. Thoning, C. Siso, E.L. Atlas, D.R. Blake, J. de Gouw, J.B. Gilman, G. Dutton, J.W. Elkins, B. Hall, H.L. Chen, M.L. Fischer, M.E. Mountain, T. Nehrkorn, S.C. Biraud, F.L. Moore, and P. Tans, Continued emissions of carbon tetrachloride from the United States nearly two decades after its phaseout for dispersive uses, *Proc. Natl. Acad. Sci.*, *113*(11), 2880–2885, doi:10.1073/pnas.1522284113, 2016a.

Hu, L., S.A. Montzka, S.J. Lehman, D.S. Godwin, B.R. Miller, A.E. Andrews, K. Thoning, J.B. Miller, C. Sweeney, C. Siso, J.W. Elkins, B.D. Hall, D.J. Mondeel, D. Nance, T. Nehrkorn, M.E. Mountain, M.L. Fischer, S.C. Biraud, H.L. Chen, and P.P. Tans, Considerable contribution of the Montreal Protocol to declining greenhouse gas emissions from the United States: U.S. CFCs, HCFCs, and HFCs Emissions, *Geophys. Res. Lett.*, *44* (15), doi:10.1002/2017GL074388, 2017.

Hu, Q., Z. Xie, X. Wang, J. Yu, and Y. Zhang, Methyl iodine over oceans from the Arctic Ocean to the maritime Antarctic, *Sci. Rep.*, *6*, 26007, doi:10.1038/srep26007, 2016b.

Hughes, C., A.L. Chuck, H. Rossetti, P.J. Mann, S.M.

Turner, A. Clarke, R. Chance, and P.S. Liss, Seasonal cycle of seawater bromoform and dibromomethane concentrations in a coastal bay on the western Antarctic Peninsula, *Global Biogeochem. Cycles*, *23*, doi:10.1029/2008gb003268, 2009.

IPCC/TEAP, *Special Report on Safeguarding the Ozone Layer and the Global Climate System: Issues Related to Hydrofluorocarbons and Perfluorocarbons*, (Intergovernmental Panel on Climate Change, and the Technical and Economic Assessment Panel) Cambridge University Press, Cambridge, United Kingdom, 2005.

Jensen, E.J., L. Pfister, D.E. Jordan, D.W. Fahey, P. Newman, T.D. Thornberry, A.W. Rollins, G.S. Diskin, T.V. Bui, M.J. McGill, D.L. Hlavka, R.P. Lawson, R.S. Gao, P. Pilewskie, J. Elkins, E.J. Hintsa, F. Moore, M.J. Mahoney, E. Atlas, J. Stutz, K. Pfeilsticker, S.C. Wofsy, S. Evan, and K. Rosenlof, The NASA Airborne Tropical TRopopause EXperiment (ATTREX), in *SPARC Newsletter No. 41*, pp. 10, SPARC, 2013.

Jensen, E.J., L. Pfister, D.E. Jordan, T.V. Bui, R. Ueyama, H.B. Singh, T.D. Thornberry, A.W. Rollins, R.S. Gao, D.W. Fahey, K.H. Rosenlof, J.W. Elkins, G.S. Diskin, J.P. DiGangi, R.P. Lawson, S. Woods, E.L. Atlas, M.A.N. Rodriguez, S.C. Wofsy, J. Pittman, C.G. Bardeen, O.B. Toon, B.C. Kindel, P.A. Newman, M.J. McGill, D.L. Hlavka, L.R. Lait, M.R. Schoeberl, J.W. Bergman, H.B. Selkirk, M.J. Alexander, J.E. Kim, B.H. Lim, J. Stutz, and K. Pfeilsticker, The NASA Airborne Tropical Tropopause Experiment: High-Altitude Aircraft Measurements in the Tropical Western Pacific, *Bull. Am. Meterol. Soc.*, *98*(1), doi:10.1175/Bams-D-14-00263.1, 2017.

Jones, C.E., K.E. Hornsby, R. Sommariva, R.M. Dunk, R. Von Glasow, G. McFiggans, and L.J. Carpenter, Quantifying the contribution of marine organic gases to atmospheric iodine, *Geophys. Res. Lett.*, *37*, doi:10.1029/2010GL043990, 2010.

Jones, C.E., S.J. Andrews, L.J. Carpenter, C. Hogan, F.E. Hopkins, J.C. Laube, A.D. Robinson, T.G. Spain, S.D. Archer, N.R.P. Harris, P.D. Nightingale, S.J. O'Doherty, D.E. Oram, J.A. Pyle, J.H. Butler, and B.D. Hall, Results from the first national UK inter-laboratory calibration for very short-lived halocarbons, *Atmos. Meas. Tech.*, *4*(5), 865–874, doi:10.5194/amt-4-865-2011, 2011.

Khalil, M.A.K., R.M. Moore, D.B. Harper, J.M. Lobert, D.J. Erickson, V. Koropalov, W.T. Sturges, and W.C. Keene, Natural emissions of chlorine-containing gases: Reactive Chlorine Emissions Inventory, *J. Geophys. Res. Atmos.*, *104*(D7), 8333–8346, doi:10.1029/1998JD100079, 1999.

Khan, M.A.H., R.C. Rhew, M.E. Whelan, K. Zhou, and S.J. Deverel, Methyl halide and chloroform emissions from a subsiding Sacramento–San Joaquin Delta island converted to rice fields, *Atmos. Environ.*, *45*(4), 977–985, doi:10.1016/j.atmosenv.2010.10.053, 2011.

Khan, M.A.H., R.C. Rhew, K. Zhou, and M.E. Whelan, Halogen biogeochemistry of invasive perennial pepperweed (Lepidium latifolium) in a peatland pasture, *J. Geophys. Res. Biogeosci.*, *118*(1), 239-247, doi:10.1002/jgrg.20020, 2013.

Kloss, C., M.J. Newland, D.E. Oram, P.J. Fraser, C.A.M. Brenninkmeijer, T. Rockmann, and J.C. Laube, Atmospheric abundances, trends and emissions of CFC-216ba, CFC-216ca and HCFC-225ca, *Atmos.*, *5*(2), 420–434, doi:10.3390/atmos5020420, 2014.

Ko, M.K.W., N.D. Sze, W.C. Wang, G. Shia, A. Goldman, F.J. Murcray, D.G. Murcray, and C.P. Rinsland, Atmospheric sulfur hexafluoride: Sources, sinks and greenhouse warming, *J. Geophys. Res. Atmos.*, *98*(D6), 10499–10507, doi:10.1029/93JD00228, 1993.

Koenig, T.K., R. Volkamer, S. Baidar, B. Dix, S. Wang, D.C. Anderson, R.J. Salawitch, P.A. Wales, C.A. Cuevas, R.P. Fernandez, A. Saiz-Lopez, M.J. Evans, T. Sherwen, D.J. Jacob, J. Schmidt, D. Kinnison, J.-F. Lamarque, E.C. Apel, J.C. Bresch, T. Campos, F.M. Flocke, S.R. Hall, S.B. Honomichl, R. Hornbrook, J.B. Jensen, R. Lueb, D.D. Montzka, L.L. Pan, J.M. Reeves, S.M. Schauffler, K. Ullmann, A.J. Weinheimer, E.L. Atlas, V. Donets, M.A. Navarro, D. Riemer, N.J. Blake, D. Chen, L.G. Huey, D.J. Tanner, T.F. Hanisco, and G.M. Wolfe, BrO and By profiles over the Western Pacific: Relevance of Inorganic Bromine Sources and a Bry Minimum in the Aged Tropical Tropopause Layer, *Atmos. Chem. Phys.*, *17* (24) 1–46, doi:10.5194/acp-2017-572, 2017.

Kohlhepp, R., R. Ruhnke, M.P. Chipperfield, M. De Maziere, J. Notholt, S. Barthlott, R.L. Batchelor, R.D. Blatherwick, T. Blumenstock, M.T. Coffey, P. Demoulin, H. Fast, W. Feng, A. Goldman, D.W.T. Griffith, K. Hamann, J.W. Hannigan, F. Hase, N.B.

Jones, A. Kagawa, I. Kaiser, Y. Kasai, O. Kirner, W. Kouker, R. Lindenmaier, E. Mahieu, R.L. Mittermeier, B. Monge-Sanz, I. Morino, I. Murata, H. Nakajima, M. Palm, C. Paton-Walsh, U. Raffalski, T. Reddmann, M. Rettinger, C.P. Rinsland, E. Rozanov, M. Schneider, C. Senten, C. Servais, B.M. Sinnhuber, D. Smale, K. Strong, R. Sussmann, J.R. Taylor, G. Vanhaelewyn, T. Warneke, C. Whaley, M. Wiehle, and S.W. Wood, Observed and simulated time evolution of HCl, $ClONO_2$, and HF total column abundances, *Atmos. Chem. Phys.*, *12*(7), 3527–3556, doi:10.5194/acp-12-3527-2012, 2012.

Kovacs, T., W.H. Feng, A. Totterdill, J.M.C. Plane, S. Dhomse, J.C. Gomez-Martin, G.P. Stiller, F.J. Haenel, C. Smith, P.M. Forster, R.R. Garcia, D.R. Marsh, and M.P. Chipperfield, Determination of the atmospheric lifetime and global warming potential of sulfur hexafluoride using a three-dimensional model, *Atmos. Chem. Phys.*, *17*(2), 883–898, doi:10.5194/acp-17-883-2017, 2017.

Kremser, S., L.W. Thomason, M. von Hobe, M. Hermann, T. Deshler, C. Timmreck, M. Toohey, A. Stenke, J.P. Schwarz, R. Weigel, S. Fueglistaler, F.J. Prata, J.-P. Vernier, H. Schlager, J.E. Barnes, J.-C. Antuña-Marrero, D. Fairlie, M. Palm, E. Mahieu, J. Notholt, M. Rex, C. Bingen, F. Vanhellemont, A. Bourassa, J.M.C. Plane, D. Klocke, S.A. Carn, L. Clarisse, T. Trickl, R. Neely, A.D. James, L. Rieger, J.C. Wilson, and B. Meland, Stratospheric aerosol—Observations, processes, and impact on climate, *Rev. Geophys.*, *54*(2), 278-335, doi:10.1002/2015RG000511, 2016.

Kreycy, S., C. Camy-Peyret, M.P. Chipperfield, M. Dorf, W. Feng, R. Hossaini, L. Kritten, B. Werner, and K. Pfeilsticker, Atmospheric test of the $J(BrONO_2)/k(BrO+NO_2)$ ratio: Implications for total stratospheric Br_y and bromine-mediated ozone loss, *Atmos. Chem. Phys.*, *13*(13), 6263–6274, doi:10.5194/acp-13-6263-2013, 2013.

Kruger, K., S. Tegtmeier, and M. Rex, Long-term climatology of air mass transport through the Tropical Tropopause Layer (TTL) during NH winter, *Atmos. Chem. Phys.*, *8*(4), 813–823, 2008.

Krysztofiak, G., Y.V. Té, V. Catoire, G. Berthet, G.C. Toon, F. Jégou, P. Jeseck, and C. Robert, Carbonyl Sulphide (OCS) Variability with Latitude in the Atmosphere, *Atmos. Ocean*, *53*(1), 89–101, doi:10.1080/07055900.2013.876609, 2015.

Langenfelds, R.L., P.J. Fraser, R.J. Francey, L.P. Steele, L.W. Porter, and C.E. Allison, The Cape Grim Air Archive: The first seventeen years, 1978-1995, edited by R.J. Francey, A.L. Dick, N. Derek, p. 53-70, Baseline Atmospheric Program Australia. [Melbourne]: Bureau of Meteorology and CSIRO Division of Atmospheric Research, 1996.

Laube, J.C., C. Hogan, M.J. Newland, F.S. Mani, P.J. Fraser, C.A.M. Brenninkmeijer, P. Martinerie, D.E. Oram, T. Rockmann, J. Schwander, E. Witrant, G.P. Mills, C.E. Reeves, and W.T. Sturges, Distributions, long term trends and emissions of four perfluorocarbons in remote parts of the atmosphere and firn air, *Atmos. Chem. Phys.*, *12*(9), 4081–4090, doi:10.5194/acp-12-4081-2012, 2012.

Laube, J.C., A. Keil, H. Bönisch, A. Engel, T. Röckmann, C.M. Volk, and W.T. Sturges, Observation-based assessment of stratospheric fractional release, lifetimes, and ozone depletion potentials of ten important source gases, *Atmos. Chem. Phys.*, *13*(5), 2779–2791, doi:10.5194/acp-13-2779-2013, 2013.

Laube, J.C., M.J. Newland, C. Hogan, C.A.M. Brenninkmeijer, P.J. Fraser, P. Martinerie, D.E. Oram, C.E. Reeves, T. Rockmann, J. Schwander, E. Witrant, and W.T. Sturges, Newly detetecd ozone-depleting substances in the atmosphere, *Nat. Geosci.*, *7*(4), 266–269, doi:10.1038/ngeo2109, 2014.

Laube, J.C., N.M. Hanif, P. Martinerie, E. Gallacher, P.J. Fraser, R. Langenfelds, C.A.M. Brenninkmeijer, J. Schwander, E. Witrant, J.L. Wang, C.F. Ou-Yang, L.J. Gooch, C.E. Reeves, W.T. Sturges, and D.E. Oram, Tropospheric observations of CFC-114 and CFC-114a with a focus on long-term trends and emissions, *Atmos. Chem. Phys.*, *6*(23), 15347–15358, doi:10.5194/acp-16-15347-2016, 2016.

Launois, T., P. Peylin, S. Belviso, and B. Poulter, A new model of the global biogeochemical cycle of carbonyl sulfide – Part 2: Use of carbonyl sulfide to constrain gross primary productivity in current vegetation models, *Atmos. Chem. Phys.*, *15*(16), 9285-9312, doi:10.5194/acp-15-9285-2015, 2015.

Lawson, S.J., M.D. Keywood, I.E. Galbally, J.L. Gras, J.M. Cainey, M.E. Cope, P.B. Krummel, P.J. Fraser, L.P. Steele, S.T. Bentley, C.P. Meyer, Z. Ristovski, and A.H. Goldstein, Biomass burning emissions of trace gases and particles in marine air at Cape Grim, Tasmania, *Atmos. Chem. Phys.*, *15*(23), 13393–13411, doi:10.5194/acp-15-13393-2015, 2015.

Le Breton, M., T.J. Bannan, D.E. Shallcross, M.A. Khan, M.J. Evans, J. Lee, R. Lidster, S. Andrews, L.J. Carpenter, J. Schmidt, D. Jacob, N.R.P. Harris, S. Bauguitte, M. Gallagher, A. Bacak, K.E. Leather, and C.J. Percival, Enhanced ozone loss by active inorganic bromine chemistry in the tropical troposphere, *Atmos. Environ., 155*, 21–28, doi:10.1016/j.atmosenv.2017.02.003, 2017.

Leedam Elvidge, E.C., D.E. Oram, J.C. Laube, A.K. Baker, S.A. Montzka, S. Humphrey, D.A. O'Sullivan, and C.A.M. Brenninkmeijer, Increasing concentrations of dichloromethane, CH_2Cl_2, inferred from CARIBIC air samples collected 1998-2012, *Atmos. Chem. Phys.*, *15*(4), 1939–1958, doi:10.5194/acp-15-1939-2015, 2015a.

Leedam Elvidge, E.C., S.M. Phang, W.T. Sturges, and G. Malin, The effect of desiccation on the emission of volatile bromocarbons from two common temperate macroalgae, *Biogeosci.*, *12*(2), 387–398, doi:10.5194/bg-12-387-2015, 2015b.

Leedham Elvidge, E.C., H. Bönisch, C.A.M. Brenninkmeijer, A. Engel, P.J. Fraser, E. Gallacher, R. Langenfelds, J. Mühle, D.E. Oram, E.A. Ray, A.R. Ridley, T. Röckmann, W.T. Sturges, R.F. Weiss, and J.C. Laube, Evaluation of stratospheric age of air from CF_4, C_2F_6, $C3F_8$, CHF_3, HFC-125, HFC-227ea and SF_6: Implications for the calculations of halocarbon lifetimes, fractional release factors and ozone depletion potentials, *Atmos. Chem. Phys.*, *18*(5), 3369–3385, doi:10.5194/acp-18-3369-2018, 2018.

Le Quéré, C., R.M. Andrew, P. Friedlingstein, S. Sitch, J. Pongratz, A.C. Manning, J.I. Korsbakken, G.P. Peters, J.G. Canadell, R.B. Jackson, T.A. Boden, P.P. Tans, O.D. Andrews, V.K. Arora, D.C.E. Bakker, L. Barbero, M. Becker, R.A. Betts, L. Bopp, F. Chevallier, L.P. Chini, P. Ciais, C.E. Cosca, J. Cross, K. Currie, T. Gasser, I. Harris, J. Hauck, V. Haverd, R.A. Houghton, C.W. Hunt, G. Hurtt, T. Ilyina, A.K. Jain, E. Kato, M. Kautz, R.F. Keeling, K. Klein Goldewijk, A. Körtzinger, P. Landschützer, N. Lefèvre, A. Lenton, S. Lienert, I. Lima, D. Lombardozzi, N. Metzl, F. Millero, P.M.S. Monteiro, D.R. Munro, J.E.M.S. Nabel, S.I. Nakaoka, Y. Nojiri, X.A. Padin, A. Peregon, B. Pfeil, D. Pierrot, B. Poulter, G. Rehder, J. Reimer, C. Rödenbeck, J. Schwinger, R. Séférian, I. Skjelvan, B.D. Stocker, H. Tian, B. Tilbrook, F.N. Tubiello, I.T. van der Laan-Luijkx, G.R. van der Werf, S. van Heuven, N. Viovy, N. Vuichard, A.P. Walker, A.J. Watson, A.J. Wiltshire, S. Zaehle, and D. Zhu, Global Carbon Budget 2017, *Earth Syst. Sci. Data*, *10*(1), 405–448, doi:10.5194/essd-10-405-2018, 2018.

Lee-Taylor, J., and K.R. Redeker, Reevaluation of global emissions from rice paddies of methyl iodide and other species, *Geophys. Res. Lett.*, *32*(15), doi:10.1029/2005GL022918, 2005.

Lejeune, B., E. Mahieu, M.K. Vollmer, S. Reimann, P.F. Bernath, C.D. Boone, K.A. Walker, and C. Servais, Optimized approach to retrieve information on atmospheric carbonyl sulfide (OCS) above the Jungfraujoch station and change in its abundance since 1995, *J. Quant. Spectrosc. Radiat. Trans.*, *186*, 81–95, available at: https://www.sciencedirect.com/science/article/pii/S0022407316300899, 2017.

Lennartz, S.T., G. Krysztofiak, C.A. Marandino, B.M. Sinnhuber, S. Tegtmeier, F. Ziska, R. Hossaini, K. Krüger, S.A. Montzka, E. Atlas, D.E. Oram, T. Keber, H. Bönisch, and B. Quack, Modelling marine emissions and atmospheric distributions of halocarbons and dimethyl sulfide: the influence of prescribed water concentration vs. prescribed emissions, *Atmos. Chem. Phys.*, *15*(20), 11753–11772, doi:10.5194/acp-15-11753-2015, 2015.

Lennartz, S.T., C.A. Marandino, M. von Hobe, P. Cortes, B. Quack, R. Simo, D. Booge, A. Pozzer, T. Steinhoff, D.L. Arevalo-Martinez, C. Kloss, A. Bracher, R. Röttgers, E. Atlas, and K. Krüger, Direct oceanic emissions unlikely to account for the missing source of atmospheric carbonyl sulfide, *Atmos. Chem. Phys.*, *17*(1), 385-402, doi:10.5194/acp-17-385-2017, 2017.

Levin, I., T. Naegler, R. Heinz, D. Osusko, E. Cuevas, A. Engel, J. Ilmberger, R.L. Langenfelds, B. Neininger, C. Von Rohden, L.P. Steele, R. Weller, D.E. Worthy, and S.A. Zimov, The global SF_6 source inferred from long-term high precision atmospheric measurements and its comparison with emission inventories, *Atmos. Chem. Phys.*, *10*(6), 2655–2662, 2010.

Li, S., J. Kim, K.R. Kim, J. Mühle, S.K. Kim, M.K. Park, A. Stohl, D.J. Kang, T. Arnold, C.M. Harth, P.K. Salameh, and R.F. Weiss, Emissions of halogenated compounds in East Asia determined from measurements at Jeju Island, Korea, *Environ. Sci. Technol., 45*(13), 5668–5675, doi:10.1021/es104124k, 2011.

Li, S., M. Park, C.O. Jo, and S. Park, Emission estimates of methyl chloride from industrial sources in China based on high frequency atmospheric observations, *J. Atmos. Chem.*, *74*(2), 227–243, doi:10.1007/s10874-016-9354-4, 2017.

Li, Z., P. Bie, Z. Wang, Z. Zhang, H. Jiang, W. Xu, J. Zhang, and J. Hu, Estimated HCFC-22 emissions for 1990–2050 in China and the increasing contribution to global emissions, *Atmos. Environ., 132*, 77–84, doi:10.1016/j.atmosenv.2016.02.038, 2016.

Liang, Q., E. Atlas, D. Blake, M. Dorf, K. Pfeilsticker, and S. Schauffler, Convective transport of very short lived bromocarbons to the stratosphere, *Atmos. Chem. Phys.*, *14*(11), 5781–5792, doi:10.5194/acp-14-5781-2014, 2014a.

Liang, Q., P.A. Newman, J.S. Daniel, S. Reimann, B.D. Hall, G. Dutton, and L.J.M. Kuijpers, Constraining the carbon tetrachloride (CCl_4) budget using its global trend and inter-hemispheric gradient, *Geophys. Res. Lett.*, *41*(14), 5307–5315, doi:10.1002/2014GL060754, 2014b.

Liang, Q., S. Reimann, and P.A. Newman, SPARC Report on the Mystery of Carbon Tetrachloride, SPARC, Volume 7, doi:10.3929/ethz-a-01069-0647, 2016.

Liu, Y., S.A. Yvon-Lewis, L. Hu, J.E. Salisbury, and J.E. O'Hern, $CHBr_3$, $CH2Br_2$, and $CHClBr_2$ in U.S. coastal waters during the Gulf of Mexico and East Coast Carbon cruise, *J. Geophys. Res. Oceans*, *116*(C10), doi:10.1029/2010JC006729, 2011.

Liu, Z., B. Yao, X. An, L. Zhou, T. Luan, H. Wang, G. Zhang, and S. Cheng, Study of Chinese HCFC-142b emission by inverse model, in Chinese with English abstract, *China Envirnomental Science*, *35*(4), 1040–1046, 2015.

Lobert, J.M., W.C. Keene, J.A. Logan, and R. Yevich, Global chlorine emissions from biomass burning: Reactive Chlorine Emissions Inventory, *J. Geophys. Res. Atmos.*, *104*(D7), 8373–8389, doi:10.1029/1998JD100077, 1999.

Logue, J.M., M.J. Small, D. Stern, J. Maranche, and A.L. Robinson, Spatial Variation in Ambient Air Toxics Concentrations and Health Risks between Industrial-Influenced, Urban, and Rural Sites, *J. Air Waste Manag. Assoc.*, *60*(3), 271–286, doi:10.3155/1047-3289.60.3.271, 2010.

Mahieu, E., M.P. Chipperfield, J. Notholt, T. Reddmann, J. Anderson, P.F. Bernath, T. Blumenstock, M.T. Coffey, S.S. Dhomse, W. Feng, B. Franco, L. Froidevaux, D.W.T. Griffith, J.W. Hannigan, F. Hase, R. Hossaini, N.B. Jones, I. Morino, I. Murata, H. Nakajima, M. Palm, C. Paton-Walsh, J.M.R. III, M. Schneider, C. Servais, D. Smale, and K.A. Walker, Recent Northern Hemisphere stratospheric HCl increase due to atmospheric circulation changes, *Nature*, *515*(7525), 104–107, doi:10.1038/nature13857, 2014a.

Mahieu, E., R. Zander, G.C. Toon, M.K. Vollmer, S. Reimann, J. Mühle, W. Bader, B. Bovy, B. Lejeune, C. Servais, P. Demoulin, G. Roland, P.F. Bernath, C.D. Boone, K.A. Walker, and P. Duchatelet, Spectrometric monitoring of atmospheric carbon tetrafluoride (CF_4) above the Jungfraujoch station since 1989: Evidence of continued increase but at a slowing rate, *Atmos. Meas. Tech.*, *7*(1), 333–344, doi:10.5194/amt-7-333-2014, 2014b.

Mahieu, E., B. Lejeune, B. Bovy, C. Servais, G.C. Toon, P.F. Bernath, C.D. Boone, K.A. Walker, S. Reimann, M.K. Vollmer, and S. O'Doherty, Retrieval of HCFC-142b (CH_3CClF_2) from ground-based high-resolution infrared solar spectra: Atmospheric increase since 1989 and comparison with surface and satellite measurements, *J. Quant. Spectrosc. Radiat. Trans.*, *186*, 96–105, doi:10.1016/j.jqsrt.2016.03.017, 2017.

Maione, M., F. Graziosi, J. Arduini, F. Furlani, U. Giostra, D.R. Blake, P. Bonasoni, X. Fang, S.A. Montzka, S.J. O'Doherty, S. Reimann, A. Stohl, and M.K. Vollmer, Estimates of European emissions of methyl chloroform using a Bayesian inversion method, *Atmos. Chem. Phys.*, *14*(18), 9755–9770, doi:10.5194/acp-14-9755-2014, 2014.

Manley, S.L., N.Y. Wang, M.L. Walser, and R.J. Cicerone, Coastal salt marshes as global methyl halide sources from determinations of intrinsic production by marsh plants, *Global Biogeochem. Cycles*, *20*(3), doi:10.1029/2005gb002578, 2006.

Mao, T., Y.S. Wang, H.H. Xu, J. Jiang, F.K. Wu, and X.B. Xu, A study of the atmospheric VOCs of Mount Tai in June 2006, *Atmos. Environ., 43*(15), 2503–2508, doi:10.1016/j.atmosenv.2009.02.013, 2009.

Marcy, T.P., P.J. Popp, R.S. Gao, D.W. Fahey, E.A. Ray, E.C. Richard, T.L. Thompson, E.L. Atlas, M. Loewenstein, S.C. Wofsy, S. Park, E.M. Weinstock, W.H. Swartz, and M.J. Mahoney, Measurements of trace gases in the tropical tropopause layer, *Atmos. Environ., 41*(34), 7253–7261, doi:10.1016/j.

atmosenv.2007.05.032, 2007.

McCulloch, A., M.L. Aucott, C.M. Benkovitz, T.E. Graedel, G. Kleiman, P.M. Midgley, and Y.-F. Li, Global emissions of hydrogen chloride and chloromethane from coal combustion, incineration and industrial activities: Reactive Chlorine Emissions Inventory, *J. Geophys. Res. Atmos.*, *104*(D7), 8391–8403, doi:10.1029/1999JD900025, 1999.

McCulloch, A., Chloroform in the environment: occurrence, sources, sinks and effects, *Chemosphere*, *50*(10), 1291–1308, doi:10.1016/s0045-6535(02)00697-5, 2003.

McNorton, J., E. Gloor, C. Wilson, G.D. Hayman, N. Gedney, E. Comyn-Platt, T. Marthews, R.J. Parker, H. Boesch, and M.P. Chipperfield, Role of regional wetland emissions in atmospheric methane variability, *Geophys. Res. Lett.*, *43*(21), 11433–11444, doi:10.1002/2016GL070649, 2016.

Mébarki, Y., V. Catoire, N. Huret, G. Berthet, C. Robert, and G. Poulet, More evidence for very short-lived substance contribution to stratospheric chlorine inferred from HCl balloon-borne in situ measurements in the tropics, *Atmos. Chem. Phys.*, *10*, 397–409, doi:10.5194/acpd-9-16163-2009, 2010.

Mendez-Diaz, J.D., K.K. Shimabuku, J. Ma, Z.O. Enumah, J.J. Pignatello, W.A. Mitch, and M.C. Dodd, Sunlight-driven photochemical halogenation of dissolved organic matter in seawater: A natural abiotic source of organobromine and organoiodine, *Environ. Sci. Technol.*, *48*(13), 7418–7427, doi:10.1021/es5016668, 2014.

Millán, L., N. Livesey, W. Read, L. Froidevaux, D. Kinnison, R. Harwood, I.A. MacKenzie, and M.P. Chipperfield, New Aura Microwave Limb Sounder observations of BrO and implications for Br_y, *Atmos. Meas. Tech.*, *5*(7), 1741-1751, doi:10.5194/amt-5-1741–2012, 2012.

Miller, B.R., M. Rigby, L.J.M. Kuijpers, P.B. Krummel, L.P. Steele, M. Leist, P.J. Fraser, A. McCulloch, C. Harth, P. Salameh, J. Mühle, R.F. Weiss, R.G. Prinn, R.H.J. Wang, S. O'Doherty, B.R. Greally, and P.G. Simmonds, HFC-23 (CHF_3) emission trend response to HCFC-22 ($CHClF_2$) production and recent HFC-23 emission abatement measures, *Atmos. Chem. Phys.*, *10*(16), 7875–7890, doi:10.5194/acp-10-7875-2010, 2010.

Montzka, S.A., J.H. Butler, B.D. Hall, D.J. Mondeel, and J.W. Elkins, A decline in tropospheric organic bromine, *Geophys. Res. Lett.*, *30*(15), doi:10.1029/2003GL017745, 2003.

Montzka, S.A., P. Calvert, B.D. Hall, J.W. Elkins, T.J. Conway, P.P. Tans, and C. Sweeney, On the global distribution, seasonality, and budget of atmospheric carbonyl sulfide (COS) and some similarities to CO_2, *J. Geophys. Res. Atmos.*, *112*(D9), doi:10.1029/2006JD007665, 2007.

Montzka, S.A., S. Reimann, (Coordinating Lead Authors) A. Engel, K. Krüger, S. O`Doherty, and W.T. Sturges, Ozone-Depleting Substances (ODSs) and Related Chemicals, Chapter 1 in *Scientific Assessment of Ozone Depletion: 2010*, Global Ozone Research and Monitoring Project–Report No. 52, World Meteorological Organization, Geneva, Switzerland, 2010.

Montzka, S.A., M. McFarland, S.O. Andersen, B.R. Miller, D.W. Fahey, B.D. Hall, L. Hu, C. Siso, and J.W. Elkins, Recent trends in global emissions of hydrochlorofluorocarbons and hydrofluorocarbons: Reflecting on the 2007 adjustments to the Montreal Protocol, *J. Phys. Chem. A*, *119*(19), 4439–4449, doi:10.1021/jp5097376, 2015.

Montzka, S.A., G.S. Dutton, P. Yu, E. Ray, R.W. Portmann, J.S. Daniel, L. Kuijpers, B.D. Hall, D. Mondeel, C. Siso, J.D. Nance, M. Rigby, A.J. Manning, L. Hu, F. Moore, B.R. Miller, and J.W. Elkins, An unexpected and persistent increase in global emissions of ozone-depleting CFC-11, *Nature*, *557*(7705), 413–417, doi:10.1038/s41586-018-0106-2, 2018.

Mühle, J., J. Huang, R.F. Weiss, R.G. Prinn, B.R. Miller, P.K. Salameh, C.M. Harth, P.J. Fraser, L.W. Porter, B.R. Greally, S. O'Doherty, and P.G. Simmonds, Sulfuryl fluoride in the global atmosphere, *J. Geophys. Res. Atmos.*, *114* D05306, doi:10.1029/2008JD011162, 2009.

Mühle, J., A.L. Ganesan, B.R. Miller, P.K. Salameh, C.M. Harth, B.R. Greally, M. Rigby, L.W. Porter, L.P. Steele, C.M. Trudinger, P.B. Krummel, S. O'Doherty, P.J. Fraser, P.G. Simmonds, R.G. Prinn, and R.F. Weiss, Perfluorocarbons in the global atmosphere: tetrafluoromethane, hexafluoroethane, and octafluoropropane, *Atmos. Chem. Phys.*, *10*(11), 5145–5164, doi:10.5194/acp-10-5145–2010, 2010.

Murphy, D.M., and D.S. Thomson, Halogen ions and NO+ in the mass spectra of aerosols in the upper troposphere and lower stratosphere, *Geophys. Res. Lett.*, *27*(19), 3217–3220,

doi:10.1029/1999GL011267, 2000.

Murphy, D.M., K.D. Froyd, J.P. Schwarz, and J.C. Wilson, Observations of the chemical composition of stratospheric aerosol particles, *Q. J. R. Meteorol. Soc.*, *140*(681), 1269–1278, doi:10.1002/qj.2213, 2014.

Myhre, G., and D.T. Shindell (Coordinating Lead Authors), F.-M. Bréon, W. Collins, J. Fuglestvedt, J. Huang, D. Koch, J.-F. Lamargue, D. Lee, B. Mendoza, T. Nakajima, A. Robock, G. Stephens, T. Takemura, and H. Zhang, Anthropogenic and Natural Radiative Forcing, Chapter 8 in *Climate Change 2013: The Physical Science Basis. Contribution of Working Group I to the Fifth Assessment Report of the Intergovernmental Panel on Climate Change*, edited by D.J. Jacob, A.R. Ravishankara, and K. Shine, p. 659–740, Cambridge University Press, Cambridge, United Kingdom, 2013.

Nadzir, M.S.M., S.M. Phang, M.R. Abas, N.A. Rahman, A. Abu Samah, W.T. Sturges, D.E. Oram, G.P. Mills, E.C. Leedham, J.A. Pyle, N.R.P. Harris, A.D. Robinson, M.J. Ashfold, M.I. Mead, M.T. Latif, M.F. Khan, A.M. Amiruddin, N. Banan, and M.M. Hanafiah, Bromocarbons in the tropical coastal and open ocean atmosphere during the 2009 Prime Expedition Scientific Cruise (PESC-09), *Atmos. Chem. Phys.*, *14*(15), 8137–8148, doi:10.5194/acp-14-8137-2014, 2014.

Navarro, M.A., E.L. Atlas, A. Saiz-Lopez, X. Rodriguez-Lloveras, D.E. Kinnison, J.F. Lamarque, S. Tilmes, M. Filus, N.R.P. Harris, E. Meneguz, M.J. Ashfold, A.J. Manning, C.A. Cuevas, S.M. Schauffler, and V. Donets, Airborne measurements of organic bromine compounds in the Pacific tropical tropopause layer, *Proc. Natl. Acad. Sci.*, *112*(45), 13789–13793, doi:10.1073/pnas.1511463112, 2015.

Nedoluha, G.E., I.S. Boyd, A. Parrish, R.M. Gomez, D.R. Allen, L. Froidevaux, B.J. Connor, and R.R. Querel, Unusual stratospheric ozone anomalies observed in 22 years of measurements from Lauder, New Zealand, *Atmos. Chem. Phys.*, *15*(12), 6817–6826, doi:10.5194/acp-15-6817-2015, 2015.

Nedoluha, G.E., B.J. Connor, T. Mooney, J.W. Barrett, A. Parrish, R.M. Gomez, I. Boyd, D.R. Allen, M. Kotkamp, S. Kremser, T. Deshler, P. Newman, and M.L. Santee, 20 years of ClO measurements in the Antarctic lower stratosphere, *Atmos. Chem. Phys.*, *16*(16), 10725–10734, doi:10.5194/acp-16-10725-2016, 2016.

Newland, M.J., C.E. Reeves, D.E. Oram, J.C. Laube, W.T. Sturges, C. Hogan, P. Begley, and P.J. Fraser, Southern hemispheric halon trends and global halon emissions, 1978–2011, *Atmos. Chem. Phys.*, *13*(11), 5551-5565, doi:10.5194/acp-13-5551-2013, 2013.

Newman, P.A., J.S. Daniel, D.W. Waugh, and E.R. Nash, A new formulation of equivalent effective stratospheric chlorine (EESC), *Atmos. Chem. Phys.*, *7*(17), 4537–4552, doi:10.5194/acp-7-4537-2007, 2007.

Nisbet, E.G., E.J. Dlugokencky, M.R. Manning, D. Lowry, R.E. Fisher, J.L. France, S.E. Michel, J.B. Miller, J.W.C. White, B. Vaughn, P. Bousquet, J.A. Pyle, N.J. Warwick, M. Cain, R. Brownlow, G. Zazzeri, M. Lanoiselle, A.C. Manning, E. Gloor, D.E.J. Worthy, E.G. Brunke, C. Labuschagne, E.W. Wolff, and A.L. Ganesan, Rising atmospheric methane: 2007-2014 growth and isotopic shift, *Global Biogeochem. Cycles*, *30*(9), 1356–1370, doi:10.1002/2016gb005406, 2016.

O'Doherty, S., D.M. Cunnold, B.R. Miller, J. Mühle, A. McCulloch, P.G. Simmonds, A.J. Manning, S. Reimann, M.K. Vollmer, B.R. Greally, R.G. Prinn, P.J. Fraser, L.P. Steele, P.B. Krummel, B.L. Dunse, L.W. Porter, C.R. Lunder, N. Schmidbauer, O. Hermansen, P.K. Salameh, C.M. Harth, R.H.J. Wang, and R.F. Weiss, Global and regional emissions of HFC-125 (CHF_2CF_3) from in situ and air archive atmospheric observations at AGAGE and SOGE observatories, *J. Geophys. Res.*, *114*, D23304, doi:10.1029/2009JD012184, 2009.

Ooki, A., D. Nomura, S. Nishino, T. Kikuchi, and Y. Yokouchi, A global-scale map of isoprene and volatile organic iodine in surface seawater of the Arctic, Northwest Pacific, Indian, and Southern Oceans, *J. Geophys. Res. Oceans*, *120*(6), 4108–4128, doi:10.1002/2014jc010519, 2015.

Oram, D.E., C.E. Reeves, W.T. Sturges, S.A. Penkett, P.J. Fraser, and R.L. Langenfelds, Recent tropospheric growth rate and distribution of HFC-134a (CF_3CH_2F), *Geophys. Res. Lett.*, *23*(15), 1949–1952, doi:10.1029/96GL01862, 1996.

Oram, D.E., Trends of Long-Lived Anthropogenic Halocarbons in the Southern Hemisphere and Model Calculation of Global Emissions, Ph.D. thesis, University of East Anglia, Norwich, United Kingdom, 249 pp., 1999.

Oram, D.E., F.S. Mani, J.C. Laube, M.J. Newland, C.E. Reeves, W.T. Sturges, S.A. Penkett, C.A.M. Brenninkmeijer, T. Rockmann, and P.J. Fraser, Long-term tropospheric trend of octafluorocyclobutane (c-C4F8 or PFC-318), *Atmos. Chem. Phys.*, *12*(1), 261–269, doi:10.5194/acp-12-261-2012, 2012.

Oram, D.E., M.J. Ashfold, J.C. Laube, L.J. Gooch, S. Humphrey, W.T. Sturges, E. Leedham-Elvidge, G.L. Forster, N.R.P. Harris, M.I. Mead, A. Abu Samah, S.M. Phang, O.Y. Chang-Feng, N.H. Lin, J.L. Wang, A.K. Baker, C.A.M. Brenninkmeijer, and D. Sherry, A growing threat to the ozone layer from short-lived anthropogenic chlorocarbons, *Atmos. Chem. Phys.*, *2017*, 1–20, doi:10.5194/acp-2017–497, 2017.

Orbe, C., D.W. Waugh, H. Yang, J.-F. Lamarque, S. Tilmes, and D.E. Kinnison, Tropospheric transport differences between models using the same large-scale meteorological fields, *Geophys. Res. Lett.*, *44*(2), 1068–1078, doi:10.1002/2016GL071339, 2017.

Ordonez, C., J.F. Lamarque, S. Tilmes, D.E. Kinnison, E.L. Atlas, D.R. Blake, G.S. Santos, G. Brasseur, and A. Saiz-Lopez, Bromine and iodine chemistry in a global chemistry-climate model: Description and evaluation of very short-lived oceanic sources, *Atmos. Chem. Phys.*, *12*(3), 1423–1447, doi:10.5194/acp-12-1423-2012, 2012.

Ostermöller, J., H. Bönisch, P. Jöckel, and A. Engel, A new time-independent formulation of fractional release, *Atmos. Chem. Phys.*, *17*(6), 3785–3797, doi:10.5194/acp-17-3785-2017, 2017.

Pan, L.L., E.L. Atlas, R.J. Salawitch, S.B. Honomichl, J.F. Bresch, W.J. Randel, E.C. Apel, R.S. Hornbrook, A.J. Weinheimer, D.C. Anderson, S.J. Andrews, S. Baidar, S.P. Beaton, T.L. Campos, L.J. Carpenter, D. Chen, B. Dix, V. Donets, S.R. Hall, T.F. Hanisco, C.R. Homeyer, L.G. Huey, J.B. Jensen, L. Kaser, D.E. Kinnison, T.K. Koenig, J.F. Lamarque, C. Liu, J. Luo, Z.J. Luo, D.D. Montzka, J.M. Nicely, R.B. Pierce, D.D. Riemer, T. Robinson, P. Romashkin, A. Saiz-Lopez, S. Schauffler, O. Shieh, M.H. Stell, K. Ullmann, G. Vaughan, R. Volkamer, and G. Wolfe, The Convective Transport of Active Species in the Tropics (CONTRAST) Experiment, *Bull. Am. Meteorol. Soc.*, *98*(1), 106–128, doi:10.1175/bams-d-14-00272.1, 2017.

Parrella, J.P., D.J. Jacob, Q. Liang, Y. Zhang, L.J. Mickley, B. Miller, M.J. Evans, X. Yang, J.A. Pyle, N. Theys, and M. Van Roozendael, Tropospheric bromine chemistry: Implications for present and pre-industrial ozone and mercury, *Atmos. Chem. Phys.*, *12*(15), 6723–6740, doi:10.5194/acp-12-6723-2012, 2012.

Pfeilsticker, K., W.T. Sturges, H. Bosch, C. Camy-Peyret, M.P. Chipperfield, A. Engel, R. Fitzenberger, M. Muller, S. Payan, and B.M. Sinnhuber, Lower stratospheric organic and inorganic bromine budget for the Arctic winter 1998/99, Geophys. Res. Lett., 27(20), 3305–3308, doi:10.1029/2000GL011650, 2000.

Plumb, I.C., P.F. Vohralik, and K.R. Ryan, Normalization of correlations for atmospheric species with chemical loss, *J. Geophys. Res. Atmos. 104*(D9), 11723–11732, doi:10.1029/1999JD900014, 1999.

Prather, M.J., J. Hsu, N.M. DeLuca, C.H. Jackman, L.D. Oman, A.R. Douglass, E.L. Fleming, S.E. Strahan, S.D. Steenrod, O.A. Sovde, I.S.A. Isaksen, L. Froidevaux, and B. Funke, Measuring and modeling the lifetime of nitrous oxide including its variability, *J. Geophys. Res. Atmos.*, *120*(11), 5693–5705, doi:10.1002/2015JD023267, 2015.

Prinn, R.G., R.F. Weiss, J. Arduini, T. Arnold, H.L. DeWitt, P.J. Fraser, A.L. Ganesan, J. Gasore, C.M. Harth, O. Hermansen, J. Kim, P.B. Krummel, S. Li, Z.M. Loh, C.R. Lunder, M. Maione, A.J. Manning, B.R. Miller, B. Mitrevski, J. Mühle, S. O'Doherty, S. Park, S. Reimann, M. Rigby, T. Saito, P.K. Salameh, R. Schmidt, P.G. Simmonds, L.P. Steele, M.K. Vollmer, R.H. Wang, B. Yao, Y. Yokouchi, D. Young, and L. Zhou, History of chemically and radiatively important atmospheric gases from the Advanced Global Atmospheric Gases Experiment (AGAGE), *Earth Syst. Sci. Data*, *10*(2), 985–1018, doi:10.5194/essd-10-985-2018, 2018.

Quack, B., E. Atlas, G. Petrick, and D.W.R. Wallace, Bromoform and dibromomethane above the Mauritanian upwelling: Atmospheric distributions and oceanic emissions, *J. Geophys. Res. Atmos.*, *112*(D9), doi:10.1029/2006JD007614, 2007.

Ramaswamy, V. (Coordinating Lead Author), O. Boucher, J.D. Haigh, D.A. Hauglustaine, J.M. Haywood, G. Myrhe, T. Nakajima, G.Y. Shi, and S. Solomon, Radiative Forcing of Climate Change, Chapter 6 in *Climate Change 2001: The Scientific Basis. Contribution of Working Group I to the Third Assessment Report of the Intergovernmental Panel on Climate Change,* edited by F. Joos and J. Srinivasan, Cambridge University Press, Cambridge,

United Kingdom and New York, New York, 2001.

Ravishankara, A.R., S. Solomon, A.A. Turnipseed, and R.F. Warren, Atmospheric Lifetimes of Long-Lived Halogenated Species, *Science*, *259*(5092), 194–199, doi: 10.1126/science.259.5092.194, 1993.

Ravishankara, A.R., J.S. Daniel, and R.W. Portmann, Nitrous Oxide (N_2O): The dominant ozone-depleting substance emitted in the 21st century, *Science*, *326*(5949), 123–125, doi:10.1126/science.1176985, 2009.

Ray, E.A., F.L. Moore, J.W. Elkins, K.H. Rosenlof, J.C. Laube, T. Rockmann, D.R. Marsh, and A.E. Andrews, Quantification of the SF_6 lifetime based on mesospheric loss measured in the stratospheric polar vortex, *J. Geophys. Res. Atmos.*, *122*(8), 4626–4638, doi:10.1002/2016JD026198, 2017.

Revell, L.E., F. Tummon, R.J. Salawitch, A. Stenke, and T. Peter, The changing ozone depletion potential of N_2O in a future climate, *Geophys. Res. Lett.*, *42*(22), 10,047-010,055, doi:10.1002/2015GL065702, 2015.

Rex, M., I. Wohltmann, T. Ridder, R. Lehmann, K. Rosenlof, P. Wennberg, D. Weisenstein, J. Notholt, K. Kruger, V. Mohr, and S. Tegtmeier, A tropical West Pacific OH minimum and implications for stratospheric composition, *Atmos. Chem. Phys.*, *14*(9), 4827–4841, doi:10.5194/acp-14-4827-2014, 2014.

Rhew, R.C., M.E. Whelan, and D.H. Min, Large methyl halide emissions from south Texas salt marshes, *Biogeosci.*, *11*(22), 6427–6434, doi:10.5194/bg-11-6427-2014, 2014.

Rhew, R.C., and J.D. Happell, The atmospheric partial lifetime of carbon tetrachloride with respect to the global soil sink, *Geophys. Res. Lett.*, *43*(6), 2889–2895, doi:10.1002/2016GL067839, 2016.

Rigby, M., J. Mühle, B.R. Miller, R.G. Prinn, P.B. Krummel, L.P. Steele, P.J. Fraser, P.K. Salameh, C.M. Harth, R.F. Weiss, B.R. Greally, S. O'Doherty, P.G. Simmonds, M.K. Vollmer, S. Reimann, J. Kim, K.R. Kim, H.J. Wang, J.G.J. Olivier, E.J. Dlugokencky, G.S. Dutton, B.D. Hall, and J.W. Elkins, History of atmospheric SF_6 from 1973 to 2008, *Atmos. Chem. Phys.*, *10*(21), 10305–10320, doi:10.5194/acp-10-10305-2010, 2010.

Rigby, M., A.L. Ganesan, and R.G. Prinn, Deriving emissions time series from sparse atmospheric mole fractions, *J. Geophys. Res. Atmos.*, *116*, doi:10.1029/2010JD015401, 2011.

Rigby, M., R.G. Prinn, S. O'Doherty, S.A. Montzka, A. McCulloch, C.M. Harth, J. Mühle, P.K. Salameh, R.F. Weiss, D. Young, P.G. Simmonds, B.D. Hall, G.S. Dutton, D. Nance, D.J. Mondeel, J.W. Elkins, P.B. Krummel, L.P. Steele, and P.J. Fraser, Re-evaluation of the lifetimes of the major CFCs and CH_3CCl_3 using atmospheric trends, *Atmos. Chem. Phys.*, *13*(5), 2691–2702, doi:10.5194/acp-13-2691-2013, 2013.

Rigby, M., R.G. Prinn, S. O'Doherty, B.R. Miller, D. Ivy, J. Mühle, C.M. Harth, P.K. Salameh, T. Arnold, R.F. Weiss, P.B. Krummel, L.P. Steele, P.J. Fraser, D. Young, and P.G. Simmonds, Recent and future trends in synthetic greenhouse gas radiative forcing, *Geophys. Res. Lett.*, *41*(7), 2623–2630, doi:10.1002/2013GL059099, 2014.

Rigby, M., S.A. Montzka, R.G. Prinn, J.W.C. White, D. Young, S. O'Doherty, M.F. Lunt, A.L. Ganesan, A.J. Manning, P.G. Simmonds, P.K. Salameh, C.M. Harth, J. Mühle, R.F. Weiss, P.J. Fraser, L.P. Steele, P.B. Krummel, A. McCulloch, and S. Park, Role of atmospheric oxidation in recent methane growth, *Proc. Natl. Acad. Sci.*, *114*(21), 5373–5377, doi:10.1073/pnas.1616426114, 2017.

Rinsland, C.P., E. Mahieu, P. Demoulin, R. Zander, C. Servais, and J.-M. Hartmann, Decrease of the carbon tetrachloride (CCl_4) loading above Jungfraujoch, based on high resolution infrared solar spectra recorded between 1999 and 2011, *J. Quant. Spectrosc. Radiat. Trans.*, *113*(11), 1322–1329, doi:10.1016/j.jqsrt.2012.02.016, 2012.

Rollins, A.W., T.D. Thornberry, L.A. Watts, P. Yu, K.H. Rosenlof, M. Mills, E. Baumann, F.R. Giorgetta, T.V. Bui, M. Höpfner, K.A. Walker, C. Boone, P.F. Bernath, P.R. Colarco, P.A. Newman, D.W. Fahey, and R.S. Gao, The role of sulfur dioxide in stratospheric aerosol formation evaluated by using in situ measurements in the tropical lower stratosphere, *Geophys. Res. Lett.*, *44*(9), 4280–4286, doi:10.1002/2017GL072754, 2017.

Russo, M.R., M.J. Ashfold, N.R.P. Harris, and J.A. Pyle, On the emissions and transport of bromoform: sensitivity to model resolution and emission location, *Atmos. Chem. Phys.*, *15*(24), 14031–14040, doi:10.5194/acp-15-14031-2015, 2015.

Saiz-Lopez, A., R.P. Fernandez, C. Ordóñez, D.E. Kinnison, J.C. Gómez Martín, J.F. Lamarque, and S. Tilmes, Iodine chemistry in the troposphere and its effect on ozone, *Atmos. Chem. Phys.*, *14*(23), 13119-

13143, doi:10.5194/acp-14-13119-2014, 2014.

Saiz-Lopez, A., S. Baidar, C.A. Cuevas, T.K. Koenig, R.P. Fernandez, B. Dix, D.E. Kinnison, J.F. Lamarque, X. Rodriguez-Lloveras, T.L. Campos, and R. Volkamer, Injection of iodine to the stratosphere, *Geophys. Res. Lett.*, *42*(16), 6852–6859, doi:10.1002/2015GL064796, 2015.

Sala, S., H. Bönisch, T. Keber, D.E. Oram, G. Mills, and A. Engel, Deriving an atmospheric budget of total organic bromine using airborne in situ measurements from the western Pacific area during SHIVA, *Atmos. Chem. Phys.*, *14*(13), 6903–6923, doi:10.5194/acp-14-6903-2014, 2014.

Sander, R., Compilation of Henry's law constants (version 4.0) for water as solvent, *Atmos. Chem. Phys.*, *15*, 4399–4981, doi:10.5194/acp-15-4399-2015, 2015.

Saunois, M., P. Bousquet, B. Poulter, A. Peregon, P. Ciais, J.G. Canadell, E.J. Dlugokencky, G. Etiope, D. Bastviken, S. Houweling, G. Janssens-Maenhout, F.N. Tubiello, S. Castaldi, R.B. Jackson, M. Alexe, V.K. Arora, D.J. Beerling, P. Bergamaschi, D.R. Blake, G. Brailsford, V. Brovkin, L. Bruhwiler, C. Crevoisier, P. Crill, K. Covey, C. Curry, C. Frankenberg, N. Gedney, L. Hoglund-Isaksson, M. Ishizawa, A. Ito, F. Joos, H.S. Kim, T. Kleinen, P. Krummel, J.F. Lamarque, R. Langenfelds, R. Locatelli, T. Machida, S. Maksyutov, K.C. McDonald, J. Marshall, J.R. Melton, I. Morino, V. Naik, S. O'Doherty, F.J.W. Parmentier, P.K. Patra, C.H. Peng, S.S. Peng, G.P. Peters, I. Pison, C. Prigent, R. Prinn, M. Ramonet, W.J. Riley, M. Saito, M. Santini, R. Schroeder, I.J. Simpson, R. Spahni, P. Steele, A. Takizawa, B.F. Thornton, H.Q. Tian, Y. Tohjima, N. Viovy, A. Voulgarakis, M. van Weele, G.R. van der Werf, R. Weiss, C. Wiedinmyer, D.J. Wilton, A. Wiltshire, D. Worthy, D. Wunch, X.Y. Xu, Y. Yoshida, B. Zhang, Z. Zhang, and Q. Zhu, The global methane budget 2000-2012, *Earth Syst. Sci. Data*, *8*(2), 697-751, doi:10.5194/essd-8-697–2016, 2016.

Schaefer, H., S.E.M. Fletcher, C. Veidt, K.R. Lassey, G.W. Brailsford, T.M. Bromley, E.J. Dlugokencky, S.E. Michel, J.B. Miller, I. Levin, D.C. Lowe, R.J. Martin, B.H. Vaughn, and J.W.C. White, A 21st-century shift from fossil-fuel to biogenic methane emissions indicated by $^{13}CH_4$, *Science*, *352*(6281), 80–84, doi:10.1126/science.aad2705, 2016.

Schmidt, J.A., D.J. Jacob, H.M. Horowitz, L. Hu, T. Sherwen, M.J. Evans, Q. Liang, R.M. Suleiman, D.E. Oram, M. Le Breton, C.J. Percival, S. Wang, B. Dix, and R. Volkamer, Modeling the observed tropospheric BrO background: Importance of multiphase chemistry and implications for ozone, OH, and mercury, *J. Geophys. Res. Atmos.*, *121*(19), 11,819–11,835, doi:10.1002/2015JD024229, 2016.

Schoenenberger, F., M.K. Vollmer, M. Rigby, M. Hill, P.J. Fraser, P.B. Krummel, R.L. Langenfelds, T.S. Rhee, T. Peter, and S. Reimann, First observations, trends, and emissions of HCFC-31 (CH_2ClF) in the global atmosphere, *Geophys. Res. Lett.*, *42*(18), 7817–7824, doi:10.1002/2015GL064709, 2015.

Schofield, R., S. Fueglistaler, I. Wohltmann, and M. Rex, Sensitivity of stratospheric Br-y to uncertainties in very short lived substance emissions and atmospheric transport, *Atmos. Chem. Phys.*, *11*(4), 1379–1392, doi:10.5194/acp-11-1379-2011, 2011.

Schwietzke, S., O.A. Sherwood, L.M.P.B. Ruhwiler, J.B. Miller, G. Etiope, E.J. Dlugokencky, S.E. Michel, V.A. Arling, B.H. Vaughn, J.W.C. White, and P.P. Tans, Upward revision of global fossil fuel methane emissions based on isotope database, *Nature*, *538*(7623), 88-91, 10.1038/nature19797, 2016.

Sheng, J.-X., D.K. Weisenstein, B.-P. Luo, E. Rozanov, A. Stenke, J. Anet, H. Bingemer, and T. Peter, Global atmospheric sulfur budget under volcanically quiescent conditions: Aerosol-chemistry-climate model predictions and validation, *J. Geophys. Res. Atmos.*, *120*(1), 256–276, 10.1002/2014JD021985, 2015.

Sherry, D., A. McCulloch, Q. Liang, S. Reimann, and P.A. Newman, Current Sources of Carbon Tetrachloride (CCl_4) in our Atmosphere, *Environ. Res. Lett.,* 13, doi:10.1088/1748-9326/oa9c87.

Sherwen, T., M.J. Evans, L.J. Carpenter, S.J. Andrews, R.T. Lidster, B. Dix, T.K. Koenig, R. Sinreich, I. Ortega, R. Volkamer, A. Saiz-Lopez, C. Prados-Roman, A.S. Mahajan, and C. Ordóñez, Iodine's impact on tropospheric oxidants: a global model study in GEOS-Chem, *Atmos. Chem. Phys., 16*(2), 1161–1186, doi:10.5194/acp-16-1161-2016, 2016.

Shi, Q., G. Petrick, B. Quack, C. Marandino, and D. Wallace, Seasonal variability of methyl iodide in the Kiel Fjord, *J. Geophys. Res. Oceans, 119*(3), doi:10.1002/2013jc009328,2014,2014.

Shimizu, Y., A. Ooki, H. Onishi, T. Takatsu, S. Tanaka, Y. Inagaki, K. Suzuki, N. Kobayashi, Y. Kamei, and K. Kuma, Seasonal variation of volatile organic

iodine compounds in the water column of Funka Bay, Hokkaido, Japan, *J. Atmos. Chem.*, *74*(2), 205–225, doi:10.1007/s10874-016-9352-6, 2017.

Simmonds, P.G., S. O'Doherty, J. Huang, R. Prinn, R.G. Derwent, D. Ryall, G. Nickless, and D. Cunnold, Calculated trends and the atmospheric abundance of 1,1,1,2-tetrafluoroethane, 1,1-dichloro-1-fluoroethane, and 1-chloro-1, 1-difluoroethane using automated in-situ gas chromatography-mass spectrometry measurements recorded at Mace Head, Ireland, from October 1994 to March 1997, *J. Geophys. Res. Atmos.*, *103*(D13), 16029–16037, doi:10.1029/98JD00774, 1998.

Simmonds, P.G., A.J. Manning, D.M. Cunnold, A. McCulloch, S. O'Doherty, R.G. Derwent, P.B. Krummel, P.J. Fraser, B. Dunse, L.W. Porter, R.H.J. Wang, B.R. Greally, B.R. Miller, P. Salameh, R.F. Weiss, and R.G. Prinn, Global trends, seasonal cycles, and European emissions of dichloromethane, trichloroethene, and tetrachloroethene from the AGAGE observations at Mace Head, Ireland, and Cape Grim, Tasmania, *J. Geophys. Res. Atmos.*, *111*(D18), doi:10.1029/2006JD007082, 2006.

Simmonds, P.G., M. Rigby, A. McCulloch, S. O'Doherty, D. Young, J. Mühle, P.B. Krummel, P. Steele, P.J. Fraser, A.J. Manning, R.F. Weiss, P.K. Salameh, C.M. Harth, R.H.J. Wang, and R.G. Prinn, Changing trends and emissions of hydrochlorofluorocarbons (HCFCs) and their hydrofluorocarbon (HFCs) replacements, *Atmos. Chem. Phys.*, *17*(7), 4641–4655, doi:10.5194/acp-17-4641-2017, 2017.

Simpson, I.J., N.J. Blake, D.R. Blake, S. Meinardi, M.P.S. Andersen, and F.S. Rowland, Strong evidence for negligible methyl chloroform (CH_3C-Cl_3) emissions from biomass burning, *Geophys. Res. Lett.*, *34*(10), doi:10.1029/2007GL029383, 2007.

Simpson, I.J., S.K. Akagi, B. Barletta, N.J. Blake, Y. Choi, G.S. Diskin, A. Fried, H.E. Fuelberg, S. Meinardi, F.S. Rowland, S.A. Vay, A.J. Weinheimer, P.O. Wennberg, P. Wiebring, A. Wisthaler, M. Yang, R.J. Yokelson, and D.R. Blake, Boreal forest fire emissions in fresh Canadian smoke plumes: C-1-C-10 volatile organic compounds (VOCs), CO_2, CO, NO_2, NO, HCN and CH_3CN, *Atmos. Chem. Phys.*, *11*(13), 6445–6463, doi:10.5194/acp-11-6445-2011, 2011.

Simpson, I.J., M.P.S. Andersen, S. Meinardi, L. Bruhwiler, N.J. Blake, D. Helmig, F.S. Rowland, and D.R. Blake, Long-term decline of global atmospheric ethane concentrations and implications for methane, *Nature*, *488*(7412), 490–494, doi:10.1038/nature11342, 2012.

Sive, B.C., R.K. Varner, H. Mao, D.R. Blake, O.W. Wingenter, and R. Talbot, A large terrestrial source of methyl iodide, *Geophys. Res. Lett.*, *34*(17), doi:10.1029/2007GL030528, 2007.

Solomon, S., D. Kinnison, R.R. Garcia, J. Bandoro, M. Mills, C. Wilka, R.R. Neely, A. Schmidt, J.E. Barnes, J.-P. Vernier, and M. Höpfner, Monsoon circulations and tropical heterogeneous chlorine chemistry in the stratosphere, *Geophys. Res. Lett.*, *43*(24), 12,624–612,633, doi:10.1002/2016GL071778, 2016.

SPARC, (Stratospheric Processes And their Role in Climate), *Lifetimes of Stratospheric Ozone-Depleting Substances, Their Replacements, and Related Species*, edited by M.K.W. Ko, P.A. Newman, S. Reimann, and S.E. Strahan, *SPARC Report No. 6*, WCRP-15/2013, 2013.

Stachnik, R.A., L. Millán, R. Jarnot, R. Monroe, C. McLinden, S. Kühl, J. Puķīte, M. Shiotani, M. Suzuki, Y. Kasai, F. Goutail, J.P. Pommereau, M. Dorf, and K. Pfeilsticker, Stratospheric BrO abundance measured by a balloon-borne submillimeterwave radiometer, *Atmos. Chem. Phys.*, *13*(6), 3307–3319, doi:10.5194/acp-13-3307-2013, 2013.

Stemmler, I., I. Hense, and B. Quack, Marine sources of bromoform in the global open ocean-global patterns and emissions, *Biogeosci.*, *12*(6), 1967–1981, doi:10.5194/bg-12-1967-2015, 2015.

Stiller, G.P., T. von Clarmann, F. Haenel, B. Funke, N. Glatthor, U. Grabowski, S. Kellmann, M. Kiefer, A. Linden, S. Lossow, and M. Lopez-Puertas, Observed temporal evolution of global mean age of stratospheric air for the 2002 to 2010 period, *Atmos. Chem. Phys.*, *12*(7), 3311–3331, doi:10.5194/acp-12-3311-2012, 2012.

Stohl, A., P. Seibert, J. Arduini, S. Eckhardt, P. Fraser, B.R. Greally, C. Lunder, M. Maione, J. Mühle, S. O'Doherty, R.G. Prinn, S. Reimann, T. Saito, N. Schmidbauer, P.G. Simmonds, M.K. Vollmer, R.F. Weiss, and Y. Yokouchi, An analytical inversion method for determining regional and global emissions of greenhouse gases: Sensitivity studies

and application to halocarbons, *Atmos. Chem. Phys.*, *9*(5), 1597–1620, doi:10.5194/acp-9-1597-2009, 2009.

Stohl, A., J. Kim, S. Li, S. O'Doherty, J. Mühle, P.K. Salameh, T. Saito, M.K. Vollmer, D. Wan, R.F. Weiss, B. Yao, Y. Yokouchi, and L.X. Zhou, Hydrochlorofluorocarbon and hydrofluorocarbon emissions in East Asia determined by inverse modeling, *Atmos. Chem. Phys.*, *10*(8), 3545–3560, doi:10.5194/acp-10-3545-2010, 2010.

Stolarski, R.S., A.R. Douglass, and S.E. Strahan, Using satellite measurements of N_2O to remove dynamical variability from HCl measurements, *Atmos. Chem. Phys.*, *18*(8), 5691–5697, doi:10.5194/acp-18-5691-2018, 2018.

Sturges, W.T., D.E. Oram, J.C. Laube, C.E. Reeves, M.J. Newland, C. Hogan, P. Martinerie, E. Witrant, C.A.M. Brenninkmeijer, T.J. Schuck, and P.J. Fraser, Emissions halted of the potent greenhouse gas SF_5CF_3, *Atmos. Chem. Phys.*, *12*(8), 3653–3658, doi:10.5194/acp-12-3653-2012, 2012.

Sulbaek Andersen, M.P., S.P. Sander, O.J. Nielsen, D.S. Wagner, T.J. Sanford, and T.J. Wallington, Inhalation anaesthetics and climate change, *Brit. J. Anaesth.*, *105*(6), 760–766, doi:10.1093/bja/aeq259, 2010.

Sulbaek Andersen, M.P., O.J. Nielsen, B. Karpichev, T.J. Wallington, and S.P. Sander, Atmospheric chemistry of isoflurane, desflurane, and sevoflurane: Kinetics and mechanisms of reactions with chlorine atoms and OH radicals and global warming potentials, *J. Phys. Chem. A*, *116*(24), 5806-5820, doi:10.1021/jp2077598, 2012.

Tegtmeier, S., K. Krüger, B. Quack, E.L. Atlas, I. Pisso, A. Stohl, and X. Yang, Emission and transport of bromocarbons: From the West Pacific ocean into the stratosphere, *Atmos. Chem. Phys.*, *12*(22), 10633–10648, doi:10.5194/acp-12-10633-2012, 2012.

Tegtmeier, S., K. Krüger, B. Quack, E. Atlas, D.R. Blake, H. Boenisch, A. Engel, H. Hepach, R. Hossaini, M.A. Navarro, S. Raimund, S. Sala, Q. Shi, and F. Ziska, The contribution of oceanic methyl iodide to stratospheric iodine, *Atmos. Chem. Phys.*, *13*(23), 11869-11886, doi:10.5194/acp-13-11869-2013, 2013.

Tegtmeier, S., F. Ziska, I. Pisso, B. Quack, G.J.M. Velders, X. Yang, and K. Krüger, Oceanic bromoform emissions weighted by their ozone depletion potential, *Atmos. Chem. Phys.*, *15*(23), 13647–13663, doi:10.5194/acp-15-13647-2015, 2015.

Thompson, R.L., K. Ishijima, E. Saikawa, M. Corazza, U. Karstens, P.K. Patra, P. Bergamaschi, F. Chevallier, E. Dlugokencky, R.G. Prinn, R.F. Weiss, S. O'Doherty, P.J. Fraser, L.P. Steele, P.B. Krummel, A. Vermeulen, Y. Tohjima, A. Jordan, L. Haszpra, M. Steinbacher, S. Van der Laan, T. Aalto, F. Meinhardt, M.E. Popa, J. Moncrieff, and P. Bousquet, TransCom N_2O model inter-comparison - Part 2: Atmospheric inversion estimates of N_2O emissions, *Atmos. Chem. Phys.*, *14*(12), 6177–6194, doi:10.5194/acp-14-6177-2014, 2014.

Thornton, B.F., A. Horst, D. Carrizo, and H. Holmstrand, Methyl chloride and methyl bromide emissions from baking: An unrecognized anthropogenic source, *Sci. Total Environ., 551*, 327–333, doi:10.1016/j.scitotenv.2016.01.213, 2016.

Toon, G.C., J.F.L. Blavier, and K. Sung, Atmospheric Carbonyl Sulphide (OCS) measured remotely by FTIR solar absorption spectrometry, *Atmos. Chem. Phys.*, *2017*, 1–37, doi:10.5194/acp-2017-404, 2017.

Trudinger, C.M., P.J. Fraser, D.M. Etheridge, W.T. Sturges, M.K. Vollmer, M. Rigby, P. Martinerie, J. Mühle, D.R. Worton, P.B. Krummel, L.P. Steele, B.R. Miller, J. Laube, F.S. Mani, P.J. Rayner, C.M. Harth, E. Witrant, T. Blunier, J. Schwander, S. O'Doherty, and M. Battle, Atmospheric abundance and global emissions of perfluorocarbons CF_4, C_2F_6 and C_3F_8 since 1800 inferred from ice core, firn, air archive and in situ measurements, *Atmos. Chem. Phys.*, *16*(18), 11,733–11,754, doi:10.5194/acp-16-11733-2016, 2016.

Turner, A.J., C. Frankenbergb, P.O. Wennberg, and D.J. Jacob, Ambiguity in the causes for decadal trends in atmospheric methane and hydroxyl, *Proc. Natl. Acad. Sci.*, *114*(21), 5367–5372, doi:10.1073/pnas.1616020114, 2017.

Umezawa, T., A.K. Baker, C.A.M. Brenninkmeijer, A. Zahn, D.E. Oram, and P.F.J. van Velthoven, Methyl chloride as a tracer of tropical tropospheric air in the lowermost stratosphere inferred from IAGOS-CARIBIC passenger aircraft measurements, *J. Geophys. Res. Atmos.*, *120*(23), doi:10.1002/2015JD023729, 2015.

UNEP (United Nations Environment Programme), *Report of the Methyl Bromide Technical Options Committee*, United Nations Environment Programme,

Ozone Secretariat, Nairobi, Kenya, 2006.

UNEP (United Nations Environment Programme), *2010 Report Of The Halons Technical Options Committee*, 187 pp., United Nations Environment Programme, Ozone Secretariat, Nairobi, Kenya, 2011.

UNEP (United Nations Environment Programme), *2014 Report of the Methyl Bromide Technical Options Committee,* edited by M. Pizano, I. Porter, and M. Besri, Nairobi, Kenya, 2014a.

UNEP (United Nations Environment Programme), *2014 Report Of The Halons Technical Options Committee*, United Nations Environment Programme, Ozone Secretariat, Nairobi, Kenya, 2014b.

UNEP(United Nations Environment Programme), Ozone Secretariat Country Data Centre (https://ozone.unep.org/countries/data), Nairobi, Kenya, 2017.

Valeri, M., F. Barbara, C. Boone, S. Ceccherini, M. Gai, G. Maucher, P. Raspollini, M. Ridolfi, L. Sgheri, G. Wetzel, and N. Zoppetti, CCl_4 distribution derived from MIPAS ESA v7 data: Intercomparisons, trend, and lifetime estimation, *Atmos. Chem. Phys.*, *17*(16), 10143–10162, doi:10.5194/acp-17-10143-2017, 2017.

van der A, R.J., B. Mijling, J. Ding, M.E. Koukouli, F. Liu, Q. Li, H. Mao, and N. Theys, Cleaning up the air: Effectiveness of air quality policy for SO_2 and NOx emissions in China, *Atmos. Chem. Phys.*, *17*(3), 1775–1789, doi:10.5194/acp-17-1775-2017, 2017.

Velders, G.J.M., and J.S. Daniel, Uncertainty analysis of projections of ozone-depleting substances: Mixing ratios, EESC, ODPs, and GWPs, *Atmos. Chem. Phys.*, *14*(6), 2757–2776, doi:10.5194/acp-14-2757-2014, 2014.

Vogt, R., P.J. Crutzen, and R. Sander, A mechanism for halogen release from sea-salt aerosol in the remote marine boundary layer, *Nature*, *383*, 327–330, doi:10.1038/383327a0, 1996.

Volkamer, R., S. Baidar, T.L. Campos, S. Coburn, J.P. DiGangi, B. Dix, E.W. Eloranta, T.K. Koenig, B. Morley, I. Ortega, B.R. Pierce, M. Reeves, R. Sinreich, S. Wang, M.A. Zondlo, and P.A. Romashkin, Aircraft measurements of BrO, IO, glyoxal, NO_2, H_2O, O_2-O_2 and aerosol extinction profiles in the tropics: comparison with aircraft-/ship-based in situ and lidar measurements, *Atmos. Meas. Tech.*, *8*(5), 2121–2148, doi:10.5194/amt-8-2121-2015, 2015.

Vollmer, M.K., L.X. Zhou, B.R. Greally, S. Henne, B. Yao, S. Reimann, F. Stordal, D.M. Cunnold, X.C. Zhang, M. Maione, F. Zhang, J. Huang, and P.G. Simmonds, Emissions of ozone-depleting halocarbons from China, *Geophys. Res. Lett.*, *36*, doi:10.1029/2009GL038659, 2009.

Vollmer, M.K., S. Reimann, M. Hill, and D. Brunner, First observations of the fourth generation synthetic halocarbons HFC-1234yf, HFC-1234ze(E), and HCFC-1233zd(E) in the atmosphere, *Environ. Sci. Technol.*, *49*(5), 2703–2708, doi:10.1021/es505123x, 2015a.

Vollmer, M.K., M. Rigby, J.C. Laube, S. Henne, T.S. Rhee, L.J. Gooch, A. Wenger, D. Young, L.P. Steele, R.L. Langenfelds, C.A.M. Brenninkmeijer, J.L. Wang, C.F. Ou-Yang, S.A. Wyss, M. Hill, D.E. Oram, P.B. Krummel, F. Schoenenberger, C. Zellweger, P.J. Fraser, W.T. Sturges, S. O'Doherty, and S. Reimann, Abrupt reversal in emissions and atmospheric abundance of HCFC-133a (C_3FCH_2Cl), *Geophys. Res. Lett.*, *42*(20), 8702–8710, doi:10.1002/2015GL065846, 2015b.

Vollmer, M.K., T.S. Rhee, M. Rigby, D. Hofstetter, M. Hill, F. Schoenenberger, and S. Reimann, Modern inhalation anesthetics: Potent greenhouse gases in the global atmosphere, *Geophys. Res. Lett.*, *42*(5), 1606–1611, doi:10.1002/2014GL062785, 2015c.

Vollmer, M.K., J. Mühle, C.M. Trudinger, M. Rigby, S.A. Montzka, C.M. Harth, B.R. Miller, S. Henne, P.B. Krummel, B.D. Hall, D. Young, J. Kim, J. Arduini, A. Wenger, B Yao., S. Reimann., S. O'Doherty, M. Maione, D.M. Etheridge, S. Li, D.P. Verdonik, S. Park, G.S. Dutton, L.P. Steele, C.P. Lunder, T.S. Rhee, O. Hermansen, N. Schmidbauer , R.H.J. Wang, M. Hill, P.K. Salameh, R.L. Langenfelds, Z. L.X. Zhou, T. Blunier, J. Schwander, J.W. Elkins, J.H. Butler, P.G. Simmonds, R.F. Weiss, R.G. Prinn, and P.J. Fraser, Atmospheric histories and global emissions of halons H-1211 ($CBrClF_2$), H-1301 ($CBrF_3$), and H-2402 ($CBrF_2CBrF_2$), *J. Geophys. Res. Atmos.*, *121*, 3663–3686, doi:10.1002/2015JD0024488, 2016.

Vollmer, M.K., D. Young, C.M. Trudinger, J. Mühle, S. Henne, M. Rigby, S. Park, S. Li, M. Guillevic, B. Mitrevski, C.M. Harth, B.R. Miller, S.Reimann, B. Yao, L.P. Steele, S.A. Wyss, C.R. Lunder, J. Arduini, A. McCulloch, S. Wu, T.S. Rhee, R.H.J. Wang, P.K. Salameh, O. Hermansen, M. Hill, R.L. Lan-

genfelds, D. Ivy, S. O'Doherty, P.B. Krummel, M. Maione, D.M. Etheridge, L. Zhou, P.J. Fraser, R.G. Prinn, R.F. Weiss, and P.G. Simmonds, Atmospheric histories and emissions of the chlorofluorocarbons CFC-13 ($CClF_3$), ΣCFC-114 ($C_2Cl_2F_4$), and CFC-115 (C_2ClF_5), *Atmos. Chem. Phys.*, *18*, 979–1002, doi:10.5194/acp-18-979-2018, 2018.

von Hobe, M., J.U. Grooß, G. Günther, P. Konopka, I. Gensch, M. Krämer, N. Spelten, A. Afchine, C. Schiller, A. Ulanovsky, N. Sitnikov, G. Shur, V. Yushkov, F. Ravegnani, F. Cairo, A. Roiger, C. Voigt, H. Schlager, R. Weigel, W. Frey, S. Borrmann, R. Müller, and F. Stroh, Evidence for heterogeneous chlorine activation in the tropical UTLS, *Atmos. Chem. Phys.*, *11*(1), 241–256, doi:10.5194/acp-11-241-2011, 2011.

Wagner-Riddle, C., K.A. Congreves, D. Abalos, A.A. Berg, S.E. Brown, J.T. Ambadan, X.P. Gao, and M. Tenuta, Globally important nitrous oxide emissions from croplands induced by freeze-thaw cycles, *Nat. Geosci.*, *10*(4), 279–283, doi:10.1038/Ngeo2907, 2017.

Wahner, A., A.R. Ravishankara, S.P. Sander, and R.R. Friedl, Absorption cross-section of BrO between 312 and 385 nm at 298 and 223 K, *Chem. Phys. Lett.*, *152*, 507–510, 1988.

Wales, P.A., R.J. Salawitch, J.M. Nicely, D.C. Anderson, T.P. Canty, S. Baidar, B. Dix, T.K. Koenig, R. Volkamer, D. Chen, L.G. Huey, D.J. Tanner, C.A. Quevas, R.P. Fernandez, D.E. Kainnison, J.-F. Lamarque, A. Saiz-Lopez, E.L. Atlas, S.R. Hall, M.A. Navarro, L.L. Pan, S.M. Schauffler, M. Stell, S. Tilmes, K. Ullmann, A.J. Weinheimer, H. Akiyoshi, M.P. Chipperfield, M. Deushi, S.S. Dhomse, W. Feng, P. Graf, R. Hossaini, P. Jöckel, E. Mancini, M. Michou, O. Morgenstern, L.D. Oman, G. Pitari, D.A. Plummer, L.E. Revell, E. Rozanov, D. Saint-Martin, R.Schofield, A. Stenke, K.A. Stone, D. Visioni, Y. Yamashita, G. Zeng, Stratospheric injection of brominated very short-lived substances: Aircraft observations in the Western Pacific and representation in global models, *J. Geophys. Res.*, doi:10.1029/2017JD027978, 2018.

Wamsley, P.R., J.W. Elkins, D.W. Fahey, G.S. Dutton, C.M. Volk, R.C. Myers, S.A. Montzka, J.H. Butler, A.D. Clarke, P.J. Fraser, L.P. Steele, M.P. Lucarelli, E.L. Atlas, S.M. Schauffler, D.R. Blake, F.S. Rowland, W.T. Sturges, J.M. Lee, S.A. Penkett, A. Engel, R.M. Stimpfle, K.R. Chan, D.K. Weisenstein, M.K.W. Ko, and R.J. Salawitch, Distribution of halon-1211 in the upper troposphere and lower stratosphere and the 1994 total bromine budget, *J. Geophys. Res. Atmos.*, *103*(D1), 1513–1526, doi:10.1029/97JD02466, 1998.

Wang, C., M. Shao, D.K. Huang, S.H. Lu, L.M. Zeng, M. Hu, and Q. Zhang, Estimating halocarbon emissions using measured ratio relative to tracers in China, *Atmos. Environ., 89*, 816–826, doi:10.1016/j.atmosenv.2014.03.025, 2014.

Wang, S., J.A. Schmidt, S. Baidar, S. Coburn, B. Dix, T.K. Koenig, E. Apel, D. Bowdalo, T.L. Campos, E. Eloranta, M.J. Evans, J.P. DiGangi, M.A. Zondlo, R.-S. Gao, J.A. Haggerty, S.R. Hall, R.S. Hornbrook, D. Jacob, B. Morley, B. Pierce, M. Reeves, P. Romashkin, A. ter Schure, and R. Volkamer, Active and widespread halogen chemistry in the tropical and subtropical free troposphere, *Proc. Natl. Acad. Sci.*, *112*(30), 9281–9286, doi:10.1073/pnas.1505142112, 2015a.

Wang, Z.Y., H.H. Yan, X.K. Fang, L.Y. Gao, Z.H. Zhai, J.X. Hu, B.Y. Zhang, and J.B. Zhang, Past, present, and future emissions of HCFC-141b in China, *Atmos. Environ., 109*, 228–233, doi:10.1016/j.atmosenv.2015.03.019, 2015b.

Warwick, N.J., J.A. Pyle, G.D. Carver, X. Yang, N.H. Savage, F.M. O'Connor, and R.A. Cox, Global modeling of biogenic bromocarbons, *J. Geophys. Res. Atmos.*, *111*(D24), doi:10.1029/2006jd007264, 2006.

Weinberg, I., E. Bahlmann, T. Eckhardt, W. Michaelis, and R. Seifert, A halocarbon survey from a seagrass dominated subtropical lagoon, Ria Formosa (Portugal): flux pattern and isotopic composition, *Biogeosci.*, *12*(6), 1697–1711, doi:10.5194/bg-12-1697-2015, 2015.

Weiss, R.F., J. Mühle, P.K. Salameh, and C.M. Harth, Nitrogen trifluoride in the global atmosphere, *Geophys. Res. Lett.*, *35*(20), doi:10.1029/2008GL035913, 2008.

Werner, B., J. Stutz, M. Spolaor, L. Scalone, R. Raecke, J. Festa, S.F. Colosimo, R. Cheung, C. Tsai, R. Hossaini, M.P. Chipperfield, G.S. Taverna, W. Feng, J.W. Elkins, D.W. Fahey, R.-S. Gao, E.J. Hintsa, T.D. Thornberry, F.L. Moore, M.A. Navarro, E. Atlas, B.C. Daube, J. Pittman, S. Wofsy, and K. Pfeilsticker, Probing the subtropical lowermost stratosphere and the tropical upper troposphere

and tropopause layer for inorganic bromine, *Atmos. Chem. Phys.*, *17*(2), 1161–1186, doi:10.5194/acp-17-1161-2017, 2017.

Wilmouth, D.M., T.F. Hanisco, N.M. Donahue, and J.G. Anderson, Fourier Transform Ultraviolet Spectroscopy of the A 2Π3/2 ← X 2Π3/2 Transition of BrO, *J. Phys. Chem. A*, *103*(45), 8935–8945, doi:10.1021/jp991651o, 1999.

Wisher, A., D.E. Oram, J.C. Laube, G.P. Mills, P. van Velthoven, A. Zahn, and C.A.M. Brenninkmeijer, Very short-lived bromomethanes measured by the CARIBIC observatory over the North Atlantic, Africa and Southeast Asia during 2009–2013, *Atmos. Chem. Phys.*, *14*(7), 3557–3570, doi:10.5194/acp-14-3557-2014, 2014.

Wofsy, S.C., and HIPPO Science Team and Cooperating Modellers, and Satellite Teams, HIAPER Pole-to-Pole Observations (HIPPO): Fine-grained, global-scale measurements of climatically important atmospheric gases and aerosols, *Philos. Trans. Roy. Soc. A*, *369*(1943), 2073–2086, doi:10.1098/rsta.2010.0313, 2011.

Wolf, J., G.R. Asrar, and T.O. West, Revised methane emissions factors and spatially distributed annual carbon fluxes for global livestock, *Carbon Balance Manag.*, *12*(1), 16, doi:10.1186/s13021-017-0084-y, 2017.

Worden, J.R., A.A. Bloom, S. Pandey, Z. Jiang, H.M. Worden, T.W. Walker, S. Houweling, and T. Röckmann, Reduced biomass burning emissions reconcile conflicting estimates of the post-2006 atmospheric methane budget, *Nat. Commun.*, *8*(1), 2227, doi:10.1038/s41467-017-02246-0, 2017.

Worton, D.R., W.T. Sturges, J. Schwander, R. Mulvaney, J.M. Barnola, and J. Chappellaz, 20th century trends and budget implications of chloroform and related tri-and dihalomethanes inferred from firn air, *Atmos. Chem. Phys.*, *6*, 2847–2863, doi:10.5194/acp-6-2847-2006, 2006.

Xiao, X., Optimal estimation of the surface fluxes of chloromethanes using a 3-D global atmospheric chemical transport model, Ph.D. thesis, Massachusetts Institute of Technology, Cambridge, Massachusetts, 2008.

Yang, G.P., B. Yang, X.L. Lu, H.B. Ding, and Z. He, Spatio-temporal variations of sea surface halocarbon concentrations and fluxes from southern Yellow Sea, *Biogeochem.*, *121*(2), 369–388, doi:10.1007/s10533-014-0007-x, 2014.

Yang, J.S., Bromoform in the effluents of a nuclear power plant: A potential tracer of coastal water masses, *J. Hydrobiologia*, *464*(1-3), 99-105, 2001.

Yang, M.M., Y. Wang, J.M. Chen, H.L. Li, and Y.H. Li, Aromatic Hydrocarbons and Halocarbons at a Mountaintop in Southern China, *Aerosol Air Qual. Res.*, *16*(3), 478–491, doi:10.4209/aaqr.2015.03.0197, 2016.

Yang, X., R.A. Cox, N.J. Warwick, J.A. Pyle, G.D. Carver, F.M. O'Connor, and N.H. Savage, Tropospheric bromine chemistry and its impacts on ozone: A model study, *J. Geophys. Res., 110*(D23), doi:10.1029/2005JD006244, 2005.

Yokouchi, Y., F. Hasebe, M. Fujiwara, H. Takashima, M. Shiotani, N. Nishi, Y. Kanaya, S. Hashimoto, P. Fraser, D. Toom-Sauntry, H. Mukai, and Y. Nojiri, Correlations and emission ratios among bromoform, dibromochloromethane, and dibromomethane in the atmosphere, *J. Geophys. Res. Atmos.*, *110*(D23), doi:10.1029/2005JD006303, 2005.

Yokouchi, Y., S. Taguchi, T. Saito, Y. Tohjima, H. Tanimoto, and H. Mukai, High frequency measurements of HFCs at a remote site in east Asia and their implications for Chinese emissions, *Geophys. Res. Lett.*, *33*(21), doi:10.1029/2006GL026403, 2006.

Yokouchi, Y., Y. Nojiri, D. Toom-Sauntry, P. Fraser, Y. Inuzuka, H. Tanimoto, H. Nara, R. Murakami, and H. Mukai, Long-term variation of atmospheric methyl iodide and its link to global environmental change, *Geophys. Res. Lett.*, *39*(23), L23805, doi:10.1029/2012GL053695, 2012.

Yokouchi, Y., A. Takenaka, Y. Miyazaki, K. Kawamura, and T. Hiura, Emission of methyl chloride from a fern growing in subtropical, temperate, and cool-temperate climate zones, *J. Geophys. Res. Biogeosci.*, *120*(6), 1142–1149, doi:10.1002/2015JG002994, 2015.

Yokouchi, Y., T. Saito, J.Y. Zeng, H. Mukai, and S. Montzka, Seasonal variation of bromocarbons at Hateruma Island, Japan: Implications for global sources, *J. Atmos. Chem.*, *74*(2), 171–185, doi:10.1007/s10874-016-9333-9, 2017.

Yuan, D., G.P. Yang, and Z. He, Spatio-temporal distributions of chlorofluorocarbons and methyl iodide in the Changjiang (Yangtze River) estuary and its adjacent marine area, *Marine Poll.*

Bull., *103*(1-2), 247–259, doi:10.1016/j.marpolbul.2015.12.012, 2016.

Zander, R., E. Mahieu, P. Demoulin, P. Duchatelet, G. Roland, C. Servais, M. De Maziere, S. Reimann, and C.P. Rinsland, Our changing atmosphere: Evidence based on long-term infrared solar observations at the Jungfraujoch since 1950, *Sci. Total Environ.*, *391*(2-3), 184–195, doi:10.1016/j.scitotenv.2007.10.018, 2008.

Zhang, J.K., Y. Sun, F.K. Wu, J. Sun, and Y.S. Wang, The characteristics, seasonal variation and source apportionment of VOCs at Gongga Mountain, China, *Atmos. Environ., 88*, 297–305, doi:10.1016/j.atmosenv.2013.03.036, 2014.

Ziska, F., B. Quack, K. Abrahamsson, S.D. Archer, E. Atlas, T. Bell, J.H. Butler, L.J. Carpenter, C.E. Jones, N.R.P. Harris, H. Hepach, K.G. Heumann, C. Hughes, J. Kuss, K. Kruger, P. Liss, R.M. Moore, A. Orlikowska, S. Raimund, C.E. Reeves, W. Reifenhauser, A.D. Robinson, C. Schall, T. Tanhua, S. Tegtmeier, S. Turner, L. Wang, D. Wallace, J. Williams, H. Yamamoto, S. Yvon-Lewis, and Y. Yokouchi, Global sea-to-air flux climatology for bromoform, dibromomethane and methyl iodide, *Atmos. Chem. Phys.*, *13*(17), 8915–8934, doi:10.5194/acp-13-8915-2013, 2013.

Ziska, F., B. Quack, S. Tegtmeier, I. Stemmler, and K. Krüger, Future emissions of marine halogenated very-short lived substances under climate change, *J. Atmos. Chem.*, *74*(2), 245–260, doi:10.1007/s10874-016-9355-3, 2017.